Environmental Effects on Stitched RTM Composites

by

Keith W. Furrow

Thesis submitted to the faculty of the
Virginia Polytechnic Institute and State University
in partial fulfillment of the requirements for the degree of
Master of Science
in
Engineering Mechanics

APPROVED:

Alfred C. Loos, Chairman

Michael W. Hyer

David A. Dillard

May 1993
Blacksburg, Virginia

C.2

Environmental Effects on Stitched RTM Composites

by
Keith W. Furrow
Dr. Alfred C. Loos, Chairman
Engineering Mechanics

ABSTRACT

The effects of temperature and humidity cycling on mechanical properties of AS4/3501-6 quasi-isotropic composites prepared from unstitched, Kevlar 29 stitched, and S-2 glass stitched uniweave fabric were determined. Data presented include compression strengths and compression-compression fatigue results for environmentally cycled and uncycled composites. Temperature cycling ranged from 60°C to -55°C. The relative humidity varied between 95 percent at the high temperature and 0 percent at the low temperature. Microcracks which were found predominantly around individual stitches were recorded using photomicrographs taken at the end of each cycling period. The glass stitched and Kevlar stitched laminates showed significant microcracking before cycling. The unstitched uniweave material developed microcracks only after cycling. The glass stitched material had lower baseline compression strength than the unstitched and Kevlar stitched materials. Temperature and humidity cycling reduced the static compression strength of the unstitched and Kevlar stitched uniweave materials nearly 10 percent. Under the same conditions the glass stitched uniweave material lost 3 percent of its baseline strength. Combined temperature and humidity cycling did not effect the fatigue properties of the uniweave materials when the test specimens were dried to their original weights before testing.

A second environment, cycling only the temperature at constant 40 percent humidity, resulted in a 5 percent decrease in static compression strength for the unstitched and Kevlar stitched material.

The last environment held a constant 60°C and 95 percent relative humidity for 80 days. After 80 days, specimens were saturated in 70°C water. After saturation, the unstitched, glass stitched and Kevlar stitched materials lost 17, 7 and 19 percent of their baseline compression strength. Moisture absorption at constant temperature and humidity lowered the fatigue strength of the uniweave materials only after saturation.

In hot humid conditions moisture diffuses into the composite. The mass diffusivities and maximum moisture uptake for the three uniweave composites were measured. Fick's law was used to predict the moisture absorption.

Braided composites including, a stitched 2-D braid, an unstitched 2-D braid and a 3-D braid were also exposed to environmental cycling. The moisture absorption in these AS4/E905L systems was lower than the AS4/3501-6 systems and consequently the cycling had little effect on the strengths of braided materials.

Acknowledgements

I would like to thank Dr. Loos, my advisor, for his support during this research and Dr. Hyer and Dr. Dillard for serving on my committee. The NASA-Virginia Tech Composites Program supported this research through NASA Langley Research Center grant NAG-1-343. Mr. H. Benson Dexter was the grant monitor.

Numerous individuals are to be thanked for their assistance on the experimental portions of this work. Bert Cano and the Technicians at NASA Langley kept track of the cycling schedules, prepared photographs and conducted the SBC tests. Bert's help and attention to detail was instrumental in completing this research on time and according to the original plan. Tamara Knot, Robert Simonds and Bob Davis are to be thanked for their assistance in laboratory and shop work at Virginia Tech.

TABLE OF CONTENTS

LIST OF FIGURES

LIST OF TABLES

1.0 INTRODUCTION

Compared to laminated composites, textile composites with through-the-thickness reinforcement show improved damage tolerance and improved resistance to delamination around holes, cutouts and free edges. Through-the-thickness reinforcement includes stitching and out-of-plane components of three dimensional braids. However, mismatches between the coefficient of thermal expansion (CTE) of the stitching and the surrounding composite may cause microcracking around the stitch.

Like any graphite/epoxy composite used in aerospace applications, textile composites will experience severe environmental conditions, including long term temperature and humidity cycling. The potential for this cycling to intensify existing microcracks or generate new ones is a concern, since microcracking will degrade mechanical properties. Additionally, moisture absorption and temperature changes affect composite mechanical properties by softening the matrix or weakening the fiber/matrix interface.

The overall objective of this investigation was to determine the combined effects of thermal cycling and absorbed moisture on the mechanical performance of stitched textile composites. Preliminary studies have shown the existence of cracks in the microstructure of textile composites with through-the-thickness stitching. This study will attempt to identify the mechanism that causes

and fatigue performance of the materials.

This investigation first characterizes moisture diffusion in glass stitched, Kevlar stitched and unstitched textile composites. Fick's Law was used to model the in-plane and the through-the-thickness moisture diffusion in textile composites. Maximum moisture uptake and the mass diffusivities were measured.

To determine the effects of cyclic temperature and humidity on mechanical performance, the composites were exposed to three different environmental cycles. The first cycle varied both the temperature and the humidity simultaneously. The second cycle varied only the temperature and maintained a constant humidity. The last cycle maintained a constant temperature and humidity. Static compression strength and compression-compression fatigue tests were used to measure mechanical performance as a function of the number of temperature and/or humidity cycles. Photomicrographs were used to record crack growth.

2.0 LITERATURE REVIEW

2.1 Toughness and Delamination

Laminated fiber-reinforced composites are useful as aerospace structures because of their high strength-to-weight ratios. Brittle graphite/epoxy laminates, however, have weak through-the-thickness strengths. This weakness becomes a problem when the composites delaminate because of free edge stresses and when the composites sustain damage from low velocity impact [1,2,3]. Methods to improve the impact resistance of fiber-reinforced composites include use of toughened epoxy [4], adhesive interleaving [4,5], hybrid fibers [6] and the use of thermoplastics [7]. Increased interlaminar fracture toughness in thermoplastic composites is attributed to energy dissipation through large amounts of plastic deformation in the matrix [7]. Rubber toughened epoxy also relies on plastic deformation for toughness. The plasticity, however, is localized in the rubbery regions and bulk stiffness is not adversely affected [8]. Adhesive interleaving increases the impact contact area minimizing transverse shear stress concentrations and subsequent cracking in the impacted layers [5]. The adhesive layer also minimizes delamination by strengthening the bond between adjacent laminae [5]. Hybrid composites contain more than one type of fiber. Plastic deformation in hybrid fibers accounts for improved impact resistance in the hybrid composite [6].

2.2 3-D and Stitched Textile Composites

Recent approaches to the impact problem involve through-the-thickness reinforcement. These approaches include stitching and 3-D weaving. Through-the-thickness reinforcement provides out-of-plane strength and better impact tolerance. When an in-plane matrix crack develops, the stiff through-the-thickness fibers carry out-of-plane loads and minimize the stress intensity around the crack tip resulting in a tougher, impact resistant material [7].

2.2.1 Stitched Textile Composites

Mechanical properties and characterization of stitched textile composites and unstitched woven composites is reviewed below. Mignery, Tan and Sun [9] showed that stitching effectively arrested edge delamination but reduced tensile strength in fiber dominated layups. Dexter and Funk [10] measured the effect of stitch pattern and stitching material on tension properties, compression properties, impact resistance and interlaminar fracture toughness of a Thornel 300/3501-6 graphite/epoxy system. An 80 percent improvement in compression after impact (CAI) strength was realized along with a 30 fold increase in mode 1 critical strain energy release rate (G_{Ic}), however, the stitching caused a 20-25 percent reduction in tension and compression strength compared to a similar tape laminate. Dow and Smith [11] studied a larger array of stitch patterns using a $(45/0/-45/90)_{6s}$ AS4/3501-6 system. They measured CAI strength, open hole compression strength, fatigue life, and a limited amount of thermal cycling effects. Stitching improved the impact strength and did not reduce fatigue life or open hole compression strength compared to the unstitched material. Thermal cycling between 93°C and -54°C did not affect the compression strength or modulus of the stitched material. Chung, et al. [12] also found increases in impact tolerance and improved flexural strength in stitched composites when compared to unstitched materials. Pelstring and Madan [13] developed semiempirical relationships correlating stitch properties with Mode I critical strain energy release rate (G_{Ic}), compression-after-impact (CAI) strength, and impact damage area.

Farley, Smith and Maiden [14] systematically studied compression properties of two stitched uniweaves, two integrally woven preforms, two tape layups and an unstitched uniweave. (Uniweave refers to the woven fabric used to lay up the composite.) The stitched uniweaves had either Kevlar or graphite stitching and the uniweave fabric contained 21K AS4 tows which were heavier than the tows used in previous investigations. The heavier tows result in thicker layers. The integrally woven materials consisted of 21K AS4 tows in the X and Y directions which were woven together in the Z direction with either graphite or Kevlar. All of the woven materials had [0/90/0/90/0/90/0/90/0] layups. One of the tape laminates had a $[(0_5/90_5)_2/0_3]_s$ ply orientation to simulate the thick layers of the woven composites and the other tape laminate had a $[(0/90)_2/0/0(0/90)_5/0/-(0/90)_3/0]_s$ layup designed to minimize interlaminar stresses. The compression strengths and CAI strengths were measured. Stitching in the thick-layer laminates reduced undamaged compression strength twice as much as stitching in the thin-layered laminates. The CAI strengths, however, were comparable between thick and thin layered laminates. Both showed improvement over the tape layups. (Thick-layer laminates are cheaper to manufacture than the thin layered laminates. If CAI strength is the design limit then the thick-layer laminate is the better choice over the thin-layer composite.)

Stitching reduces composite compression strength compared to the unstitched material or similar tape layups [10,14]. Farley [15] suggested that stitch induced kinking of the outer layers causes the reduction. Machining off the kinked layers resulted in a 35 percent improvement in compression strength. Farley et al. [15] repeated the experiment using similar materials and measured CAI strength. The machined composites had 14 percent higher CAI strength compared to the unmachined composites.

Portanova, Poe and Whitcomb [16] initiated fatigue studies of stitched composites. Their work characterized open hole and post-impact compression fatigue of

stitched graphite/epoxy and unstitched toughened graphite/epoxy composites. Stitching did not improve open hole fatigue life or static compression strength in comparison to the toughened system. After impact damage, however, the compressive static and fatigue strengths of the stitched composite were greater than those of the toughened tape composite. Vandermey, Morris and Masters [17] described damage development under compressive fatigue loading using X-ray photography, edge replication, residual strength, stiffness loss and S-N curves. They used $(45/0/-45/90)_{6s}$ glass stitched graphite/epoxy composites and found that damage initiated at the stitching and propagated from that point.

Since the stitched materials in this study were fabricated from woven material, a brief review of woven composite static and fatigue behavior is given. The conclusions are from a review by Wagnecz [18].

> "Damage development studies on woven materials show that the woven architecture limits delamination and 0 degree matrix splitting in graphite-epoxy. As a result, failure surfaces are more localized, although significant nonlinear strain response occurs near notches prior to ultimate material failure. Fatigue studies showed that woven laminates had less global delamination and splitting than non-woven laminates, but also had lower residual strength. Local delaminations at fiber bundle crossovers resulted in 0 degree fiber damage and strength degradation. The weave constrains global damage development, but may at the same time cause local damage."

2.2.2 3-D Textile Composites

Current 3-D textile composite literature mainly concerns weaving methods for various shapes and preforms. Ko [19], however, reviews fiber architecture and mechanical properties of composites made from 3-D wovens, 3-D orthogonal nonwovens (XYZ fabrics), knitted fabrics and 3-D braids.

The XYZ composites demonstrate higher interlaminar shear [19], tensile, compressive and flexural fatigue strengths compared to a 2-D woven material [20]. These properties increase with increasing reinforcement in the Z direction [20]. In

3-D braids, as the braiding percentage is increased a maximum compression strength is reached so that the braided material has a higher compression strength than unidirectional material [21]. Three-dimensional braids show sensitivity to cut edges and strength can depend on tow size and the resulting degree of crimping [22].

Impact and notch studies have shown that the through-the-thickness reinforcement in 3-D textile composites improves their damage resistance [19,23,24]. For example, open hole test results show that a 3-D braid maintains 90 percent of its tensile strength compared to 50 percent for a quasi-isotropic layup [19]. Under impact, 3-D laminates show a similar damage threshold compared to 2-D layups, but the damage area is significantly reduced [22].

2.3 The Moisture Problem

Environmental exposure can affect the performance of many materials, including fiber-reinforced composites. The type of environmental exposure depends on the application. In the case of commercial aircraft, temperature and humidity extremes can be expected along with exposure to solvents and other chemicals. When exposed to a flight environment of variable temperature and humidity, a graphite/epoxy composite will absorb moisture and be subject to temperature gradients. To obtain a reliable structural design, composite performance must be understood as a function of temperature distribution, moisture distribution and total moisture content [25]. Through-the-thickness reinforcement complicates the moisture problem since stitching adds flaws and may provide preferential moisture ingression into the interior of the composite. For example, Whiteside, et al. [26] measured preferential moisture ingression in a stitched skin-to-spar joint which failed prematurely due to increased moisture diffusion along the stitching.

As a starting point for the study of moisture absorption in stitched composites, the following sections review moisture diffusion in laminated composites and hygrothermal effects on laminated composite performance. A series of papers by Komorowski [27-30] reviews moisture diffusion in composites and hygrothermal effects on laminated composites through the year 1982. Wolfe [31] reviewed moisture diffusion in the context of dimensional stability.

2.4 Diffusion in Composites

2.4.1 Fick's Law

Diffusion in polymers is a two step process beginning with adhesion of the solute to the solid surface followed by diffusion through the bulk of the polymer [32]. Random molecular motion drives the diffusion process. Molecular motion also drives the heat conduction process. Therefore, by analogy to Fourier's law of heat conduction, Fick's law is often used to describe the diffusion process. Fick's law states that the mass flux of a diffusing material is proportional to its concentration gradient and is given by

$$\bar{F} = -\bar{\bar{D}}\nabla C \tag{1}$$

where F is the mass flux, D is the diffusivity matrix and C is the concentration of the diffusing material. When combined with the continuity equation, Fick's law becomes

$$\frac{\partial C}{\partial t} = \nabla \cdot \bar{\bar{D}}\nabla C \tag{2}$$

The initial and boundary conditions are analogous to those in heat transfer. The initial concentration distribution is specified. The boundary conditions may include evaporation(convection), a constant mass flux(insulation or heat source) or a specified surface concentration(temperature). Crank [33] gives solutions to this problem for infinite plates, cylinders and spheres. The total mass uptake is

generally of interest and is obtained by integrating the concentration distribution over the volume.

Shen and Springer [34] found that moisture diffusion in laminated composites follows Fick's law. For a constant temperature thin plate with infinite dimensions in X and Y and a constant diffusion coefficient, Fick's Law becomes one-dimensional and is given by

$$\frac{\partial C}{\partial t} = D_z \frac{\partial^2 C}{\partial z^2} \tag{3}$$

where D_z is the diffusion coefficient in the Z direction. When the composite is exposed to humid air, the surface concentration is assumed to instantaneously reach a known value equal to the maximum equilibrium moisture concentration in the composite, C_m . The initial moisture distribution C_o is usually taken to be a small constant value or zero. However, laminates leaving the autoclave can have moisture contents between 0.1 and 0.4 percent [35].

Using the separation of variables technique to solve equation (3) subject to the boundary and initial conditions given in the preceding paragraph, the transient concentration profile is given by [33]

$$\frac{C - C_o}{C_m - C_o} = 1 - \frac{4}{\pi} \sum_{n=0}^{\infty} \frac{1}{2n+1} e^{-D_z (2n+1)^2 \pi^2 t / h^2} \sin \frac{(2n+1)\pi z}{h} \tag{4}$$

where h is the plate thickness shown in Figure 1. Experimentally, the concentration profile is difficult to measure, so the total mass uptake is measured. Integrating the equation for the concentration profile (equation 4) through the thickness results in an expression for the total mass absorbed

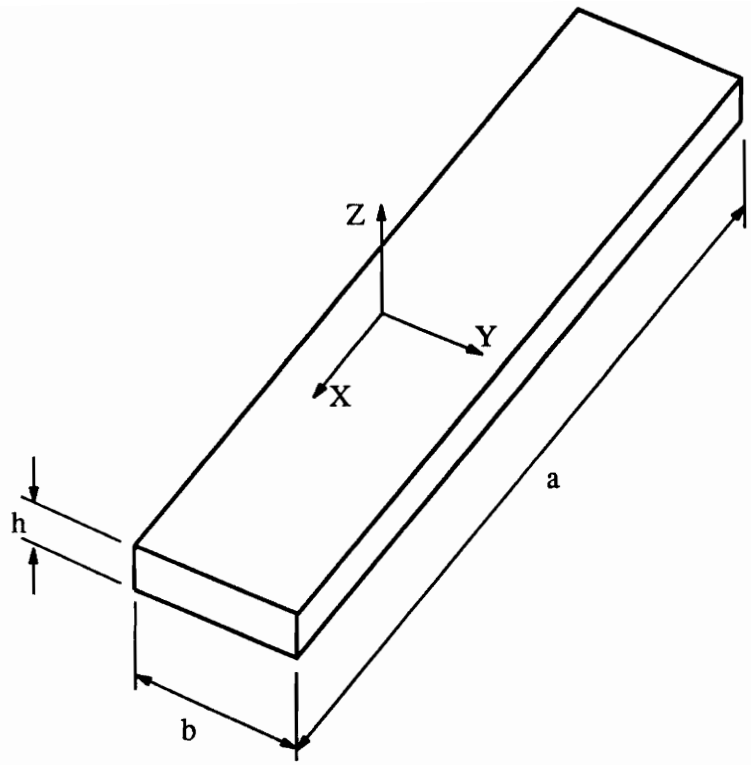

Figure 1. Coordinates and dimensions for the diffusion problem

$$\frac{M_t - M_o}{M_m - M_o} = 1 - \sum_{n=0}^{\infty} \frac{8}{(2n+1)^2\pi^2} e^{-D_z(2n+1)^2\pi^2 t/h^2} \quad (5)$$

where M_o , M_t and M_m are the initial moisture content, the moisture absorbed at time t and the maximum amount of absorbed moisture, respectively.

Shown below is a Laplace transform solution to Fick's Law describing the moisture absorption in a semi-infinite solid. The solution is valid for a flat plate at short times when the top and bottom halves of the plate can be modeled as semi-infinite solids [33].

$$\frac{M_t}{M_m} = 4\sqrt{\frac{D_z t}{\pi h^2}} \quad (6)$$

For a flat plate exposed to constant temperature and humidity, a plot of the mass absorbed against the square root of time (Figure 2) initially yields a straight line whose slope is related to the diffusivity, D_z , as shown in equation 6. After a long period of time the plate reaches its maximum moisture content, M_m . The diffusivity and the maximum moisture adsorption are the two parameters used to describe the one-dimensional moisture absorption process

2.4.2 Maximum Moisture Absorption

In the absence of applied stress, the maximum moisture absorption is a function of the relative humidity, RH, and experimentally [34,36-39] follows the equation

$$C_m = a(RH)^b \quad (7)$$

where a and b are experimentally determined constants. Voids and cracks also influence total moisture content. Harper, Staab and Chen [40] studied AS4/3502 with void content between 0 and 6 percent and found that a 5 percent void content increased the maximum moisture content by approximately 50 percent over a material with a 1 percent void content. Weitsman [41] also suggests a relationship between damage and moisture content.

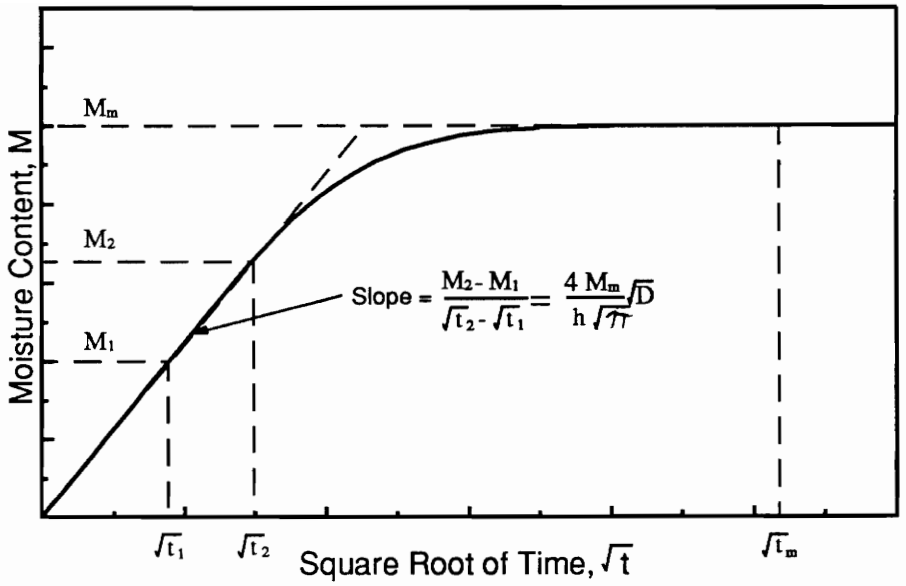

Figure 2. Illustration of the change of moisture content with the square root of time for one dimensional Fickian diffusion in a flat plate exposed to constant temperature and humidity. (after ref. 25)

Aramid fibers will absorb moisture [42] but in glass and graphite composites the matrix accounts for all of the absorbed moisture. If the maximum moisture content of the matrix and fiber are known, then the rule of mixtures gives the maximum moisture content of the composite. Enhanced moisture absorption at fiber matrix interfaces [43] and voids create deviations from the rule of mixtures. For epoxy between 21°C and 82°C, maximum moisture content is nearly independent of temperature [38,44]. Under applied stress the maximum moisture content increases with the volume strain of the matrix [44]. Weitsman [41] also predicts a linear relationship between applied stress and maximum moisture content.

2.4.3 Diffusivity

The diffusivity quantifies the ability of moisture to diffuse through a polymer matrix. In a polymer, voids of atomic scale or free volume exist due to polymeric chain motion. Temperature regulates the polymer chain motion which in turn regulates the size and distribution of free volume. For diffusion to take place, a free volume large enough for the diffusing species must be created [32]. Consequently, the diffusivity is primarily a function of temperature and can be written [32,36]

$$D = D_o e^{-E_a/RT} \tag{8}$$

where D_o and the activation energy, E_a, are determined experimentally. T is the absolute temperature and **R** is the gas constant. Numerous researchers [36,37,45-46] have reported values of D_o and E_a for diffusion perpendicular to the fiber direction. The values vary considerably due to variation in cure cycle [36], fiber volume fraction [34], void content [40] and extent of damage [36,41]. Void content and damage act to increase the diffusivity. By analogy to thermal conductivity [46,34], the transverse and longitudinal diffusivities decrease with fiber volume fraction and can be described by

$$D_{11} = D_r(1 - \nu_f) \qquad D_{22} = D_r(1 - 2\sqrt{\nu_f/\pi}) \tag{9}$$

The subscripts 11 and 22 are longitudinal and transverse values, respectively, v_f is the fiber volume fraction and D_r is the diffusivity of the pure resin when it is cured identically to the composite. The equations are valid for nonabsorbing fibers when $v_f \leq 0.78$. Carslaw [48] developed transformations for thermal conductivities in anisotropic media. Shen and Springer [34] applied these transformations to mass diffusivities in layered fiber reinforced composites. Consequently, the diffusivities D_{11} and D_{22} obtained from unidirectional materials can be used to determine the diffusivity in angle ply laminates.

2.4.4 3-D Diffusion

For diffusion in one direction, the maximum moisture content and the diffusivity in that direction characterize the moisture absorption process. For the three-dimensional case, Carslaw [48] shows that the solution to Fourier's law (and by analogy Fick's law) is the product of the three one dimensional solutions. For the full three dimensional case two more diffusivities are required. Whitney [49] suggest a method to experimentally determine the remaining two in-plane diffusivities using a short time three dimensional solution. Shen and Springer [34] obtain the same results by neglecting the interaction between the sides of a parallelepiped. Consequently, at short times, the estimated moisture uptake is the sum of moisture diffusing through each side of the parallelepiped. Whitney's three-dimensional equivalent to equation (6) is written

$$\frac{M_t}{M_m} = 1 - \left(1 - 4\sqrt{\frac{D_z t}{\pi h^2}}\right)\left(1 - 4\sqrt{\frac{D_x t}{\pi a^2}}\right)\left(1 - 4\sqrt{\frac{D_y t}{\pi b^2}}\right) \qquad (10)$$

The coordinates and the dimensions a , b and h are described in Figure 1.

With the exception of reference 22 which analyzed diffusion into a stitched wing to spar joint, the diffusion in a stitched material has not been characterized. The closest treatment of diffusion in a composite with through-the-thickness reinforcement would be the work of Singh, Singh and Rao [50] which characterized

woven roving and chopped strand mat composites. The chopped strand mat had a higher diffusivity than the woven roving composite due to either its lower fiber volume fraction or its higher proportion of fibers with through-the-thickness components.

2.5 Hygrothermal Effects

Moisture absorption and temperature changes affect the mechanical properties of composites. Moisture induced swelling causes dimensional instability and changes in the stress state [31,51]. The coefficient of thermal expansion (CTE) causes analogous changes in the case of temperature [31]. Thermal cycling between -150°C and 100°C will cause matrix cracking in graphite/epoxy systems due to mismatches in the CTE between layers. These temperature ranges are studied in the context of space structures [52-54]. Thermal spikes, or high temperature excursions (typically up to 130°C) associated with supersonic flight, can induce cracking and interface damage which increases the amount and rate of moisture absorption. As a result, strength and stiffness are reduced [55-58].

Absorbed moisture reduces graphite/epoxy composite strength and stiffness by plasticizing the matrix and weakening the fiber/matrix interface. These reductions are particularly significant at elevated temperatures [59-64]. Failure surfaces showing bare fiber surfaces are cited as evidence for weakened fiber/matrix interfaces [59]. Decreased elastic moduli and lowered glass transition temperatures are evidence of matrix plasticization. The effects of moisture and temperature on moduli, strength and fatigue performance are reviewed below.

2.5.1 Elastic Moduli

Shen and Springer [64] reviewed experimental data for graphite/epoxy composites and concluded that in fiber dominated layups temperatures up to 177°C have a negligible effects on the elastic moduli of dry materials. Between 25°C and 150°C Haque et.al. [62] found a 28 percent decrease in the longitudinal tensile modulus

of a dry unidirectional graphite/epoxy while Ankara [60] found no change in a similar material. In the case of matrix dominated properties (transverse tension, shear and compression), previous studies [60-63] have all shown decreasing moduli with increasing temperature especially when absorbed moisture was present. The results vary considerably, with 20 to 30 percent reductions in the moduli being common at temperatures above 100°C.

2.5.2 Strength

Shen and Springer [63] indicate a negligible change in the tensile strength for dry, fiber dominated layups up to 110°C. Above 110°C, a 20 percent decrease in tensile strength was observed. For transverse tensile strength they report 30 percent decreases up to 170°C. When moisture is present, the strengths (especially matrix dominate strengths) decline even faster with temperature. For example, for a graphite/epoxy composite containing 1.6 percent moisture at 120°C, Bergmann et.al. [59] report 28, 75 and 36 percent decreases in longitudinal, transverse and shear strengths, respectively compared to the strengths at dry ambient conditions.

Appreciable data scatter and differences in materials and test conditions preclude any specific conclusions. In graphite/epoxy composites, however, the data supports the generalization that absorbed moisture reduces moduli and strength especially at high temperatures.

2.5.3 Fatigue

Bergmann et al. [59] produced S-N curves at 28°C and 80°C for $(0,45,-45,90)_s$ graphite/epoxy laminates conditioned at 5, 40 and 95 percent humidity. They concluded that temperature and moisture did not significantly influence the tensile fatigue life of carbon fiber reinforced laminates. In angle-ply laminates, the simultaneous presence of temperature and moisture causes an increase in the fatigue data scatter but the slope of the S-N curve remains essentially unaffected.

Additionally, Komorowski's review [30] of moisture effects on fatigue concluded: 1. large data scatter appeared at high temperature and humidity; 2. environment had little effect on fiber dominated layups; 3. the effects on matrix dominated layups depend on the matrix material and 4. wet elevated temperature conditions and environmental cycling reduce the fatigue resistance of composites.

2.6 Summary

Based on the literature review, stitched textile composites and braided composites have a promising future. Their advantages include easier handling and improved impact resistance. Stitched composites have lower undamaged or pre-impact strengths than comparable tape laminates. Experimental studies on textile composites have concentrated on measuring physical properties and CAI properties of dry or as received materials.

Available literature indicates that moisture absorption reduces laminated composite strength and stiffness. The degree of the reduction depends on the amount of absorbed moisture, the test temperature and the composite layup. The epoxy matrix in textile composites also absorbs moisture and as a consequence, the matrix loses stiffness. Therefore, absorbed moisture is expected to affect the strength and stiffness of textile composites. The effect of absorbed moisture on stitched textile composite strength and stiffness needs to be determined.

Compared to tape laminates, stitched and braided fiber architectures will generate different stress states when subject to temperature cycling. Microcracking from thermal stresses may affect the mechanical properties of textile composites. Microcracking, due to curing stresses, has already been observed around individual stitches in stitched textile composites. The effect of temperature cycling on stitched textile composites needs to be determined.

Fick's law describes moisture diffusion in laminated composites. The additional through-the-thickness reinforcement in stitched textile composites may enhance moisture diffusion into the composite. Therefore, moisture absorption in stitched composites needs to be characterized.

3.0 MATERIALS

Six textile preforms were used in this investigation. These included an unstitched uniweave, a glass stitched uniweave, a Kevlar stitched uniweave, an unstitched 2-D braided fabric, a glass stitched 2-D braided fabric and a 3-D braided fabric.

3.1 Uniweave Materials

The uniweave preforms were quasi-isotropic $(0,45,90,-45)_{4s}$ lay-ups of uniweave fabric. Each layer of fabric consists of unidirectional Hercules AS4 carbon fiber tows woven together with 225 denier glass fibers. The weave fibers made up a small portion (~2%) of the weight of the fabric. The fabric was laid up into a dry preform and infiltrated with 3501-6 epoxy resin using the resin film infusion (RFI) process. The resin was cured using the manufacture's recommended cycle.

In the case of the stitched uniweave materials, the dry preforms were stitched through-the-thickness with either 1000 denier Kevlar 29 thread or 449-1500 denier S-2 glass thread. In each case a two-end, 200 denier Kevlar 29 twisted needle thread was used to make a modified lock stitch with the glass and Kevlar threads. The rows of through-the-thickness stitching were 0.48 cm. (3/16 in.). apart with a 0.32 cm. (1/8 in.) step (i.e. a stitched penetrated the preform every 0.32 cm. (1/8 in.) in the stitching direction.) The stitch rows were oriented in the zero degree direction. Stitch spacing and terminology are illustrated in Figure 3.

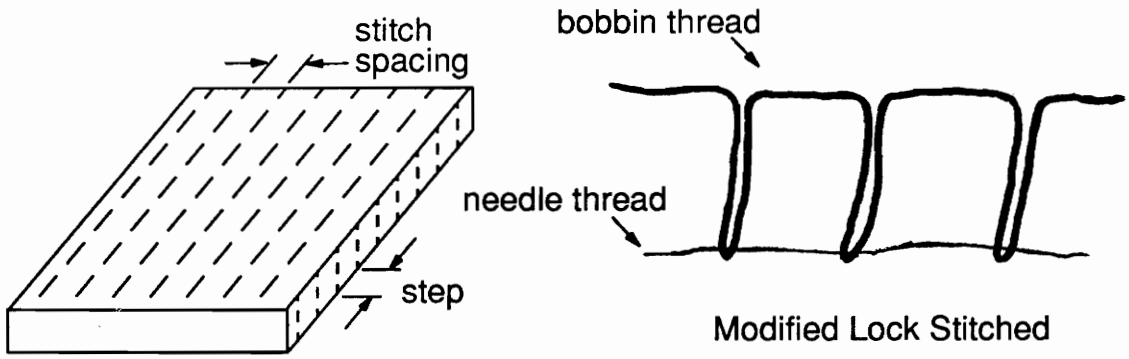

Figure 3. Stitching terminology and lock stitch diagram

The resin content from the manufacturer was reported as 33 percent by weight. The resin content was measured as 33 percent for the unstitched material, 33 percent for the glass stitched material and 36 percent for the Kevlar stitched material. The unstitched panels were 0.445-cm. thick. The glass stitched panels were 0.478 to 0.493-cm. thick and the Kevlar stitched panels were 0.457 to 0.465-cm. thick.

3.2 Braided Materials

Three braided composites were investigated. These included a 2-D braided fabric preform, a stitched 2-D braided fabric preform and a 3-D braided fabric preform.

Fiber Innovations Inc. braided the 2-D fabric preforms. Three separate bundles of Hercules AS4 fiber were braided in the +30°, -30° and 0° directions. Bundles braided in +30° and -30° directions consisted of two ends of 12K tow. The 0° bundles consisted of two ends of 12K tow and one additional end of 3K tow. The result was a braided sheet with fiber reinforcement in the +30°, -30° and 0° directions. Six of these sheets were braided at the same time using multiple passes and then resin transfer molded with British Petroleum E905L resin. To make the stitched 2-D braid, the six layers were stitched together with a glass fiber lock stitch before molding. The unstitched 2-D braided material had a fiber volume fraction of 59 percent. The thickness of both braided composites was 0.61 cm.

Atlantic Research Company braided the 3-D preforms with 12K Hercules AS4 graphite tow in each of the +30°, -30° and 0° directions. The resulting preform had equal amounts of graphite fibers in each reinforcement direction. The tows traverse the laminate thickness giving the preform through-the-thickness reinforcement. The 3-D preform was resin transfer molded with E905L resin. The resulting material had a fiber volume fraction of 53 percent and the thickness was 0.61 cm.

4.0 EXPERIMENTAL PROCEDURES

This study exposed stitched and unstitched uniweave composites and 2-D and 3-D braided textile composites to temperature and humidity environments that simulated commercial aircraft flight cycles. The uniweave materials were also exposed to cyclic temperature under constant humidity and to high temperature, high humidity environments. After environmental cycling, short-block-compression (SBC) and compression-compression fatigue tests were performed. Additional specimens were photographed to determine the extent of microcracking due to environmental cycling. In separate experiments, diffusion coefficients and maximum moisture contents were determined for the uniweave material exposed to humid environments.

The following sections detail the experimental procedures for environmental cycling, SBC testing, fatigue testing, and diffusion characterization.

4.1 Environmental Cycling

The materials were received as 30 cm. by 30 cm. panels which were C-scanned then cut up into SBC and compression-compression fatigue specimens. The specimens were labeled and weighed prior to cycling.

The specimens were placed on a wire rack inside a programmable environmental

chamber (Tenney Engineering Model T30RC). Wet/dry bulb humidity measurements and thermocouples were used to control the humidity and temperature. Circulation fans maintained uniform conditions inside the chamber. A chart recorder monitored conditions inside the chamber. Three environmental cycles were developed to determine the effects of absorbed moisture and temperature cycling on stitched textile composites.

4.1.1 Combined Temperature and Humidity Cycling

The first cycle, shown in Figure 4, varied both the temperature and humidity simultaneously. The cycle imitates the temperature and humidity extremes encountered by primary structures on commercial aircraft [65]. This cycle allows extensive moisture absorption and the low temperature portion generates thermal stress between laminae and between the stitching and surrounding composite. The cycle starts at 60°C and 95 percent relative humidity. These conditions are maintained for 45 minutes, representing conditions on the ground. The temperature was elevated from normal ambient conditions to facilitate moisture absorption. Forty-five minutes was chosen so that after 80 days of cycling the absorbed moisture had reached the center of the uniweave composites. The moisture absorption was estimated using a 1-D transient moisture absorption computer program W8GAIN2[66]. Diffusion coefficients were estimated from published values for graphite/epoxy composites. After the first 45 minutes the temperature was reduced to -55°C and the humidity to zero percent over 20 minutes. These conditions were held for 10 minutes. This portion of the cycle represents take off and high altitude conditions. Ten minutes at the cold/dry conditions allows the entire specimen to reach the cold temperature. Finally, the temperature and humidity return to 60°C over fifteen minutes.

SBC tests were performed before cycling and after 160, 480, 720 and 1280 cycles(10, 30, 45 and 80 days). The sampling frequency was chosen to highlight moisture absorption at the beginning of the cycling and the potential effects of

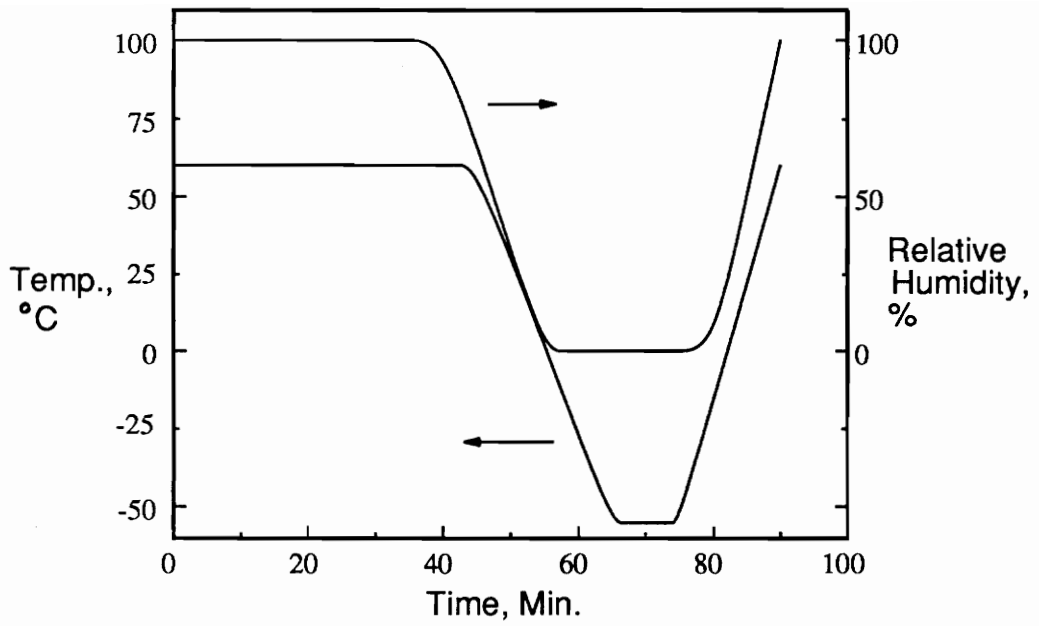

Figure 4. Environmental cycle simultaneously varying both the temperature and the humidity. The cycle imitates the ground-air-ground cycle of a commercial aircraft.

repeated temperature cycling towards the end of the cycling period. Fatigue tests were performed before environmental cycling and after 480 cycles and 1280 cycles.

4.1.2 Temperature Cycling

The second environmental cycle, shown in Figure 5, varied only the temperature while maintaining constant 40 percent relative humidity. The temperature variation was identical to the temperature variation in the first cycle (Figure 4). This cycle determines the effects of cyclic temperature at reduced moisture contents in the composites. SBC tests were performed at the same frequency as those in the temperature and humidity cycle. Fatigue tests were not performed for this environmental cycle.

4.1.3 Constant Temperature and Humidity

The final environmental cycle, shown in Figure 6, maintained constant 60°C and 95 percent relative humidity. This cycle determined the effect of absorbed moisture. SBC compression tests were performed after 4, 10, 14, 27, and 40 days. The sampling frequencies were chosen to match the moisture uptakes of the first cycle. After 40 days the remaining SBC specimens were transferred to a water bath at 70°C and allowed to reach saturation. The specimens were then tested. (Transfer to the water bath made the chamber available for the next cycle) Fatigue specimens were sampled after 40 days and after saturation.

4.2 Thermal Stress Cracking

Cycled SBC specimens were periodically removed from the environmental chamber to asses the presence and degree of thermal stress cracking around the stitching. These specimens were cut along their length to reveal a row of internal stitches as shown in Figure 7. The edge was polished and photographed under a Nikon EPIphoto light microscope to determine the degree of microcracking. One additional specimen was designated as a trailer specimen. The edge of this

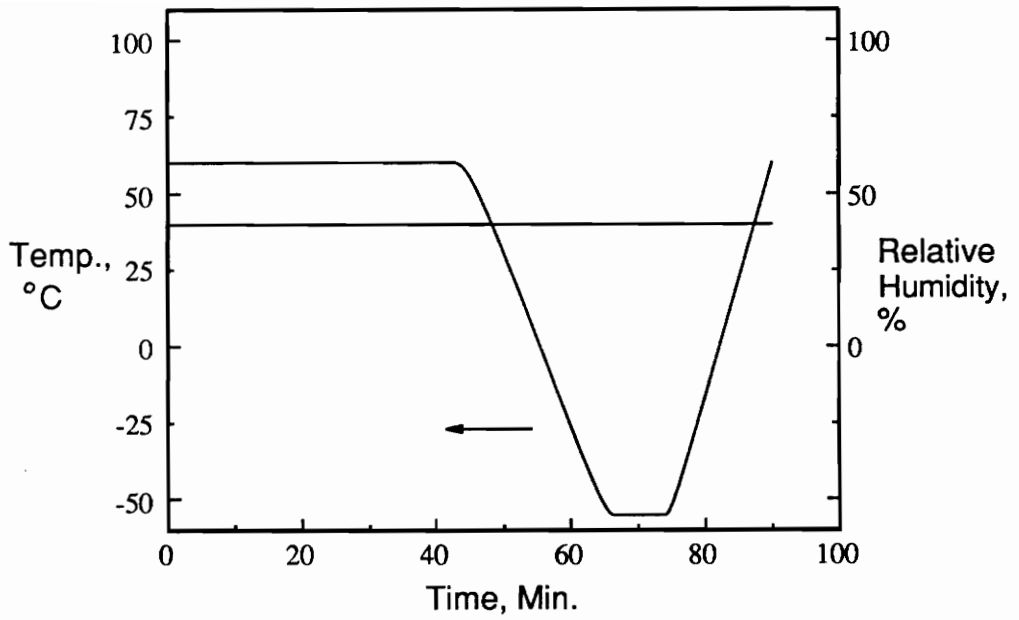

Figure 5. Environmental cycle varying only the temperature while holding constant humidity.

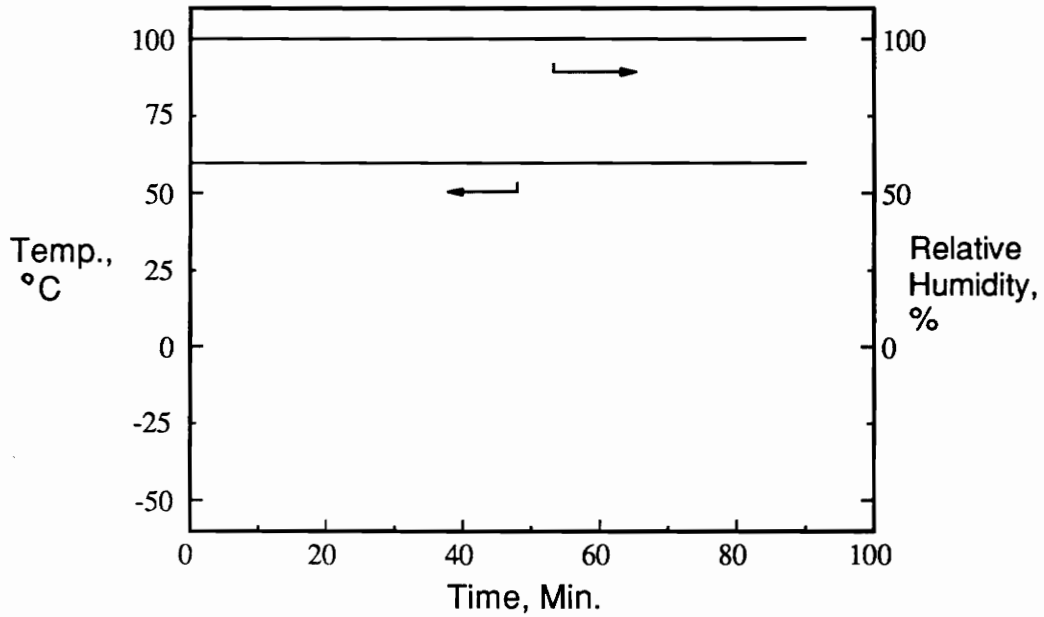

Figure 6. Constant temperature and humidity cycle.

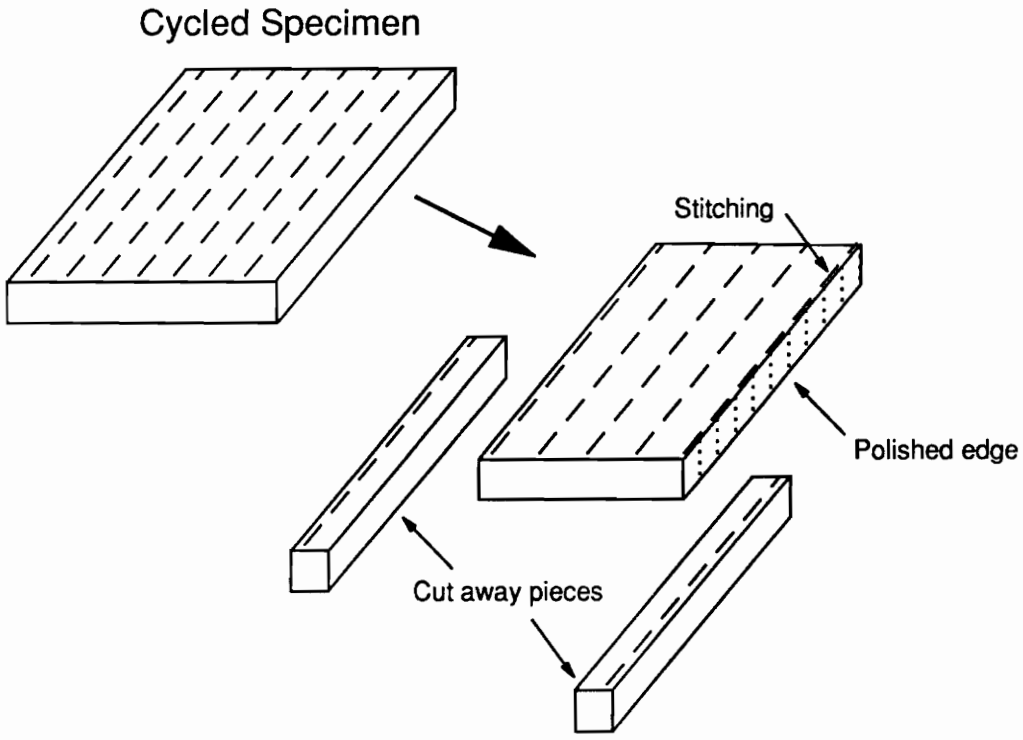

Figure 7. Sample preparation for light microscopy. Cycled specimens were machined so that a row of internal stitches were visible on the edge. This edge was polished and viewed under a light microscope to reveal cracks around the stitching.

specimen was polished so that the stitching was visible. This trailer specimen remained in the chamber and was viewed periodically to determine if the microcracks grew after extended temperature cycling.

4.3 Short-Block-Compression Test

A 120-kip hydraulic load frame was used to measure compressive properties. The platens on the load frame were adjusted parallel to each other before each round of testing. The short-block-compression fixture (Figure 8) fit between the platens. A 16-bit A/D micro computer based data acquisition system collected strain gauge and load cell data to determine the modulus, Poisson's ratio and ultimate strength of the short block specimen.

The compression specimens were 3.8 cm. wide by 4.5 cm. long. The ends of the specimens were ground flat, square to the sides and parallel to each other. The stitching followed the length of the specimen and the load was applied in the direction of the stitching.

Baseline room temperature dry (RTD) properties were determined for as-fabricated specimens with a moisture content resulting from normal laboratory exposure. Three replicates were used to measure the compression properties of both the baseline materials and the environmentally cycled materials. Upon removal from the environmental chamber, each exposed specimen was weighed and its moisture weight gain was determined. Specimens were immediately strain gaged on the front and back with Micro-Measurements CEA-06-125WT-350 strain gages as shown in Figure 9. Specimens were then gripped in the SBC fixture and the entire assembly was placed between the load frame platens. Load was applied at a displacement rate of 0.13 cm/min. Tests were conducted at room temperature at NASA Langley Research Center. Table 1 is a summary of the environmental cycles and the specimens used in the SBC tests.

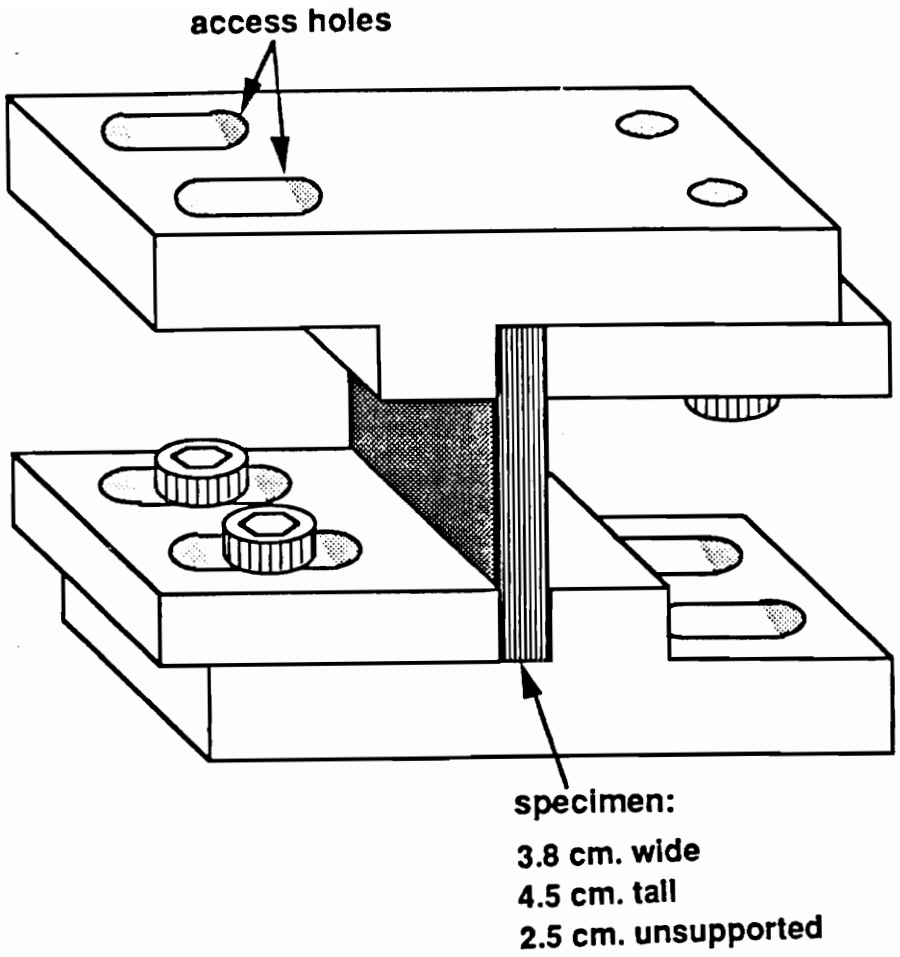

Figure 8. Short-block-Compression test fixture. The assembled fixture is compressed between the load frame platens. (from ref. [67])

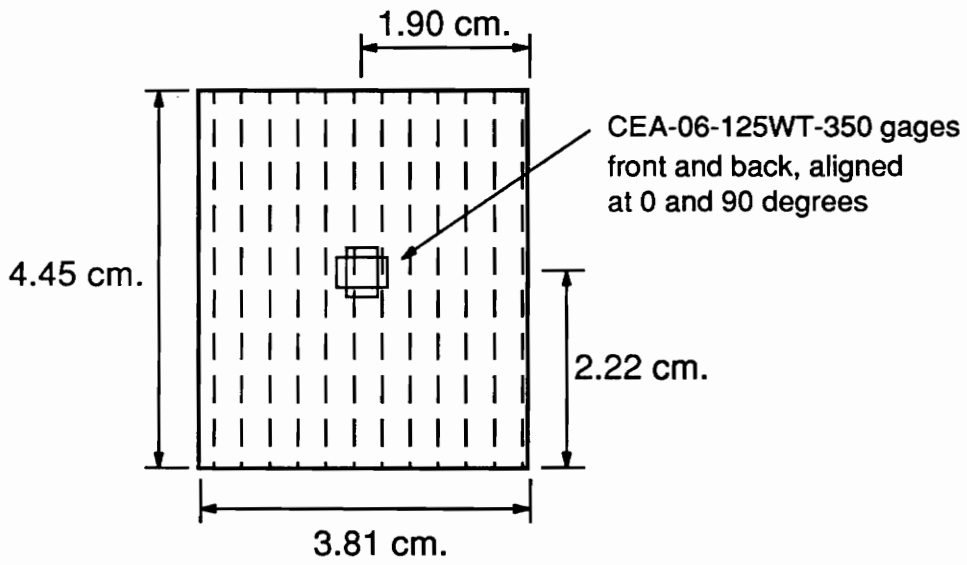

Figure 9. Dimensions and strain gage placement on short-block-compression specimens. The ends are ground flat, parallel to each other and square to the sides.

Table 1. Sampling schedule for Short-Block-Compression (SBC) and compression-compression fatigue (CCF) tests for the uniweave materials. The braided materials were only exposed to the temperature and humidity cycle.

Environmental Cycle	Test	Sampling Schedule (days)
Temperature and Humidity	SBC	0, 10, 30, 45 and 80
	CCF	0, 30 and 80
Temperature Only	SBC	0, 10, 30, 45 and 80
	CCF	no samples were taken
Constant Temperature and Humidity	SBC	4, 10, 14, 27, 40 and after saturation in 70°C water
	CCF	40 and after saturation in 70°C water

4.4 Compression-Compression Fatigue Test

Fatigue properties were determined on a 20-kip Instron model 1321 load frame using the fixture shown in Figure 10. Four alignment rods rolling on linear bearings kept the fixture in-line. The end stops were machined 0.25 mm. thinner than the specimen. Load was transferred through the ends of the specimens via the end stops. The grips held the specimen in place. The end stops and grips resulted in a 2.54 cm. gage section. Each fatigue specimen was 2.5 cm. by 10.2 cm. with the ends ground flat, square to the sides and parallel to each other. The stitching followed the length of the specimen and the load was applied in the direction of the stitching.

The specimen was first placed on the bottom end stop and secured in place with the grip plate by tightening the four bolts finger tight. The bottom of the fixture was then raised until the specimen reached the top end stop where a ~1 kN load was applied. Then the top grip plate was secured in place by tightening the bolts finger-tight. With the specimen in place, all eight bolts were alternately tightened in 8 N-m increments. The four inner bolts were tightened to 90 N-m and the four outer bolts were tightened to 55 N-m. This configuration maintained the best fixture alignment and resulted in fewer grip failures. Then the specimen was loaded to the minimum compressive load in the fatigue cycle.

The fatigue tests were run in load control at 5 Hz. using a sinusoidal loading cycle with a ratio of the maximum compressive load to the minimum compressive load of 10. A function generator (Exact model 340A) provided a sinusoidal zero to ten volt signal to the controller. The controller gain setting scaled the zero volt signal from the function generator to the minimum compressive load and scaled the 10 volt signal to the maximum compressive load.

The specimens were cycled to failure and 1 million cycles was considered a runout. The uniweave material failed suddenly and catastrophically making the

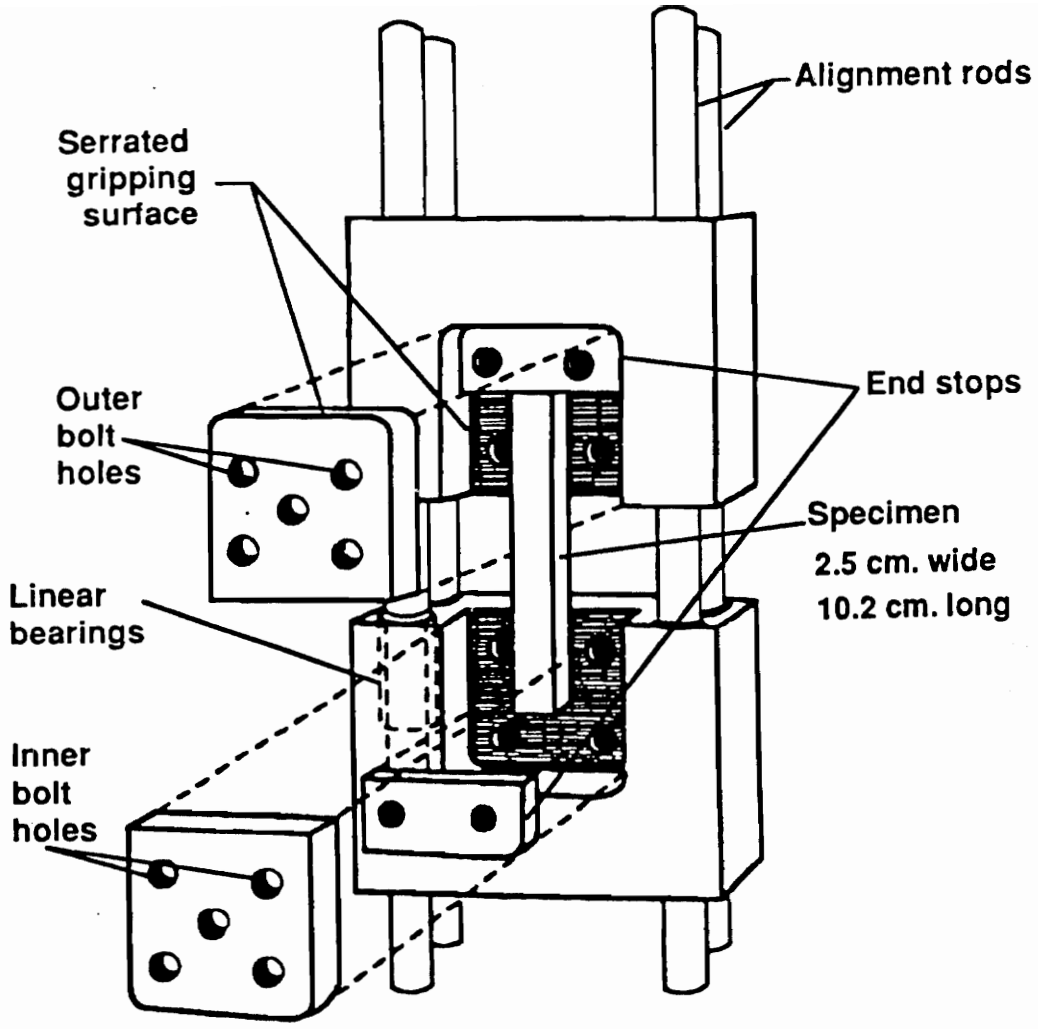

Figure 10. Compression-compression fatigue fixture. The end stops are thinner than the specimen and are used to end load the specimen. (from ref. 67)

failure criterion obvious. For the 2-D and 3-D braided materials, failure was defined as a 0.08 cm. displacement beyond the maximum displacement recorded at the start of the test. The maximum compressive load level and cycles to failure were recorded for each test.

After a predetermined number of temperature and humidity cycles (Table 1), six to eight specimens of each material were fatigue tested. After a predetermined time of exposure to constant temperature and humidity (Table 1), 12 to 16 specimens were fatigue tested.

Uniweave specimens exposed to combined temperature and humidity cycling were dried in a vacuum oven at 80°C before testing. In all of the remaining tests, the specimens were refrigerated until test time to minimize any moisture loss. During the test, a damp cloth was wrapped around these specimens in an effort to minimize moisture loss.

Fatigue damage progression in the uniweave materials was recorded using a stereo microscope (WILD model M3Z) set up to view the edge of the specimen while the specimen was loaded in the fixture. (The set up was modeled after the apparatus described in reference [68]). The specimens were prepared by grinding the edges with 600 grit sand paper. The resulting flat finish showed fatigue damage more clearly than a highly polished surface. Photographs were taken as the damage appeared at the edge of the specimen. Cycling was stopped and a compressive load was applied to open up the cracks before taking the picture. The resulting photographs were scanned and dark lines were used to enhance the cracks. For these specimens the maximum compressive fatigue load was 60 percent of their ultimate compressive strength.

4.5 Diffusion Characterization

Moisture absorption was characterized for all three uniweave materials. Diffusion

Table 2: Test temperatures and humidities for moisture diffusion characterization. Both in-plane and through-the-thickness diffusivities were measured.

Diffusivity	Glass Stitched	Kevlar Stitched	Unstitched
	Temperature/Humidity		
In-plane 0° direction (D_x)	60°C/ 75%RH		
	70°C/ 81%RH		
	80°C/ 95%RH		
In-plane 90° direction (D_y)	60°C/ 75%RH		
	70°C/ 81%RH		
	80°C/ 95%RH		
Through-the-thickness (D_z)	85°C/ 65%RH	85°C/ 65%RH	85°C/ 65%RH
	85°C/ 75%RH	85°C/ 75%RH	85°C/ 75%RH
	85°C/ 95%RH	85°C/ 95%RH	85°C/ 95%RH
	65°C/ 75%RH	65°C/ 75%RH	65°C/ 75%RH
	45°C/ 75%RH	45°C/ 75%RH	45°C/ 75%RH

coefficients and maximum moisture contents were determined at three temperatures and three humidities according the test matrix shown in Table 2. Specimens for the in-plane measurements were cut from the edges of a 64-ply quasi-isotropic glass stitched panel (Figure 11). Each specimen used to measure moisture absorption transverse to the stitching, D_y, contained one row of stitches. Each specimen used to measure moisture absorption in the stitching direction, D_x, contained single stitches spaced randomly. The edges parallel to the diffusion direction were sealed with a silicon sealant. (A 1.81 gm. sample of the sealant did not absorb a measurable amount of water after 8 days at 80°C and 95 percent relative humidity.)

The through-the-thickness specimens were cut from the Kevlar stitched, glass stitched and unstitched uniweave materials. The specimens varied in size. Specimen dimensions are discussed in the diffusion analysis section. The edges of the through-the-thickness specimens exposed to 45°C were sealed with red insulating varnish. (One of two identical specimens of unstitched uniweave material was completely coated with sealant. Then both were exposed to 60°C air at 100 percent relative humidity. After 35 days, the sealed specimen gained 0.1 percent moisture compared two the bare specimen which gained 0.6 percent moisture.) The edges of the through-the-thickness specimens exposed to 65°C and 85°C were not sealed.

Saturated salt solutions, listed in Table 3, were used to control the humidity inside constant temperature water baths. The specimens were placed in racks above the solution where they absorbed moisture from the humid air. The specimens were periodically removed from the water baths and weighed using an analytical balance (Mettler model AE 100). The test was stopped when the weight gain of the specimens leveled off.

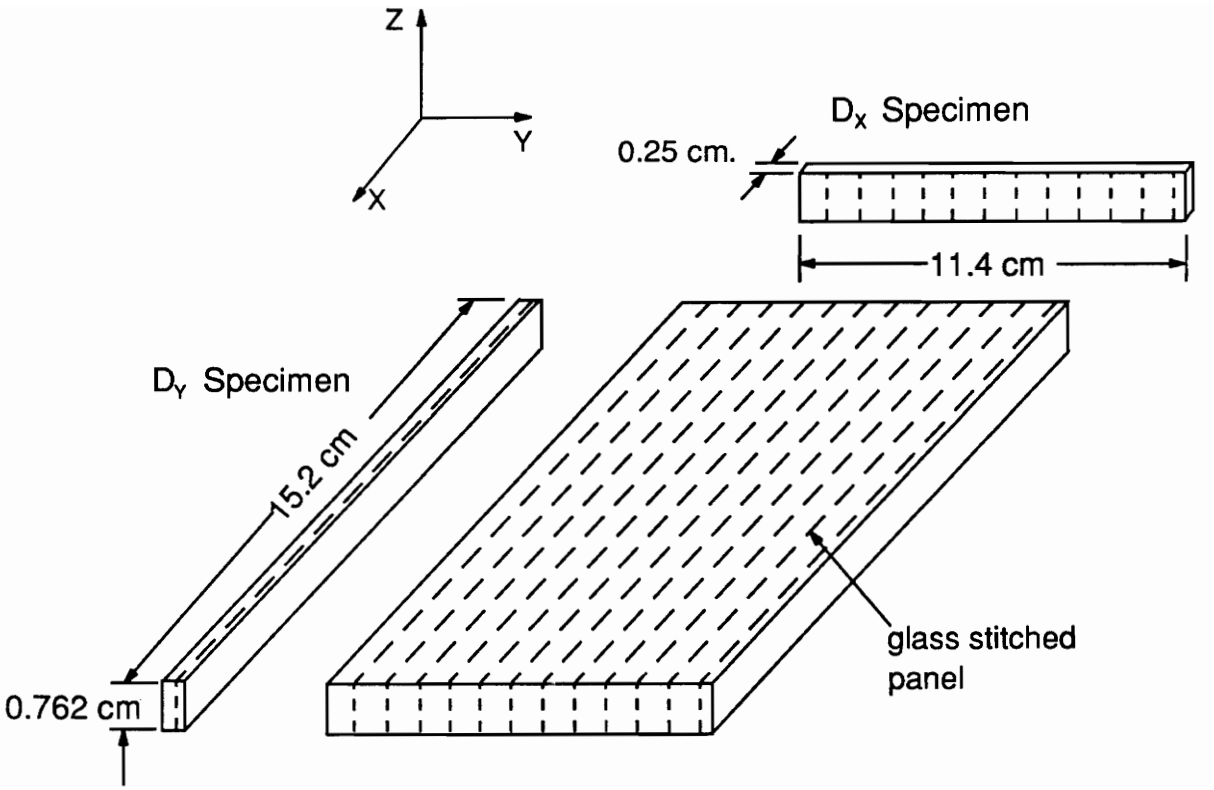

Figure 11. Sample size for in-plane diffusion measurements. Each specimen was cut from a 64-ply quasi-isotropic glass stitched panel.

Table 3. Saturated salt solutions used to maintain constant humidity conditions. The solution is in a closed temperature controlled bath. The air directly above the solution has a constant humidity.

Type of Salt	K_2SO_4	NaCl	Na_2CO_3	KNO_3
Relative Humidity (%)	95	75	81	65

5.0 DIFFUSION ANALYSIS

5.1 1-D, In-Plane Diffusion

The analysis used for the in-plane diffusion tests is the 1-D solution to Fick's Law described in the literature review (section 2.4.1). Equation (6) describes the initial straight line portion of a plot of absorbed moisture versus the square root of time. A linear least squares fit to the straight line portion of the absorption curve gives a slope which is equated with the slope of equation (6). The resulting equation is then solved for the diffusivity and the diffusivity is used to predict the moisture absorption as a function of time, equation (5).

5.2 3-D Diffusion

The specimen dimensions used for the 3-D absorption experiments are shown in Table 4. Specimens with these thicknesses require an exposure time of over six months to reach saturation. Furthermore, finding a moisture impermeable sealant that would bond to the edges of the absorption specimens for six months was considered unlikely. An effective edge sealant would permit the moisture absorption problem to be modeled as a 1-D Fickian moisture diffusion problem. Ineffective sealants and the specimen length to thickness ratios necessitated a full 3-D solution of Fick's Law.

Table 4. Dimensions for through-the-thickness moisture absorption specimens. The high thickness to length ratio necessitates a 3-D approach. The dimensions a and b correspond to the dimensions in figure 2.

Temp., (°C)	RH, (%)	Unstitched		Kevlar Stitched		Glass Stitched	
		a, (cm)	b, (cm)	a, (cm)	b, (cm)	a, (cm)	b, (cm)
85	65	7.59	1.83	8.10	1.78	8.66	2.03
	75	1.38	1.78	8.26	1.52	7.95	2.24
	95	8.92	2.01	8.10	1.78	7.90	2.03
65	75	8.13	1.70	8.79	1.70	8.64	2.06
Thickness,h		0.432		0.462		0.495	

The analysis used in the through-the-thickness absorption tests follows that of Whitney [49] and Aronhime [70]. The analysis involves approximate solutions to Fick's Law valid at short times and series solutions valid over all time. Using the notation in Figure 1 the diffusion equation for orthotropic materials is

$$\frac{\partial C}{\partial t} = D_x \frac{\partial^2 C}{\partial x^2} + D_y \frac{\partial^2 C}{\partial y^2} + D_z \frac{\partial^2 C}{\partial z^2} \qquad (11)$$

where D_x, D_y and D_z are the principal diffusivities. The in-plane diffusivities, D_x and D_y, are taken to be equal based on the quasi-isotropic lay-up. The diffusion coefficients are assumed not to be a function of moisture content. Local changes in diffusion coefficients are averaged together so that the diffusion coefficients are not functions of position.

The initial condition for the solution of equation (11) is

$$C=0 \text{ at } t=0 \text{ and } \begin{array}{r} -a/2 \le x \le a/2 \\ -b/2 \le y \le b/2 \\ -h/2 \le z \le h/2 \end{array}$$

the boundary conditions are

$$C=C_m \text{ at } \begin{array}{c} x = \pm a/2 \\ y = \pm b/2 \\ z = \pm h/2 \end{array} \text{ and } t \ge 0$$

Fick's Law is solved in one dimension giving the moisture content as a function of position and time. Carslaw [48] showed that with the above assumptions and boundary conditions, the solution to the 3-D form of Fourier's Law, and by analogy Fick's Law, is the product of the 1-D solutions.

To determine D_x and D_z, Fick's Law in one dimension is solved using the Laplace transform method which results in an infinite series of error functions [33]. For

moisture absorption in the Z-direction, the moisture concentration is

$$\frac{C}{C_m} = \sum_{n=0}^{\infty} (-1)^n erf\alpha + \sum_{n=0}^{\infty} (-1)^n erf\beta \qquad (12)$$

where

$$\alpha = \frac{(2n+1)(h/2)-z}{2(D_z t)^{1/2}} \qquad \beta = \frac{(2n+1)(h/2)+z}{2(D_z t)^{1/2}}$$

The 3-D solution [48] is then the product of the 1-D solutions for the X, Y and Z directions. Integrating this solution over the volume [33] yields

$$\frac{M(t)}{M_m} = 1 - \left(1 - \frac{4}{h}(D_z t)^{\frac{1}{2}}\left[\pi^{-\frac{1}{2}} + 2\sum_{n=1}^{\infty}(-1)^n ierfc\left[\frac{nh}{2(D_z t)^{\frac{1}{2}}}\right]\right]\right) \times \left(1 - \frac{4}{a}(D_x t)^{\frac{1}{2}}\left[\pi^{-\frac{1}{2}} + 2\sum_{n=1}^{\infty}(-1)^n ierfc\left[\frac{na}{2(D_x t)^{\frac{1}{2}}}\right]\right]\right) \times \left(1 - \frac{4}{b}(D_x t)^{\frac{1}{2}}\left[\pi^{-\frac{1}{2}} + 2\sum_{n=1}^{\infty}(-1)^n ierfc\left[\frac{nb}{2(D_x t)^{\frac{1}{2}}}\right]\right]\right) \qquad (13)$$

Using only the first two terms in equation (13) yields

$$\frac{M(t)}{M_m} = 1 - \left(1 - \frac{4}{h}\left[\frac{D_z t}{\pi}\right]^{\frac{1}{2}}\right)\left(1 - \frac{4}{a}\left[\frac{D_x t}{\pi}\right]^{\frac{1}{2}}\right)\left(1 - \frac{4}{b}\left[\frac{D_x t}{\pi}\right]^{\frac{1}{2}}\right) \qquad (14)$$

For short times, small diffusivities and thick specimens the terms in the infinite series of equation (13) are small compared to $\pi^{-\frac{1}{2}}$. Dropping the series terms results in a solution valid over short times. Expanding equation (14) yields

$$\frac{M(t)}{M_\infty} = \frac{4}{\pi^{\frac{1}{2}}}\left(\frac{D_z^{\frac{1}{2}}}{h} + D_x^{\frac{1}{2}}\left[\frac{1}{a}+\frac{1}{b}\right]\right)t^{\frac{1}{2}} - \frac{16}{\pi}\left(\frac{D_x}{ab} + D_x^{\frac{1}{2}}D_z^{\frac{1}{2}}\left[\frac{1}{ha}+\frac{1}{hb}\right]\right)t + \frac{64}{\pi^{\frac{3}{2}}}\left(\frac{D_x D_z^{\frac{1}{2}}}{abh}\right)t^{\frac{3}{2}} \qquad (15)$$

At short times, the third term in equation (15) is small in comparison to the other two and the experimental data can be fit to an equation of the form

$$\frac{M(t)}{M_\infty} = At^{\frac{1}{2}} + Bt \qquad (16)$$

The coefficients A and B are then equated with the corresponding terms in equation (15) to obtain

$$A = \frac{4}{\pi^{\frac{1}{2}}}\left(\frac{D_z^{\frac{1}{2}}}{h} + D_x^{\frac{1}{2}}\left[\frac{1}{a}+\frac{1}{b}\right]\right)$$
$$B = -\frac{16}{\pi}\left(\frac{D_x}{ab} + D_x^{\frac{1}{2}}D_z^{\frac{1}{2}}\left[\frac{1}{ha}+\frac{1}{hb}\right]\right) \qquad (17)$$

Equations (17) are solved for D_x and D_z which are then used to fit the moisture absorption data over all time. Equation (13) could be used to fit the moisture absorption data but the series solution obtained from the separation of variables technique is easier to use since it does not require evaluation of error functions. The solution obtained from separation of variables is

$$\frac{M(t)}{M_m} = 1 - \frac{512}{\pi^6} \sum_{n=0}^{\infty} \sum_{m=0}^{\infty} \sum_{k=0}^{\infty} \frac{1}{(2n+1)^2(2m+1)^2(2k+1)^2} \exp\left[-\pi^2 t \left[D_x \frac{(2n+1)^2}{a^2} + D_x \frac{(2m+1)^2}{b^2} + D_z \frac{(2k+1)^2}{h^2}\right]\right] \quad (18)$$

where the notation is described in the literature review (Figure 1).

6.0 RESULTS AND DISCUSSION

6.1 Short-Block-Compression for Uniweave Materials

6.1.1 Baseline Compression Properties

The compressive properties of the uniweave materials prior to environmental exposure are shown in Table 5 Stitching causes a decrease in ultimate static

Table 5. Baseline, room temperature compressive properties of the uniweave materials before environmental cycling. The results are the average of three specimens where ± indicates the standard deviation.

Material	Compressive Strength, MPa±MPa	Modulus, GPa±GPa
Unstitched	667±14	46.6±4.6
Glass Stitched	558±5.5	43.3±3.0
Kevlar Stitched	635±6.9	43.7±1.9

compression strength and stiffness. Compared to the unstitched material, glass stitching reduces the compressive strength 16 percent and Kevlar stitching reduces the compressive strength 5 percent.

Compared to the unstitched material, the glass stitched and Kevlar stitched materials had stiffness reductions of 7 percent and 6 percent, respectively. The standard deviations for the stiffnesses, however, suggests that each material had the same stiffness.

Previous researchers [10,15,17] have noted that stitching damages the surrounding tows. The damage may include kinked fibers on the surface [15] or broken fibers around the stitching [17]. Straight and undamaged fibers in the unstitched material are seen in Figure 12. Broken fibers and fibers displaced around the glass and Kevlar stitching are shown in Figures 13 and 14. In Figures 13 and 14, cross sections of stitch fibers are visible while the graphite fibers lie in the plane of the page. The fiber damage is greater in the glass stitched composite than in the Kevlar stitched composite since the glass stitch is bigger. Cracking around a glass stitch and irregularities in fiber architecture around both the glass and the Kevlar stitches are shown in section 6.6.1 where the entire length of the stitch is shown. Stitch induced fiber damage and microcracking around the stitching are the probable cause for reduced strength and stiffness in the stitched composites when compared to the unstitched composite.

6.1.2 Combined Temperature and Humidity Cycling

Compression properties for the uniweave materials exposed to combined temperature and humidity cycling are shown in Table 6. The strengths as a function of the number of cycles are compared in Figure 15. Compressive strength decreased in all three uniweave materials after cycling. (Zero cycles represents the baseline properties.) After 160 cycles, the compressive strength of unstitched and Kevlar stitched material decreased 6.4 and 4.8 percent, respectively. Following the initial strength reduction, the strengths continue declining but at a slower rate. After 1280 cycles, the unstitched and Kevlar stitched materials lost 10.3 and 9.6 percent of their original baseline strength, respectively. The glass stitched material lost 2.5 percent of its baseline strength after 160 cycles and remained unchanged through the remaining cycles.

As pointed out in the literature review, absorbed moisture degrades graphite/epoxy composite mechanical properties. Figure 16 shows the compressive strength

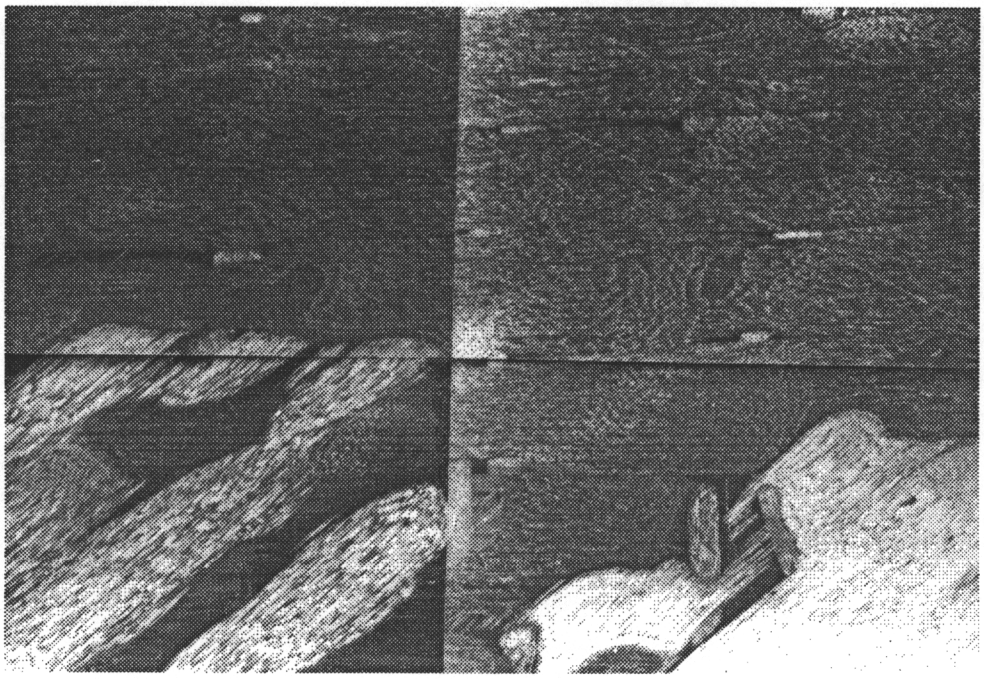

Figure 12. Plane section view of an unstitched uniweave composite showing the X-Y plane.

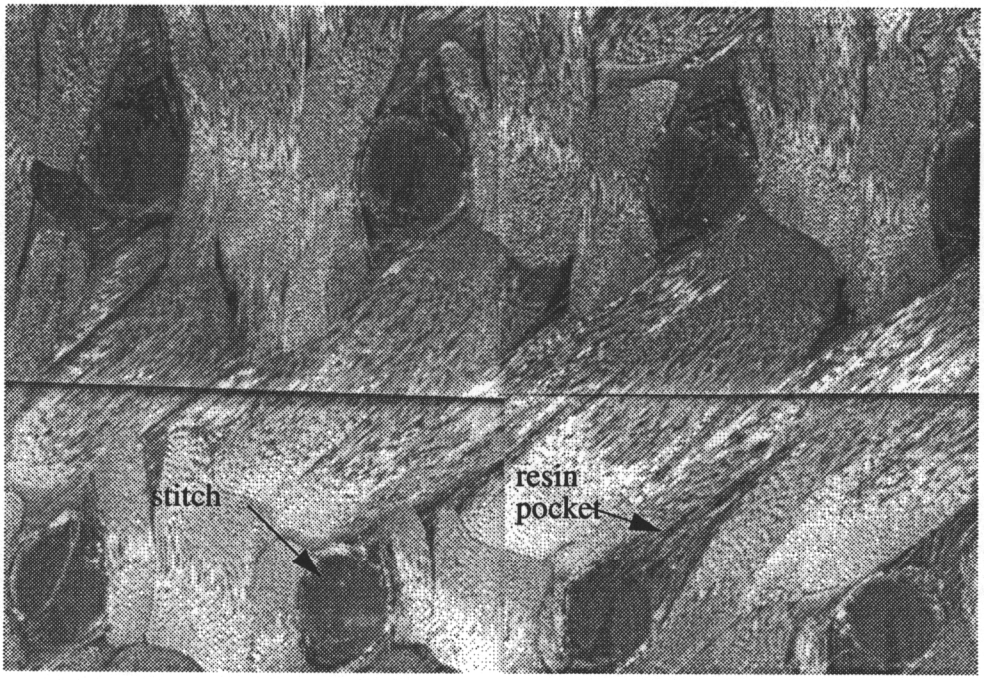

Figure 13. Plane section view of a glass stitched uniweave composite showing the X-Y plane.

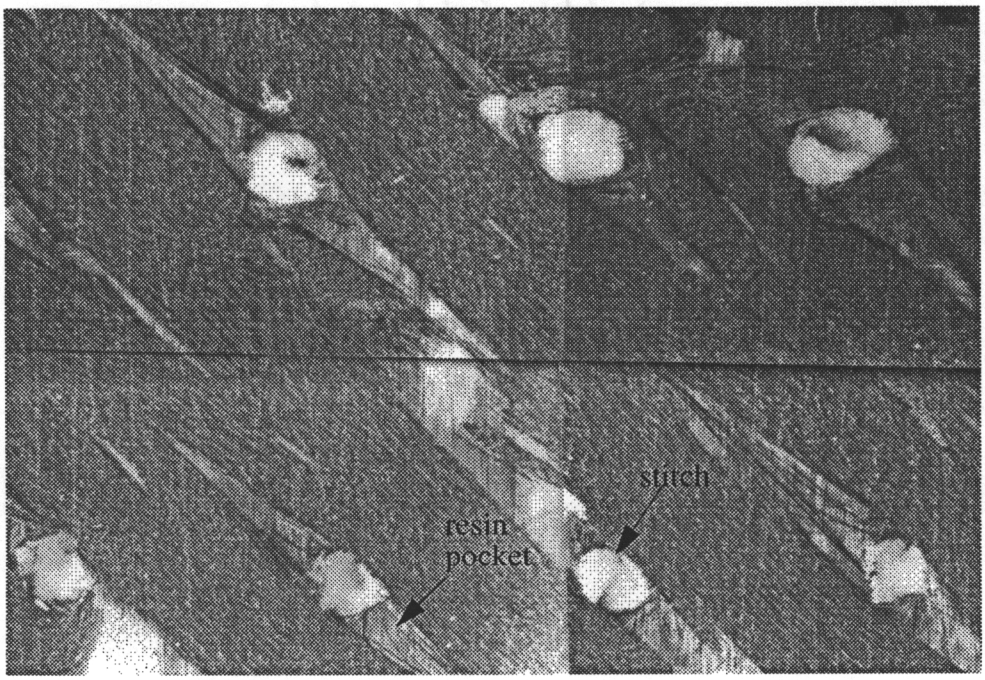

Figure 14. Plane section view a Kevlar stitched uniweave composite showing the X-Y plane.

Table 6. Short-block-compression properties of uniweave materials exposed to combined temperature and humidity cycling. The results are the average of three specimens where ± indicates the standard deviation.

Material	Environmental Cycles	Water Absorption, wt%	Compression Strength, MPa±MPa	Modulus, GPa±GPa
Unstitched	0	0.000	667±14	47.6±4.6
	160	0.169	624±10	44.7±0.62
	480	0.251	656±21	44.6±0.55
	720	0.357	609±14	44.5±0.14
	1280	0.510	598±12	44.6±0.34
Glass Stitched	0	0.000	558±5.5	43.3±3.04
	160	0.300	544±3.4	42.3±0.83
	720	0.617	546±9.6	41.6±0.90
	1280	0.783	545±5.5	39.6±0.83
Kevlar Stitched	0	0.000	635±6.9	43.7±1.9
	160	0.231	605±12	44.7±0.48
	720	0.583	581±14	43.9±1.1
	1280	0.748	574±6.9	42.3±0.76

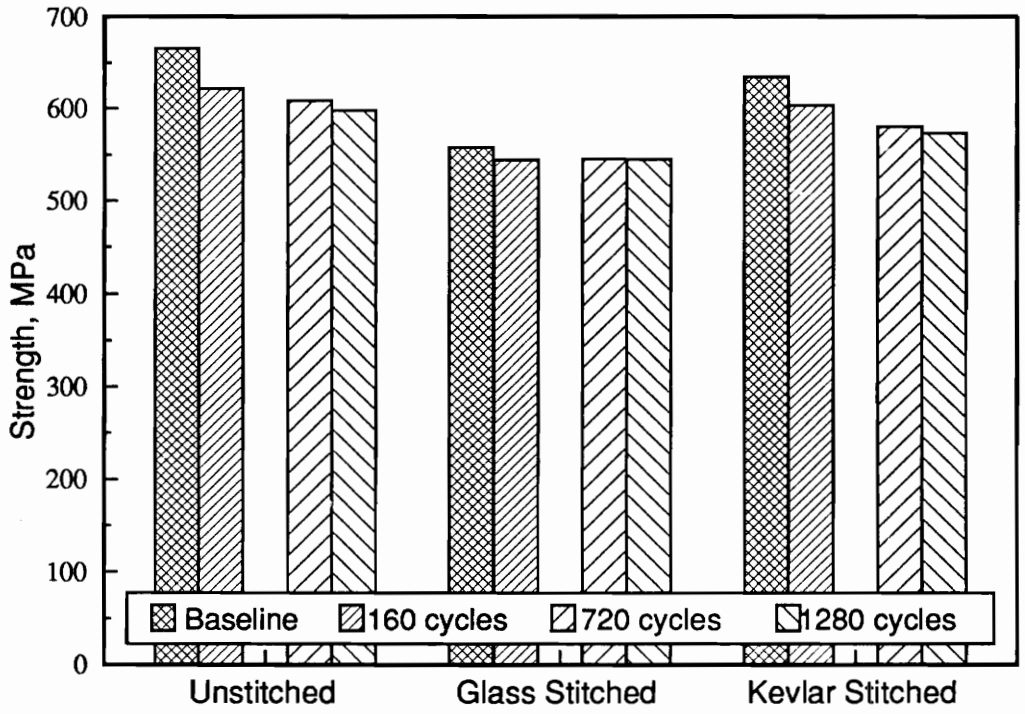

Figure 15. Short-block-compression strength of uniweave materials exposed to combined temperature and humidity cycling.

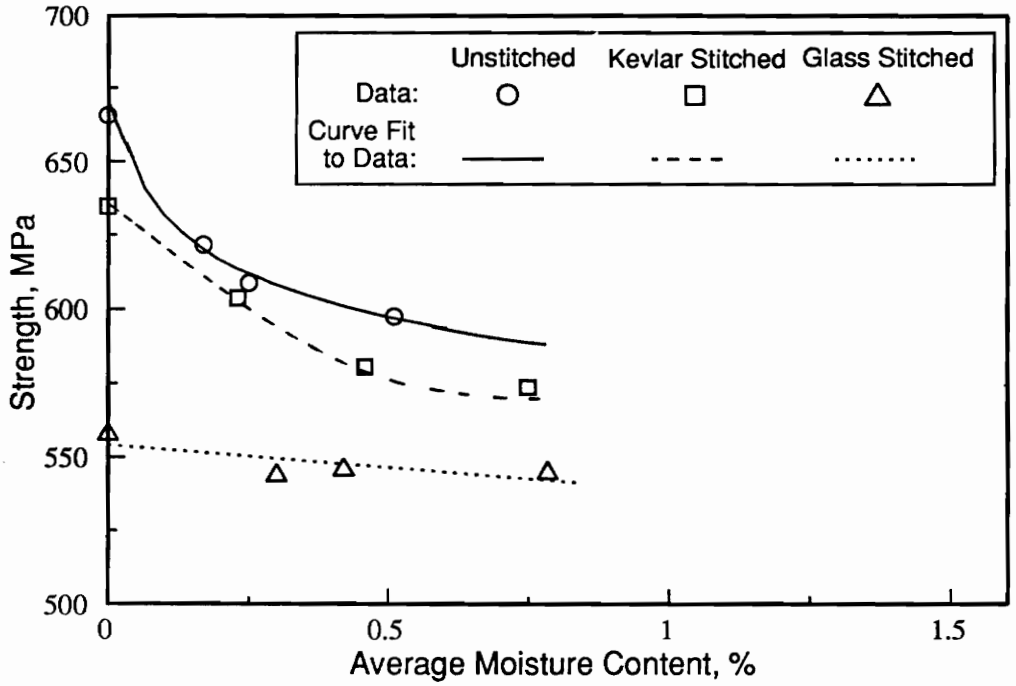

Figure 16. Short-block-compression strength as a function of moisture content during combined temperature and humidity cycling.

plotted as a function of average moisture content during the combined temperature and humidity cycle. The compressive strength of the unstitched and Kevlar stitched materials decreases with an increase in moisture absorption. The compression strength of the glass stitched material remains unchanged despite absorbed moisture. The glass stitched material developed cracks after fabrication which did not grow during cycling. These cracks may have caused a larger reduction in the compression strength of the material than absorbed moisture. Therefore, temperature and humidity cycling did not affect the compression strength of the glass stitched composites.

For all three materials, the elastic moduli remained unchanged after temperature and humidity cycling. The tests were conducted at room temperature. Testing above the glass transition temperature would be expected to cause a measurable decrease in the modulus.

6.1.3 Temperature Cycling

Compression properties for the uniweave materials exposed to temperature cycling at a constant 40 percent humidity are shown in Table 7. The strengths as a function of the number of temperature cycles are compared in Figure 17. Compressive strength decreases in the unstitched and Kevlar stitched uniweave materials after temperature cycling. (Zero cycles again represents the baseline or as received strengths. Glass stitched material was not available for this set of tests.) The unstitched material had an initial decrease of 6.3 percent after 160 cycles. The Kevlar stitched material had a initial decrease of 7.3 percent after 480 cycles. The strengths remained constant after the initial reduction.

Figure 18 shows the compressive strength plotted as a function of average moisture content during temperature cycling. After gaining 0.08 percent moisture (160 cycles), the compressive strength of the unstitched material decreases. Likewise, the compression strength of the Kevlar stitched material decreases after

Table 7. Short-block-compression properties of uniweave materials exposed to temperature cycling at constant humidity. The results are the average of three specimens where ± indicates the standard deviation.

Material	Environmental Cycles	Water Absorption, wt%	Compression Strength, MPa±Mpa	Modulus, GPa±GPa
Unstitched	0	0.000	667±14	46.6±4.6
	160	0.080	625±28	43.3±1.9
	480	0.101	618±5.5	43.1±0.28
	720	0.120	616±23	42.8±0.28
	1280	0.130	629±46	44.0±0.41
Glass Stitched	material unavailable for testing			
Kevlar Stitched	0	0.000	635±6.7	43.7±1.9
	160	0.110	630±21	42.7±1.1
	480	0.144	589±12	41.4±0.14
	720	0.176	586±24	42.8±0.28
	1280	0.200	596±9.0	42.1±0.62

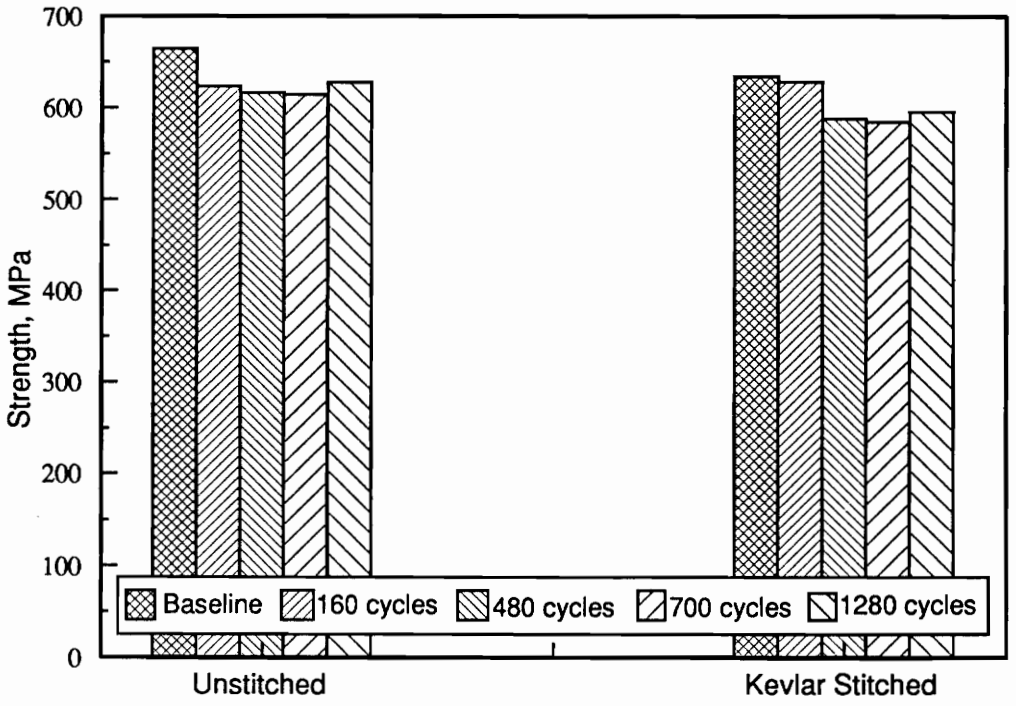

Figure 17. Short-block-compression strength of uniweave materials exposed to temperature cycling at constant humidity.

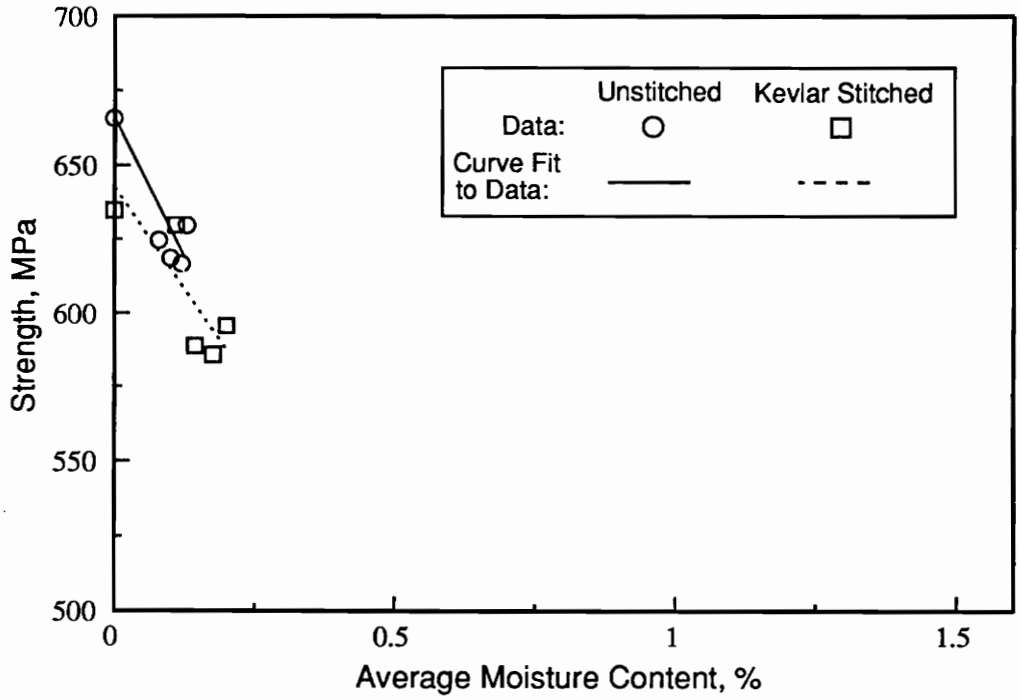

Figure 18. Short-block-compression strength of uniweave materials as a function of moisture content during temperature cycling at constant humidity

0.11 percent moisture.

6.1.4 Constant Temperature and Humidity

Compression properties for the uniweave materials exposed to constant temperature and humidity are show in Table 8. The strengths as a function of the time are compared in Figure 19. Compressive strength decreased in all three uniweave materials after exposure to the hot/wet conditions (Zero cycles represents the baseline strengths). After 4 days, the unstitched and Kevlar stitched material had initial strength decreases of 9.3 and 6.5 percent, respectively. Following the initial strength reduction, the strength remained constant through 40 days. After complete saturation (200 days), the unstitched and Kevlar stitched materials respectively lost 17.3 and 18.8 percent of their original baseline strength. The glass stitched material lost 4.3 percent of its baseline compression strength after 4 days and the strength remained constant through 40 days. The saturated glass stitched material lost 7.4 percent of the baseline strength.

The compressive strength as a function of moisture absorbed at constant temperature and humidity is shown in Figure 20. The compression strength of the unstitched and Kevlar stitched materials decreased with increasing moisture content. The compression strength of the glass stitched material also decreased with moisture content but at a slower rate than the unstitched and Kevlar stitched materials. For all three materials, the elastic moduli remained unchanged after exposure to constant temperature and humidity.

6.1.5 Overall Trends

The ultimate compressive strength of unstitched and Kevlar stitched uniweave composites decreased after exposure to elevated temperature and humidity environments. Approximately half of the strength loss occurs near 0.15 percent moisture content. The remaining strength loss occurs only after saturation in water at 1.5 percent moisture content. When testing at 25°C, moisture contents greater

Table 8. Short-block-compression properties of uniweave materials exposed to constant temperature and humidity. The results are the average of three specimens where ±indicates the standard deviation.

Material	Exposure Time, Days	Water Absorption, wt%	Compression Strength, MPa±MPa	Modulus, GPa±GPa
Unstitched	0	0.000	667±14	46.6±4.6
	4	0.164	605±26	44.7±0.62
	10	0.191	592±13	44.6±0.55
	14	0.347	618±8.3	44.5±0.14
	27	0.499	597±21	44.6±0.34
	40	0.561	612±24	44.6±0.34
	Saturated*	1.701	552±12	41.3±0.41
Glass Stitched	0	0.000	558±5.5	43.3±3.0
	4	0.305	534±10	40.6±0.28
	10	0.276	541±3.4	41.6±0.07
	14	0.554	542±19	39.7±0.55
	27	0.700	522±9.7	39.6±0.21
	40	0.725	539±8.3	43.0±1.7
	Saturated*	1.564	514±7.6	40.0±0.76
Kevlar Stitched	0	0.000	635±6.9	43.7±1.9
	4	0.246	594±5.5	43.0±0.96
	10	0.253	581±29	42.7±0.01
	14	0.476	597±12	41.8±0.69
	27	0.629	571±41	41.8±1.4
	40	0.683	576±19	43.0±1.7
	Saturated*	1.666	516±11	41.0±0.90

* After 40 days at 60°C and 95 percent relative humidity, the remaining specimens were placed in a 70°C water bath until the material was saturated.

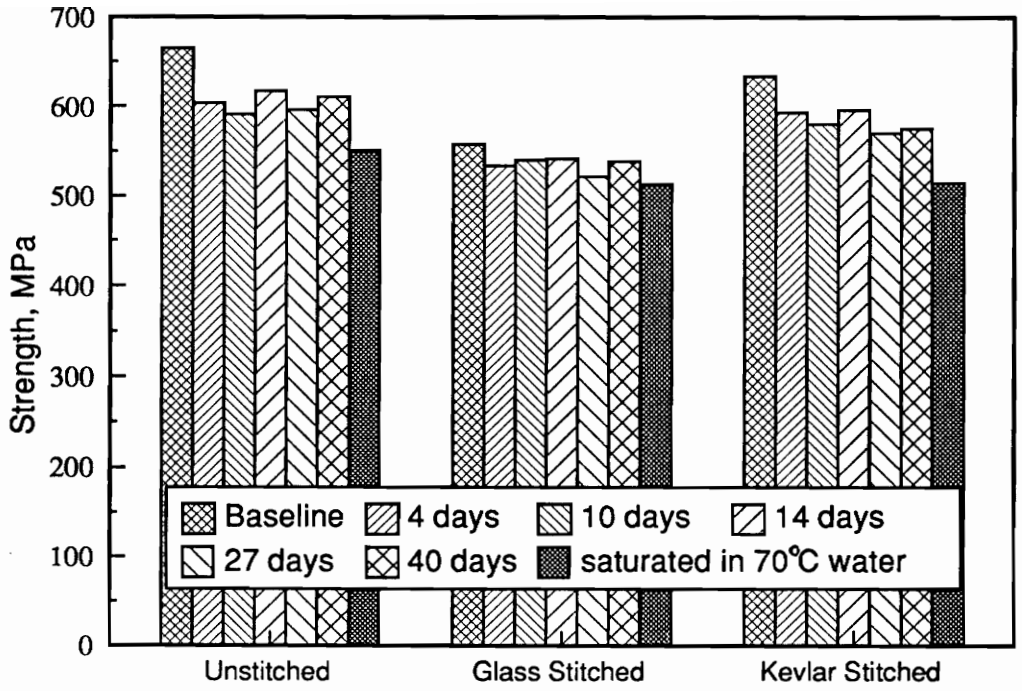

Figure 19. Short-block-compression strength of uniweave materials exposed to constant temperature(60°C) and humidity(95% RH).

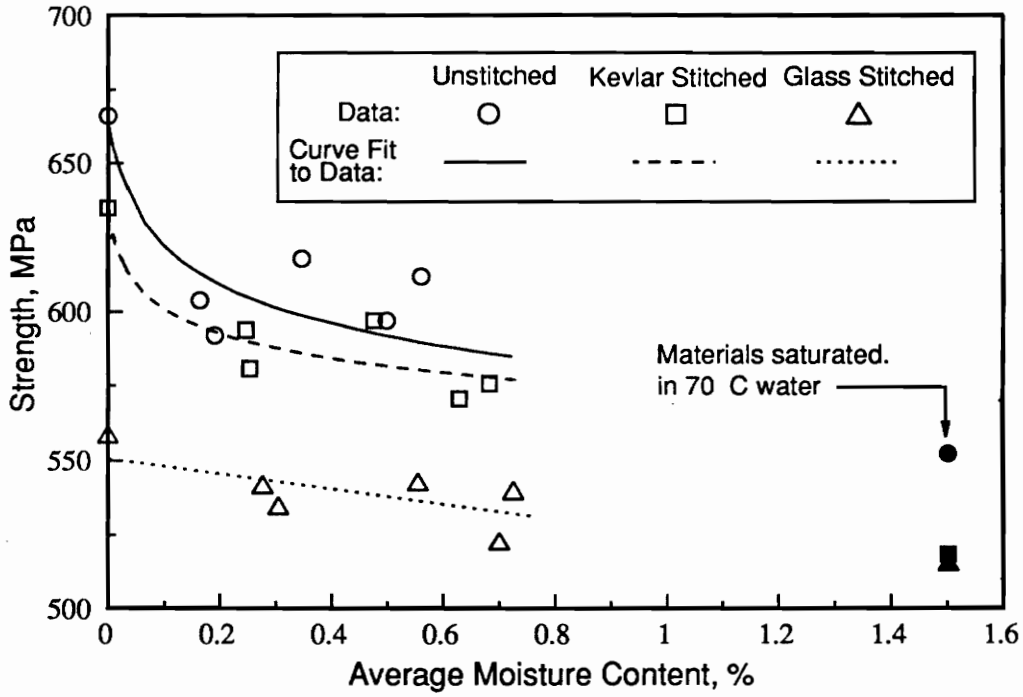

Figure 20. Short-block-compression strength as a function of moisture absorbed at constant temperature and humidity.

than 0.15 percent had comparatively little affect on compressive properties. Strength losses in both the combined temperature and humidity cycle and constant temperature and humidity cycle showed similar trends, therefor, the strength losses were attributed primarily to absorbed moisture. Furthermore, temperature cycling at constant humidity did not result in additional strength loss after the materials gained 0.1 percent moisture which implies that temperature cycling did not have a measurable effect on the material.

6.2 Short-Block-Compression for Braided Materials

6.2.1 Temperature and Humidity Cycling

The compression properties of the AS4/E905L braided materials are presented in Table 9 and Figure 21. In Figure 21, the baseline compression strengths from reference [69] are compared to the compression strengths obtained from specimens exposed to combined temperature and humidity cycling (Figure 4). The glass stitching in the 2-D braid results in a 5 percent strength reduction compared to the unstitched 2-D braid. The stitched 2-D braided material lost 8.3 percent of its baseline compression strength after 1280 temperature and humidity cycles. Temperature and humidity cycling did not affect the unstitched 2-D and 3-D braids. The slight increase in the strength of the 3-D braid may have resulted from the baseline strength being taking from the results of a separate investigation. These results are not surprising since the moisture absorption of the AS4/E905L material was significantly lower than that for the AS4/3501-6 uniweave materials.

Like the uniweave materials, temperature and humidity cycling did not affect the moduli of the braided material. The moduli of the braided materials are essentially the same within the scatter of the data. Furthermore, the braided tows are approximately ⅛" wide which is the width of the strain gage used to obtain the stiffness. Therefore, the strain gage measures local strains near the braids. The local strains will vary considerably over the specimen surface resulting in the high data scatter.

Table 9. Short-block-compression properties of AS4/E905L braided materials exposed to combined temperature and humidity cycling. The results are the average of three specimens where ± indicates the standard deviation.

Material	Environmental Cycles	Water Absorption, wt%	Compression Strength, MPa±MPa	Modulus, GPa±GPa
Unstitched 2-D Braid	0	0.000	404±6.7	*****
	160	0.091	386±4.8	58±3.4
	720	0.122	404±8.3	61±4.8
	1280	0.100	400±15	57±3.4
Stitched 2-D Braid	0	0.000	383±16	57±2.8
	160	0.158	346±13	54±6.9
	720	0.175	359±9.0	61±5.5
	1280	0.143	351±2.9	51±4.1
3-D Braid	0	0.000	447±13	50±4.1
	160	0.097	465±40	68±6.9
	720	0.176	483±10	60±2.1
	1280	0.206	472±10	60±4.8

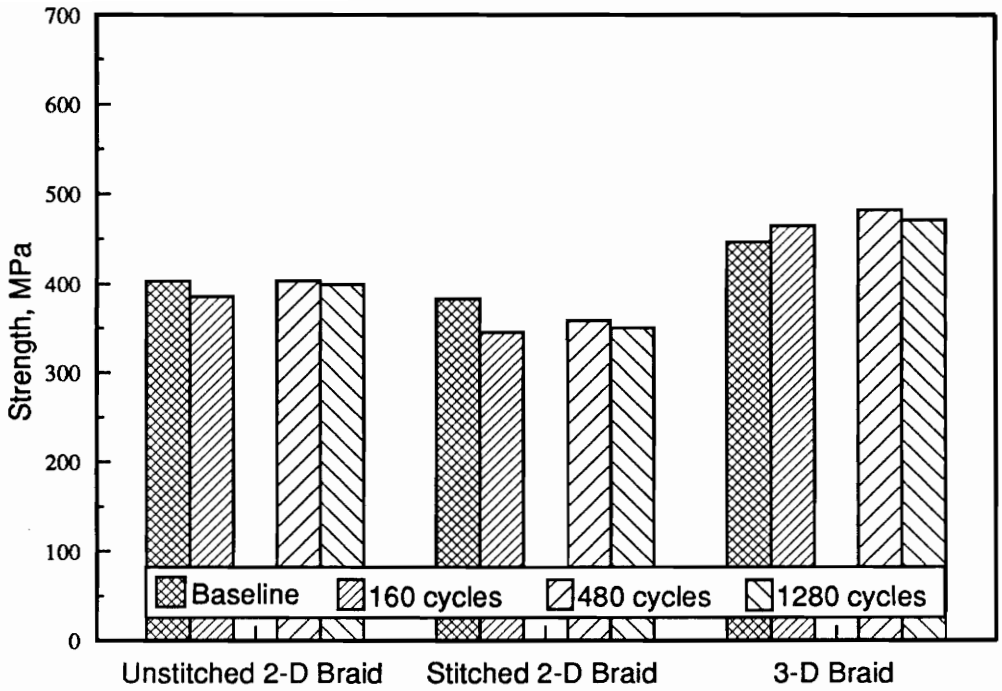

Figure 21. Short-block-compression strength of braided materials exposed to combined temperature and humidity cycling.

6.3 Compression-Compression Fatigue for Uniweave Materials

6.3.1 Baseline Fatigue Properties

The baseline fatigue properties of the uniweave materials are shown in Figure 22. Logarithmic regression S-N curves represent trends in the fatigue data. The SBC strength of each material is plotted at one cycle on the S-N curve. The curves are least squares regression fits of all the data points for each material excluding the SBC strength and the runouts. The fatigue sensitivity or the slope of the S-N curve was nearly the same for each material. The run-out strength was defined as the maximum compressive load reaching one million fatigue cycles. For the uniweave materials the run-out strength was approximately 50 percent of the ultimate baseline compressive strength. Comparing the fatigue results of the unstitched and stitched material shows that Kevlar stitching does not adversely affect the fatigue performance. The glass stitched material has lower fatigue strength than either the Kevlar stitched or the unstitched material. The lower fatigue strength in the glass stitched material may result from crack growth initiating from pre-existing, processing induced cracks found around the stitching.

6.3.2 Combined Temperature and Humidity Cycling

The fatigue properties of uniweave specimens exposed to combined temperature and humidity cycling are shown in Figures 23 through 25. The solid curves in each figure are least squares regression fits to all of the data points excluding run-outs and the SBC strength which is plotted at one cycle. As shown in Figure 23, temperature and humidity cycling did not measurably influence fatigue properties of the unstitched laminates. Run-out strength and fatigue sensitivity remained unchanged. The glass stitched material similarly appeared unaffected by temperature and humidity cycling (Figure 24). Likewise, in Figure 25, temperature and humidity cycling did not affect the Kevlar stitched material. Recall, the test specimens were dried to their original weights before testing.

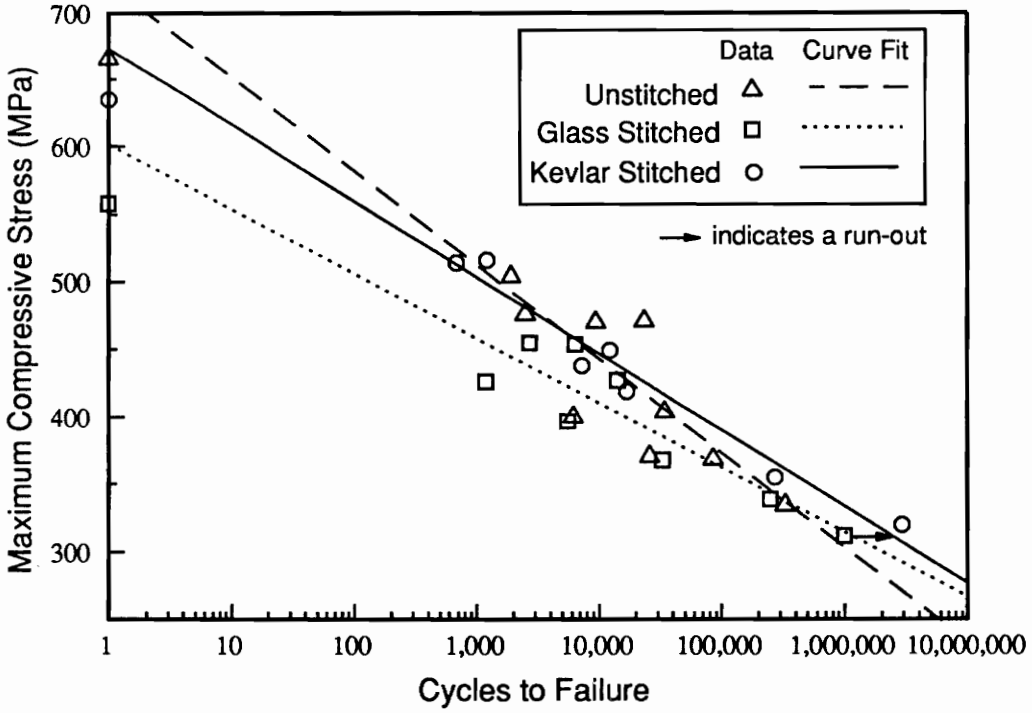

Figure 22. Baseline S-N curves for uniweave materials.

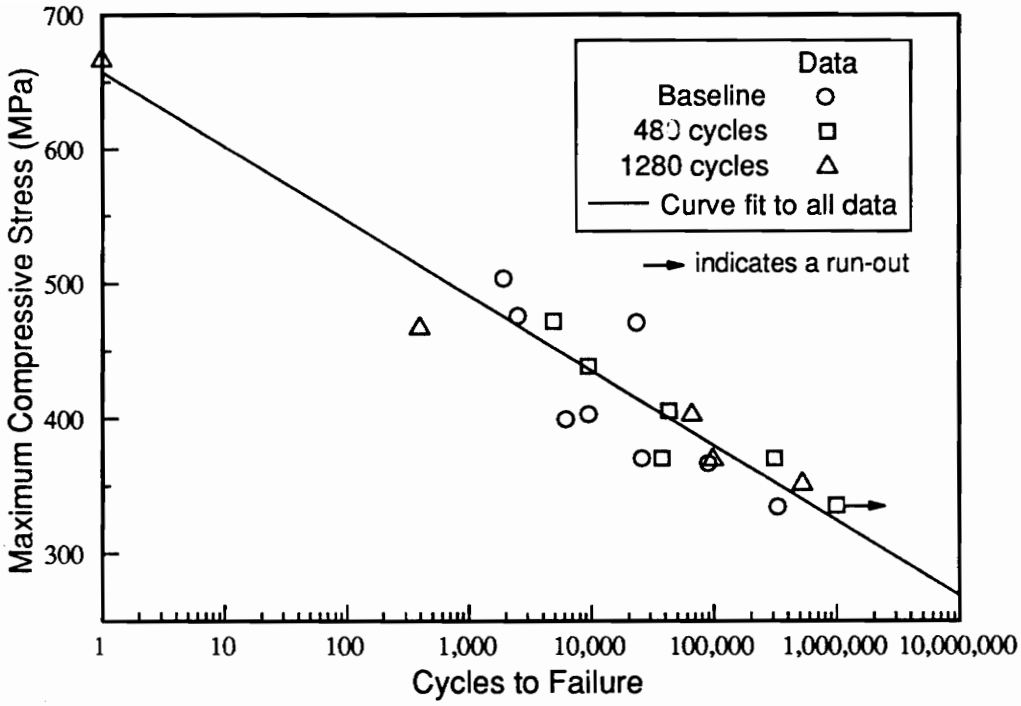

Figure 23. S-N curve for the unstitched uniweave material exposed to combined temperature and humidity cycling.

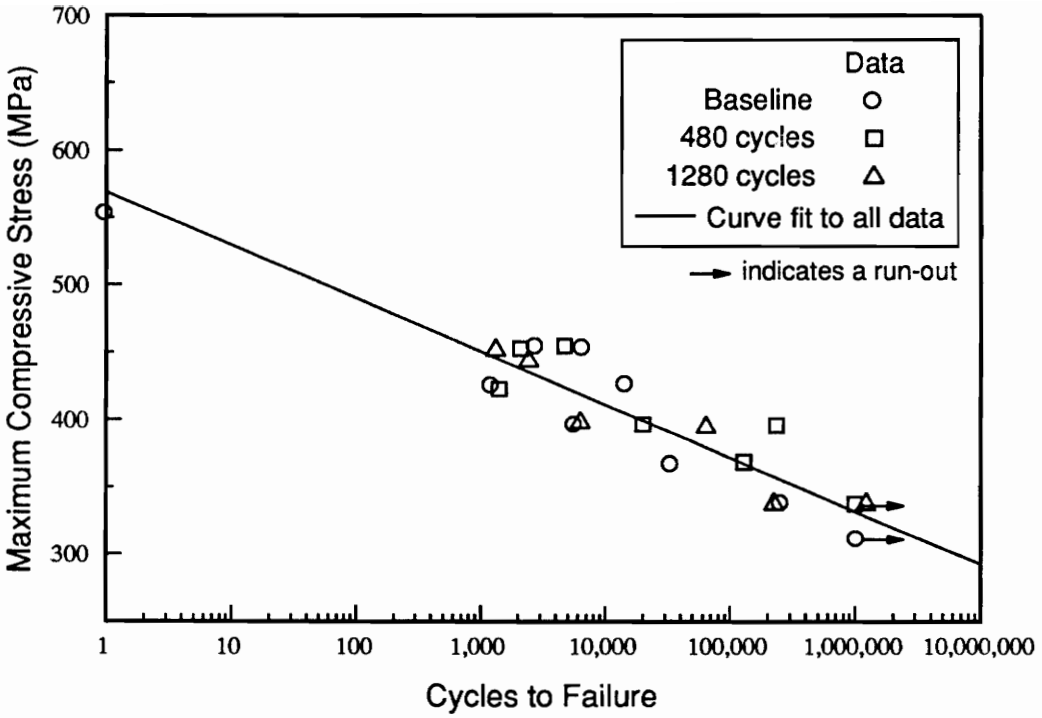

Figure 24. S-N curve for the glass stitched uniweave material exposed to combined temperature and humidity cycling.

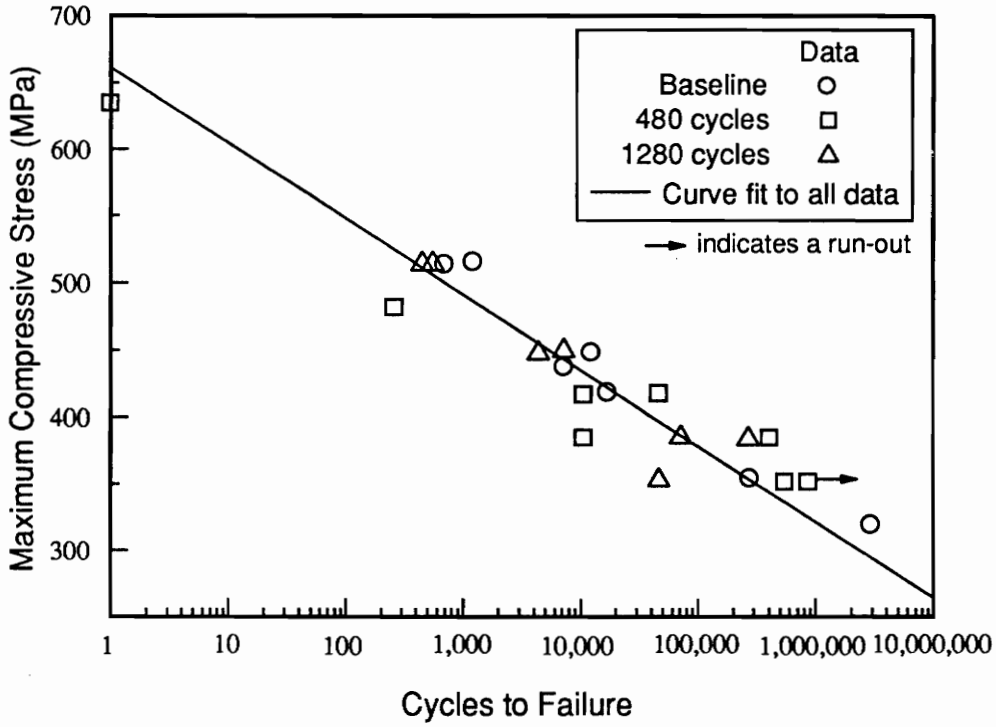

Figure 25. S-N curve for the Kevlar stitched uniweave material exposed to combined temperature and humidity cycling.

6.3.3 Constant Temperature and Humidity

Since the combined temperature and humidity cycle had no effect on the fatigue properties of uniweave specimens that were dried to their original weight before testing, the specimens exposed to constant temperature and humidity were tested while they still contained absorbed moisture. The fatigue properties of the uniweave materials exposed to constant temperature (60°C) and humidity (95 percent) are show in Figures 26 through 28. The solid curves in each figure are least squares regression fits to each set of data points excluding runouts and the SBC strength which is plotted at one cycle. The constant temperature and humidity environment does not significantly affect the fatigue properties of the unstitched material until the material is saturated (Figure 26). Based on the trends in the data, the baseline runout strength decreased from ~325 MPa to ~275 MPa for the saturated unstitched material. Data scatter between the baseline and 40 day results preclude any specific conclusion regarding the fatigue sensitivity. The S-N curves for the glass stitched material exposed to the constant temperature and humidity environment are shown in Figure 27. The trend in the data suggest that absorbed moisture reduces the baseline run-out strength of the glass stitched material from ~325 MPa to ~300 MPa. The fatigue sensitivity for the glass stitched material remains unchanged. The fatigue results for the Kevlar stitched material exposed the constant temperature and humidity environment are shown in Figure 28. The fatigue sensitivity decreases while the run-out strength remains unchanged.

6.4 Compression-Compression Fatigue for Braided Materials

6.4.1 Combined Temperature and Humidity Cycling

The fatigue properties of the environmentally cycled braided specimens are compared to the baseline fatigue properties in Figures 29 through 31. The lines in each figure are least squares regression fits to the fatigue data obtained at each level of environmental cycling. Run-outs and SBC strengths are excluded from the regression fit. Combined temperature and humidity cycling did not measurably

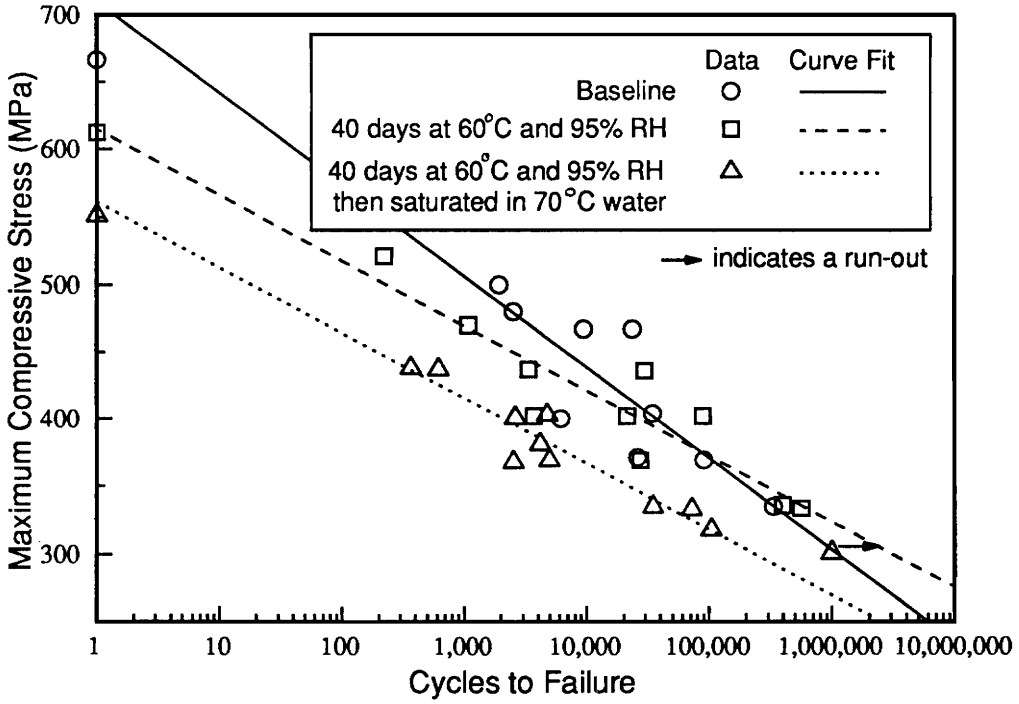

Figure 26. S-N curves for the unstitched uniweave materials exposed to constant temperature and humidity.

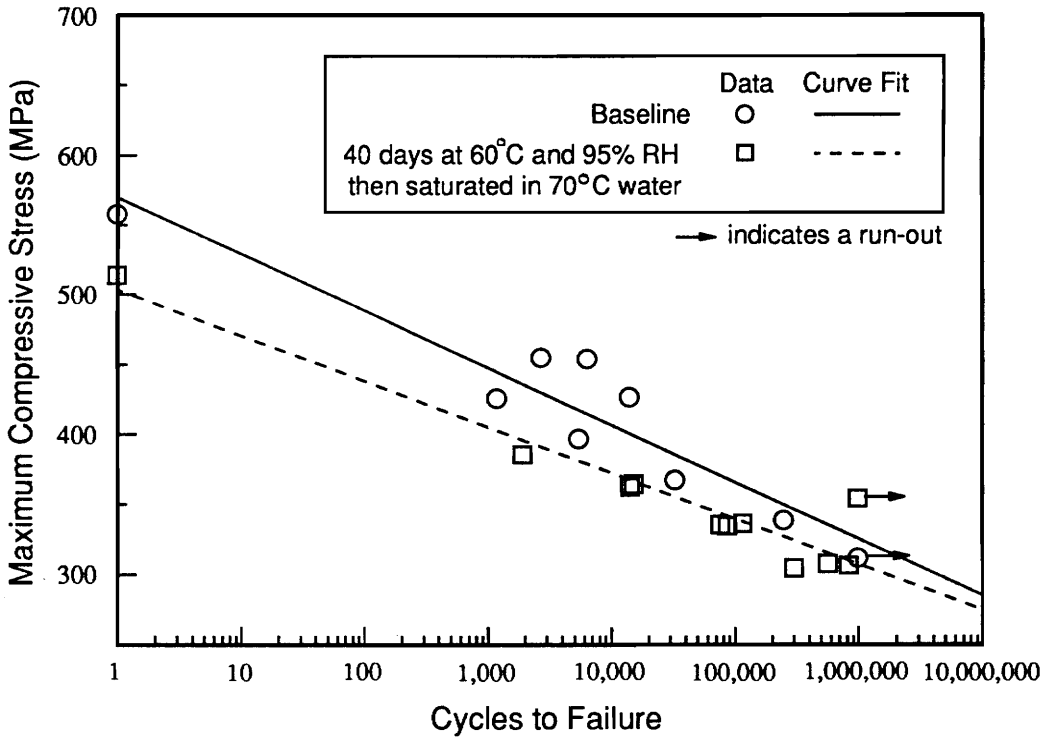

Figure 27. S-N curves for the glass stitched uniweave materials exposed to constant temperature and humidity.

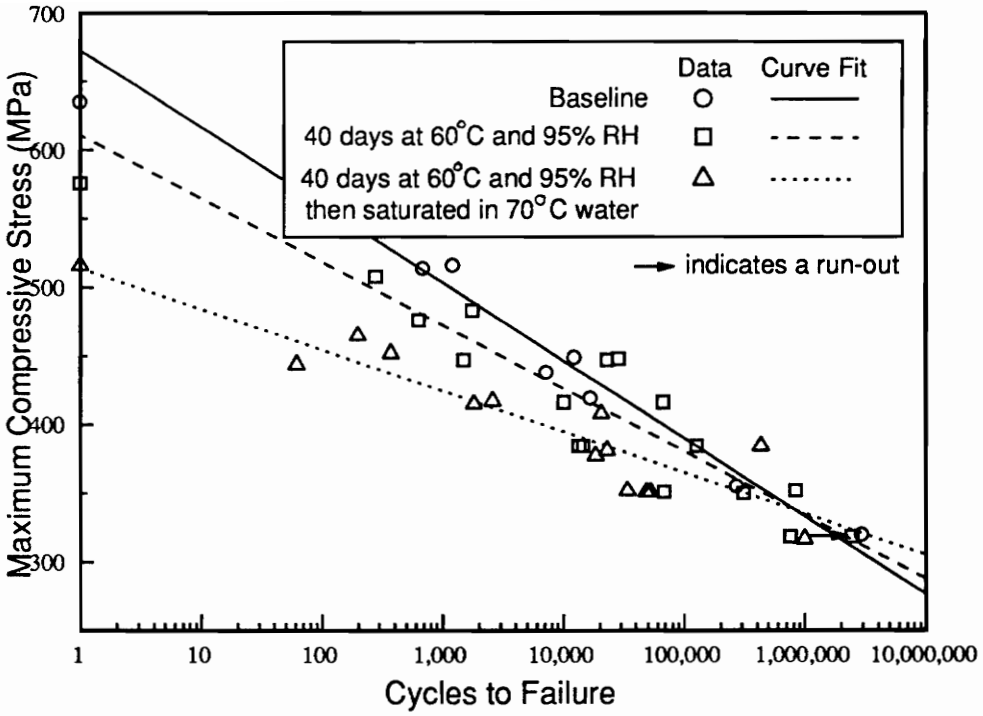

Figure 28. S-N curves for the Kevlar stitched uniweave materials exposed to constant temperature and humidity.

influence fatigue properties of the unstitched 2-D braid (Figure 29). Run-out strength and fatigue sensitivity remained unchanged. The stitched 2-D braid (Figure 30) similarly appeared unaffected by combined temperature and humidity cycling. Likewise, combined temperature and humidity cycling did not significantly affect the fatigue properties of the 3-D braid (Figure 31). For each material, the run-out strength was 50 to 60 percent of the ultimate compressive strength. Recall, the absorbed moisture remained in the specimens during testing.

6.5 Fatigue Damage Progression and Failure Surfaces

6.5.1 Uniweave Materials

Photographs of edge damage development were taken with the specimen mounted in the grips. The maximum compressive fatigue load for this set of tests was 60 percent of the short-block-compression strength. Fatigue damage in the uniweave materials initiates at the edge of the specimens and propagates to the interior before ultimate failure occurs [17]. Damage progression and the failure surfaces did not change with environmental exposure or with maximum fatigue load levels below 65 percent of ultimate compression strength which was the highest level tested. Damage progression and failure surfaces varied considerably between stitched and unstitched materials.

In the unstitched uniweave material, fatigue damage initiates with complete delamination of the top 0° layer as shown in Figure 32. After the top layer delaminates, a delamination crack appears in the second 0° layer. The crack quickly propagates along the length of the specimen. The crack may propagate into the 45° layers by following matrix pockets between tows. Shortly after the second 0° layer has cracked along the entire gage length, the specimen fails by delamination. Prior to failure, no cracks appear below the second 0° layer. (In Figures 32 to 34 the cracks are enhanced with darker lines drawn over the scanned image.)

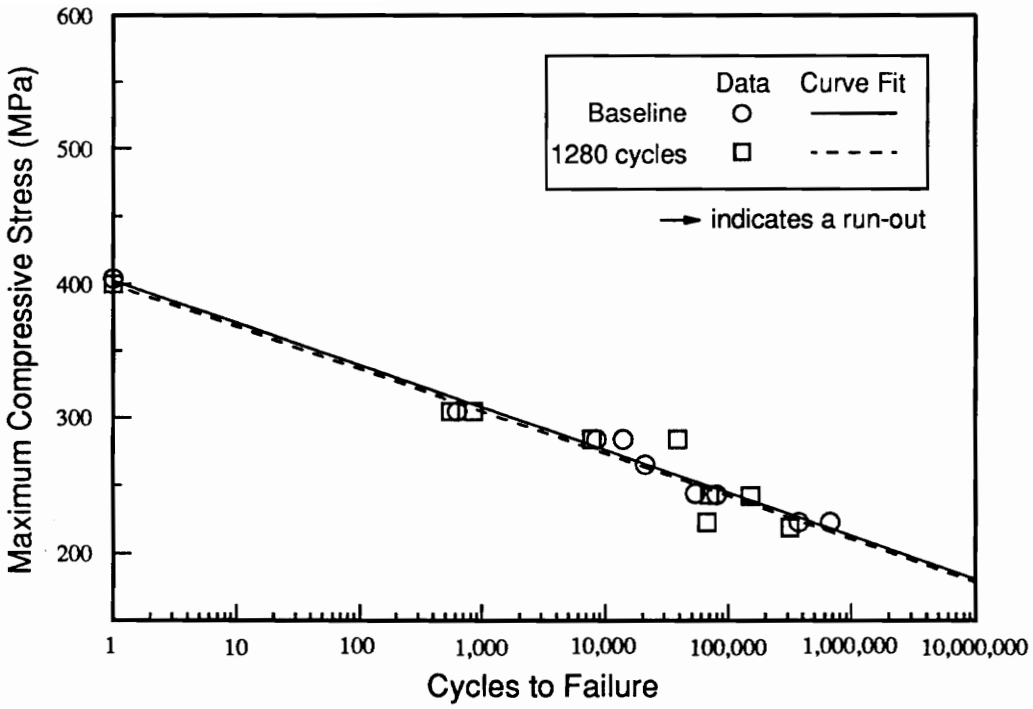

Figure 29. S-N curves for unstitched 2-D braids exposed to the combined temperature and humidity cycling.

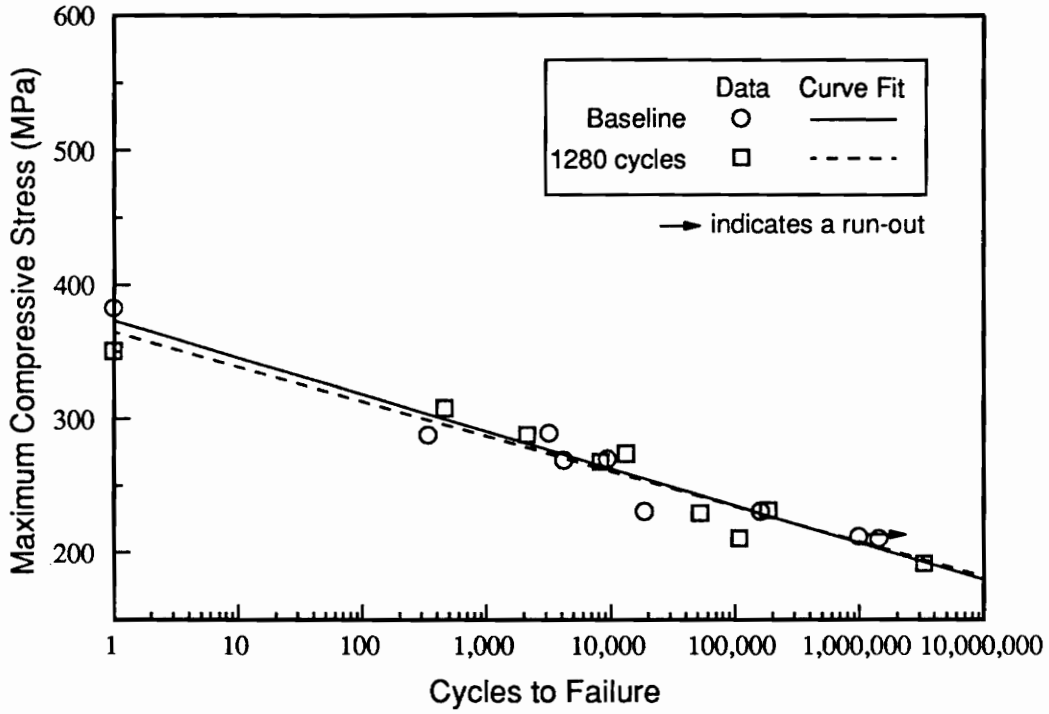

Figure 30. S-N curves for stitched 2-D braids exposed to combined temperature and humidity cycling.

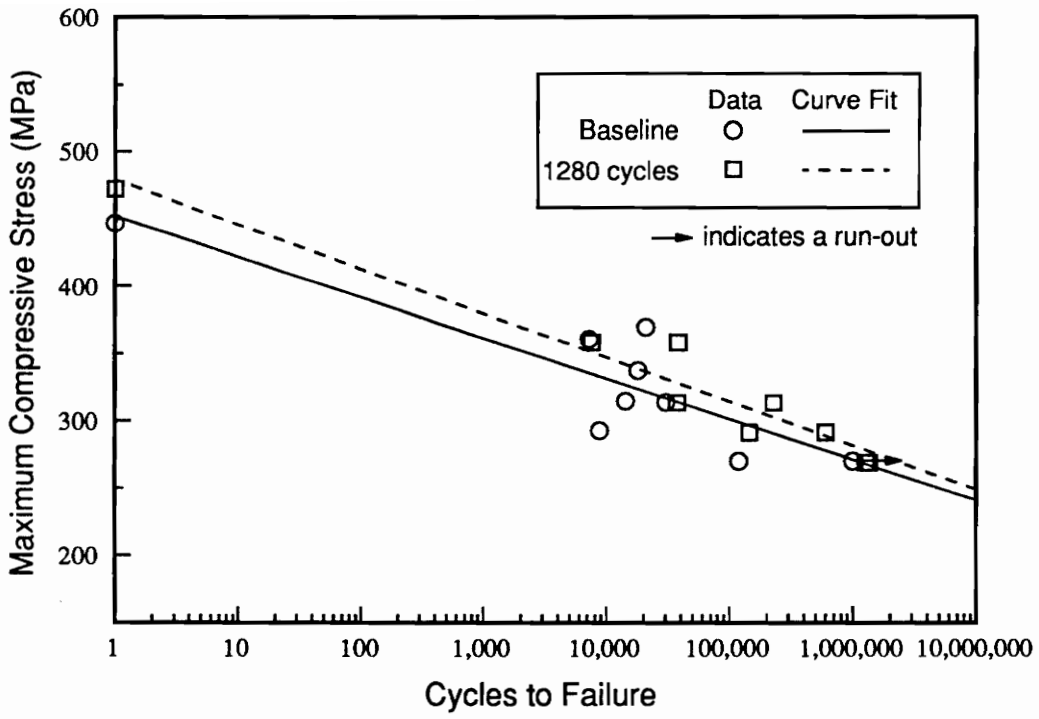

Figure 31. S-N curves for 3-D braids exposed to combined temperature and humidity cycling.

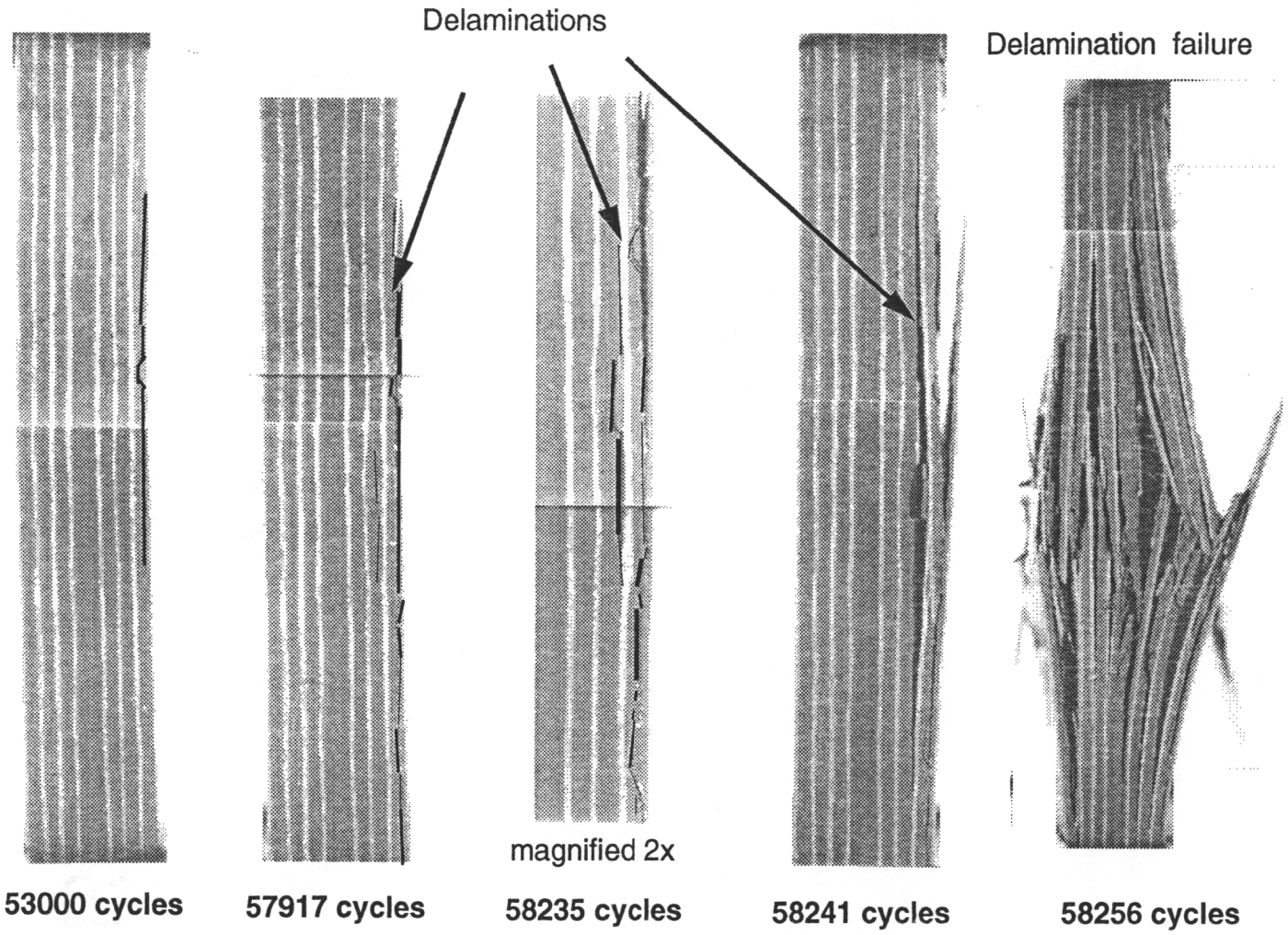

Figure 32. Fatigue damage development and delamination failure in an unstitched uniweave material.

In the glass stitched uniweave material, the top 0° layer opposite of the needle thread delaminates first (Figure 33). The needle thread is not visible in the picture. The delamination propagates over the entire gage length. After the first delamination, cracks appear in the lower 0° layers. These subsequent cracks are confined to the area around the stitching. They do ultimately propagate along the length but at a slower pace than in the unstitched material. Once cracks appear throughout the thickness, the specimen fails in a diagonal, shear mode type failure. The Kevlar stitched material, shows behavior similar to the glass stitched material (Figure 34).

6.6 Microcracking

6.6.1 Uniweave Materials

Photomicrographs of each of the three uniweave materials are presented in Figures 35 through 37. For each material type, a representative photomicrograph is presented for an uncycled specimen and a specimen after 1280 combined temperature and humidity cycles. The unstitched material, Figure 35, did not show any microcracks in the uncycled specimens. Microcracking between some of the outer plies did develop after temperature and humidity cycling. Only one side of the composite showed signs of microcraking, indicating the possibility of uneven temperature distributions inside the chamber.

As shown in Figure 36, the glass stitched material had significant microcracking around each individual stitch. These microcracks did not appear to grow with temperature and humidity cycling as evident in the photomicrograph of the glass stitched specimen after 1280 cycles. The microcracks in the specimen with 1280 combined temperature and humidity cycles appear to be similar in severity to the uncycled specimen.

The Kevlar stitched material, Figure 37, also showed microcracking around the stitching but not to the degree that the glass stitched material microcracked. As

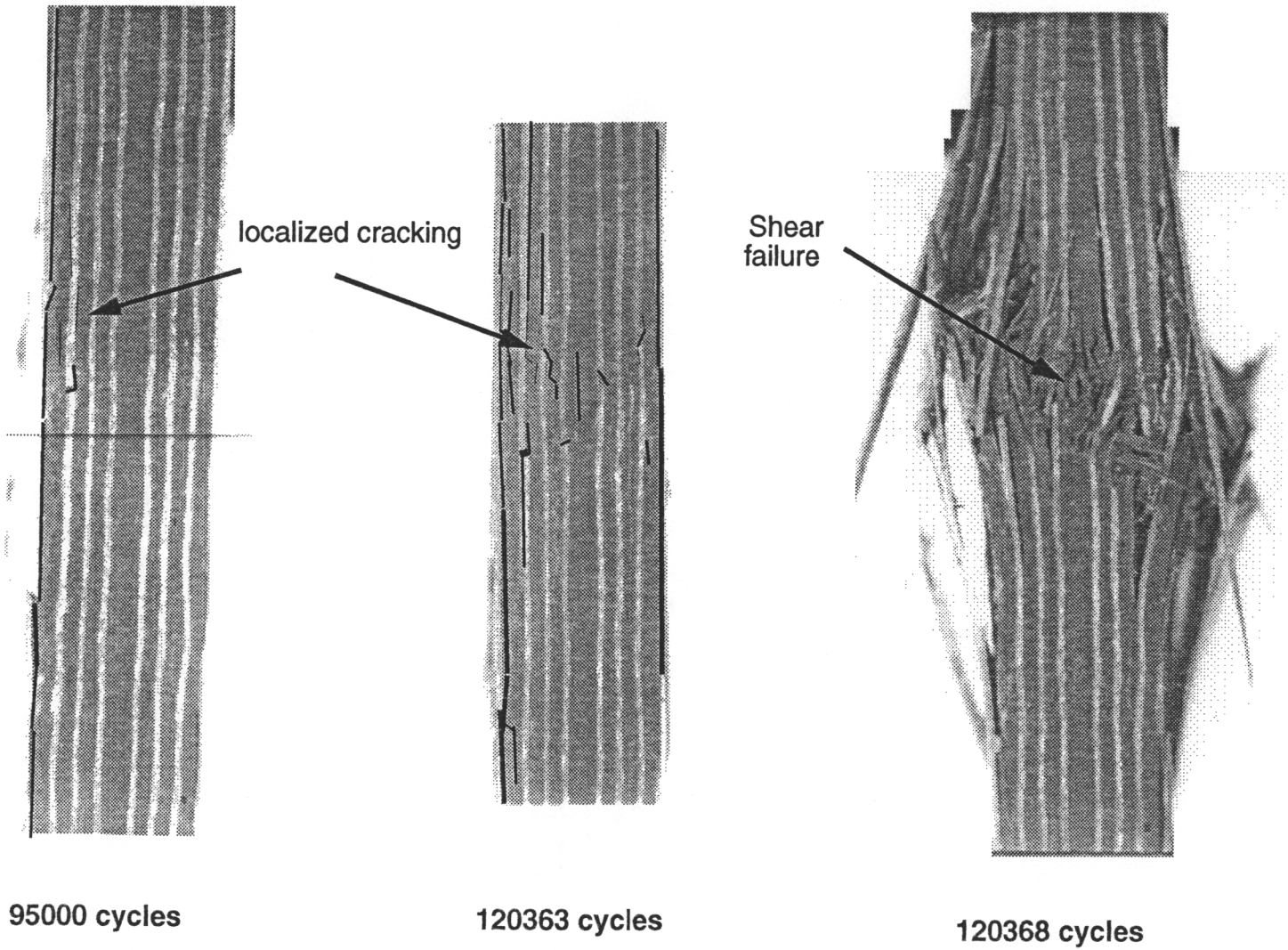

Figure 33. Fatigue damage development and shear mode failure in glass stitched uniweave material.

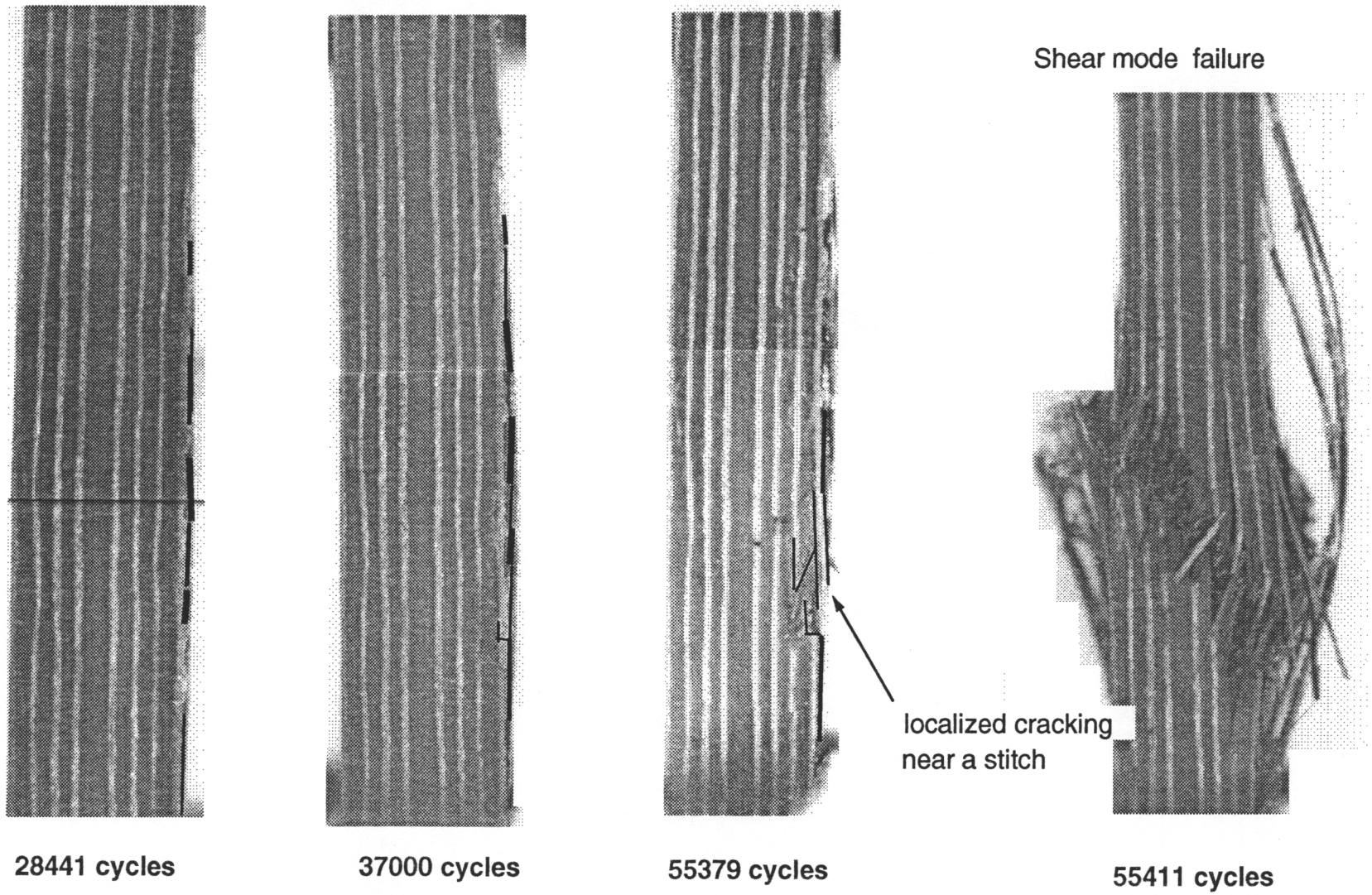

Figure 34. Fatigue damage development and shear mode failure in a Kevlar stitched uniweave.

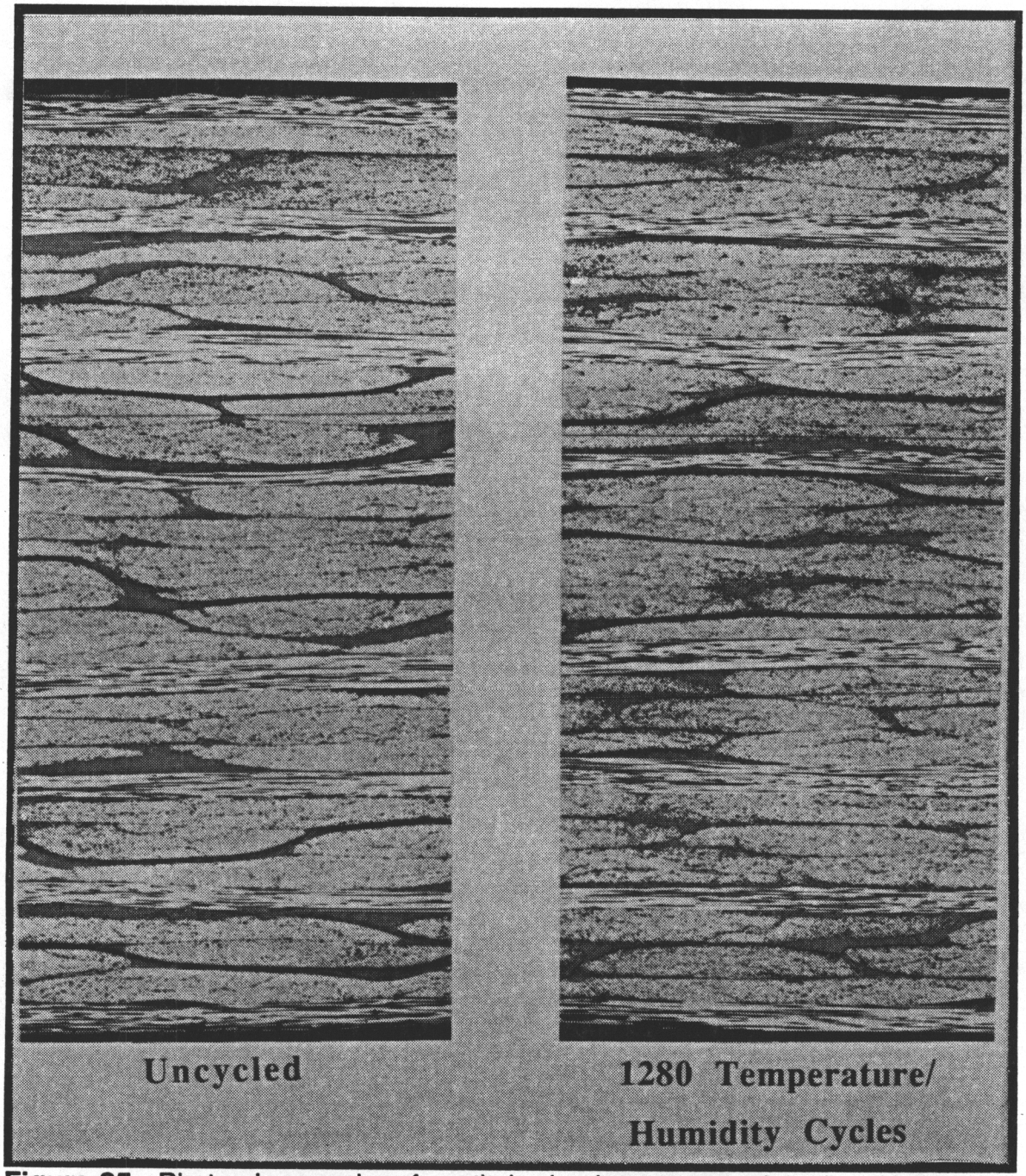

Figure 35. Photomicrographs of unstitched uniweave material taken before and after 1280 combined temperature and humidity cycles

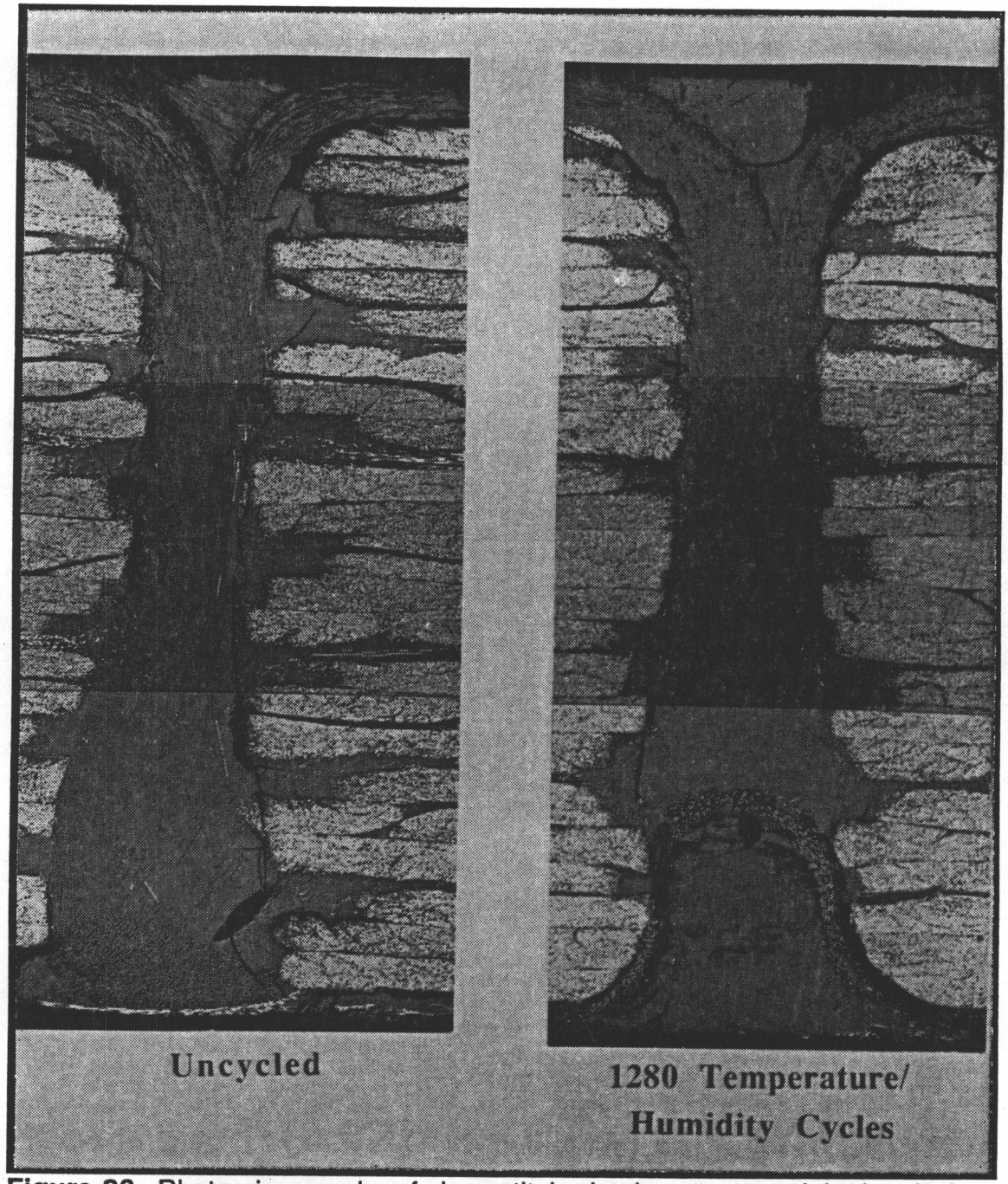

Figure 36. Photomicrographs of glass stitched uniweave material taken before after 1280 combined temperature and humidity cycles.

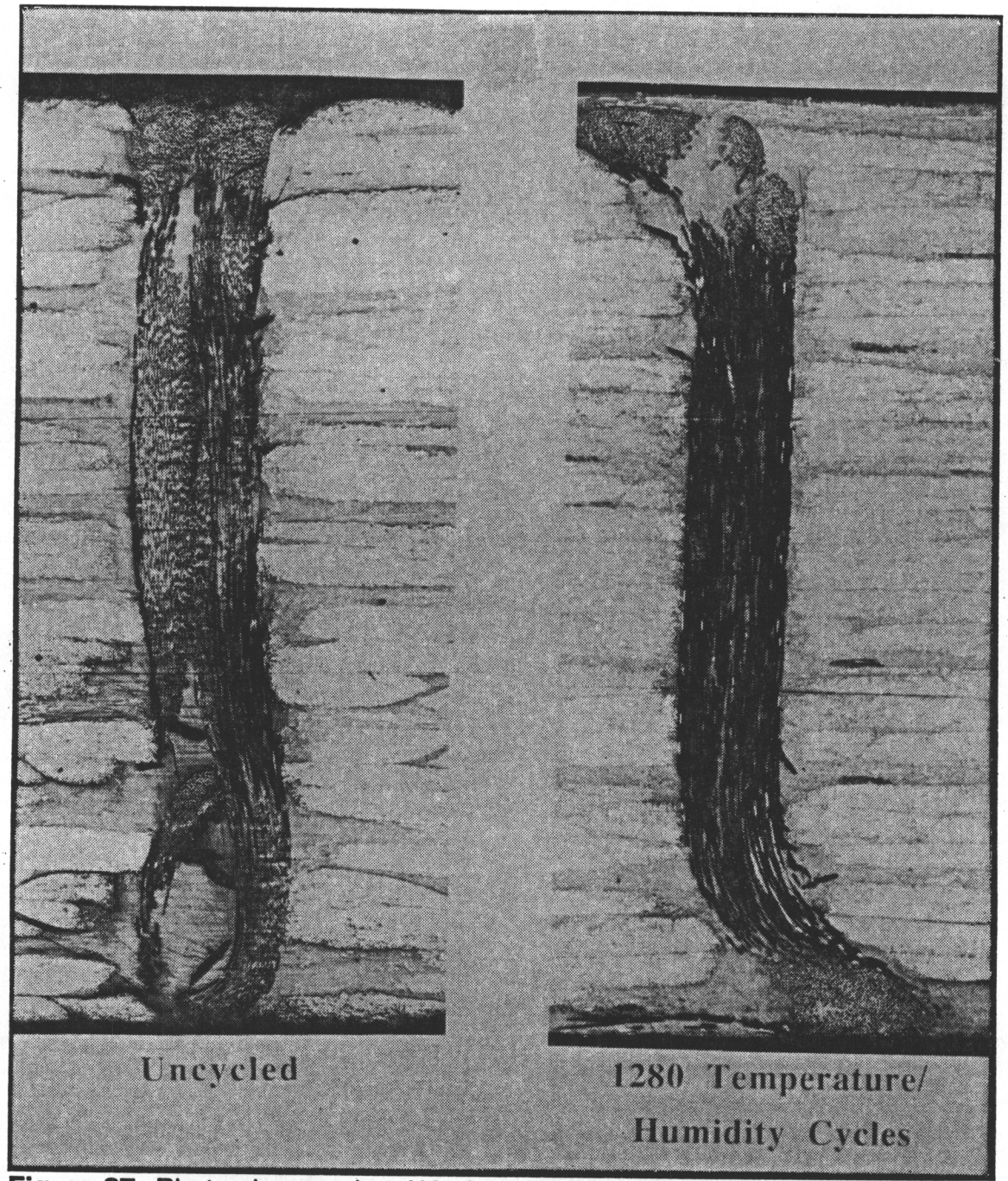

Figure 37. Photomicrographs of Kevlar stitched uniweave material taken before and after 1280 combined temperature and humidity cycles.

observed in the glass stitched material, the microcracks in the Kevlar stitched material did not appear to increase in severity with temperature and humidity cycling.

6.6.2 Braided Materials

Photomicrographs for the braided materials are presented in Figures 38-40. As observed in the glass stitched uniweave material, the glass stitched 2-D braid, Figure 38, experienced significant microcracking around the stitching before and after cycling. The unstitched 2-D material, Figure 39, and the 3-D braided material, Figure 40, did not appear to develop any microcracking from temperature and humidity cycling.

6.7 Diffusion Tests Results

6.7.1 One-Dimensional In-Plane Diffusion

The calculated diffusivities are show in Table 10 and were used to fit the in-plane moisture absorption data shown in Figures 41 and 42. In each figure, the ratio of moisture absorbed to the total moisture absorbed is plotted against the square root of time for temperatures of 60°C, 70° and 80°C. The experimental points are the average of three specimens and the curves are calculated from the 1-D series solution to Fick's Law. The series solution fits the data well at short times but over predicts the moisture uptake in the knee of the curve before reaching the maximum moisture content.

For the quasi-isotropic lay-up and the stitched pattern used in these tests, the two in-plane diffusivities are similar at a given temperature. The in-plane diffusivities vary with temperature as shown in Figure 43. Figure 43 is an Arrhenius plot which plots the logarithm of the diffusivity against the reciprocal of the absolute temperature. The data is fit to the Arrhenius equation (equation 8) shown below.

$$D_x = D_y = 0.452e^{-4512/T} (mm^2/sec)$$

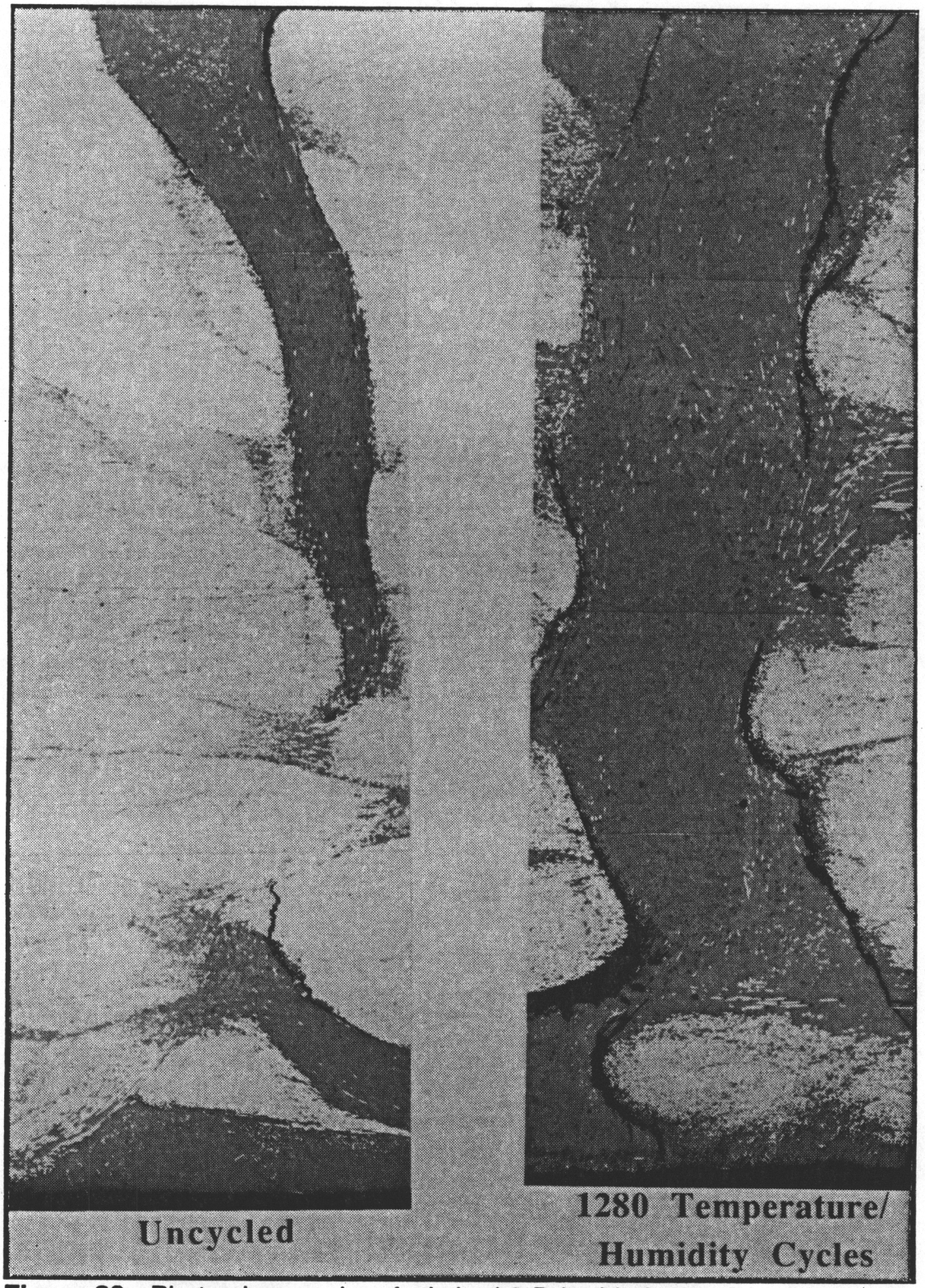

Figure 38. Photomicrographs of stitched 2-D braided material taken before and after 1280 combined temperature and humidity cycles.

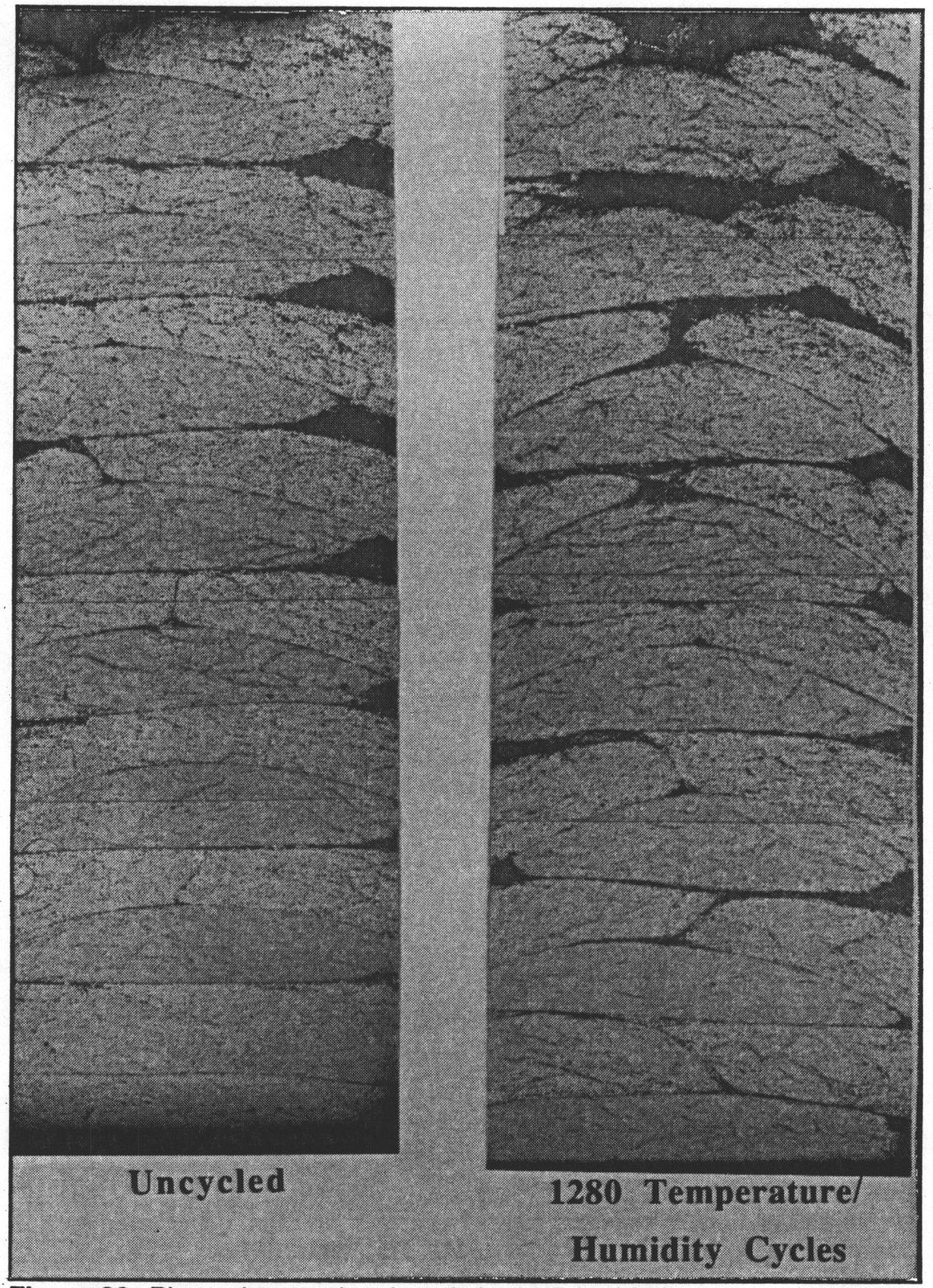

Figure 39. Photomicrographs of unstitched 2-D braided material taken before and after 1280 combined temperature and humidity cycles

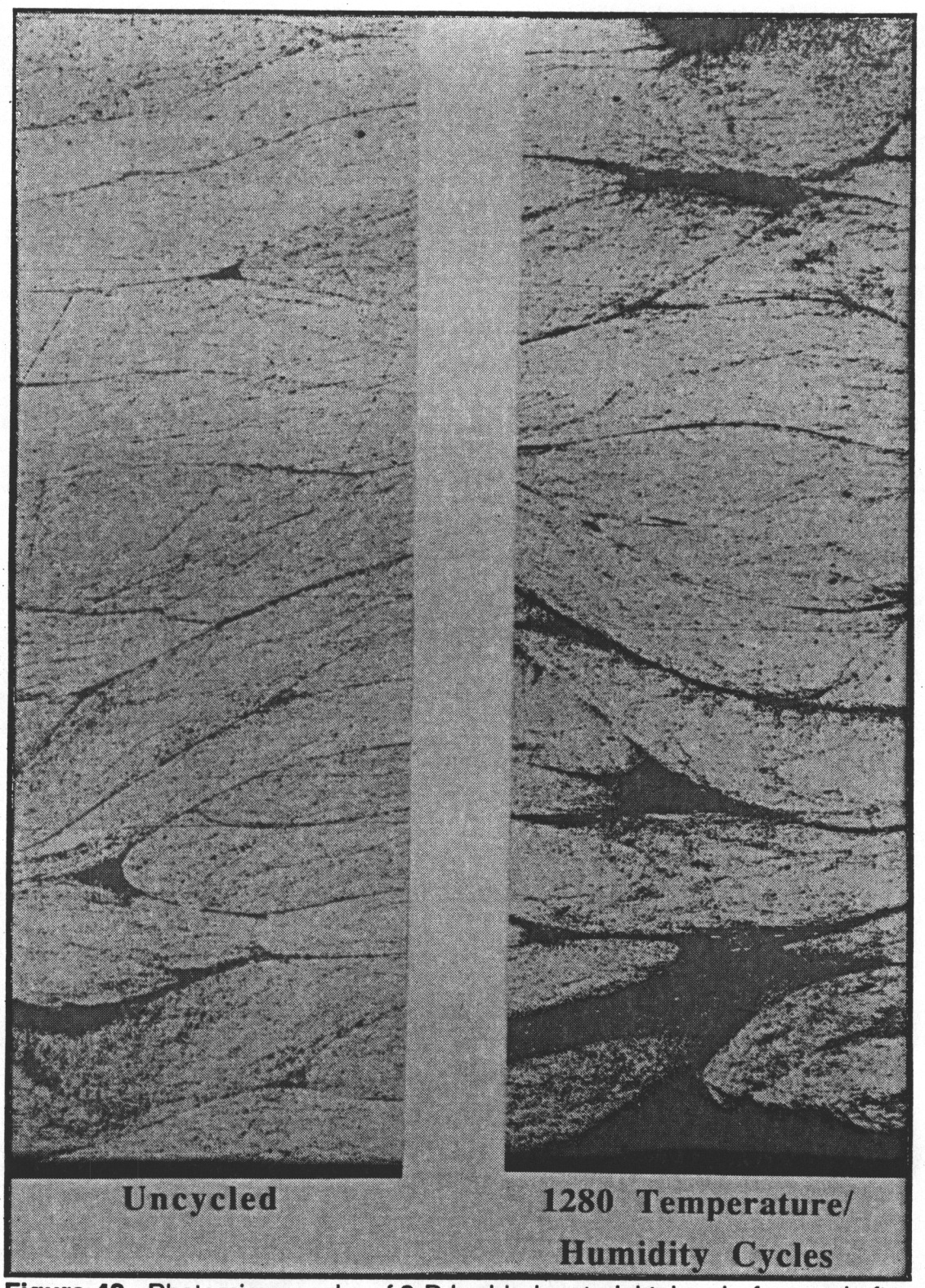

Figure 40. Photomicrographs of 3-D braided material taken before and after 1280 combined temperature and humidity cycles

Table 10. In-plane diffusivities for quasi-isotropic, glass stitched composite

	60°C, 75% RH	70°C, 80% RH	80° C, 90% RH
D_X, (mm^2/sec)	6.4E-7	7.5E-7	1.3E-6
D_Y, (mm^2/sec)	6.4E-7	7.0E-7	1.4E-6

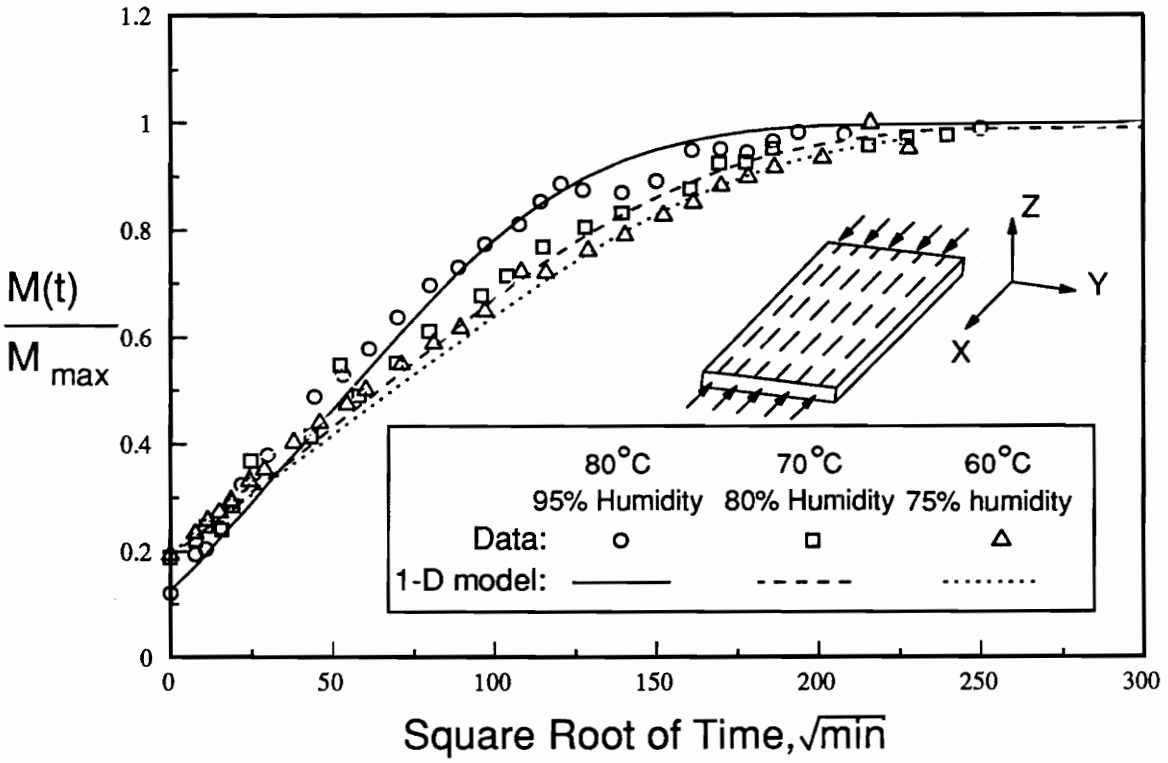

Figure 41. In-Plane (D_x) moisture absorption curves. The 1-D series solution to Fick's law fits the experimental data points.

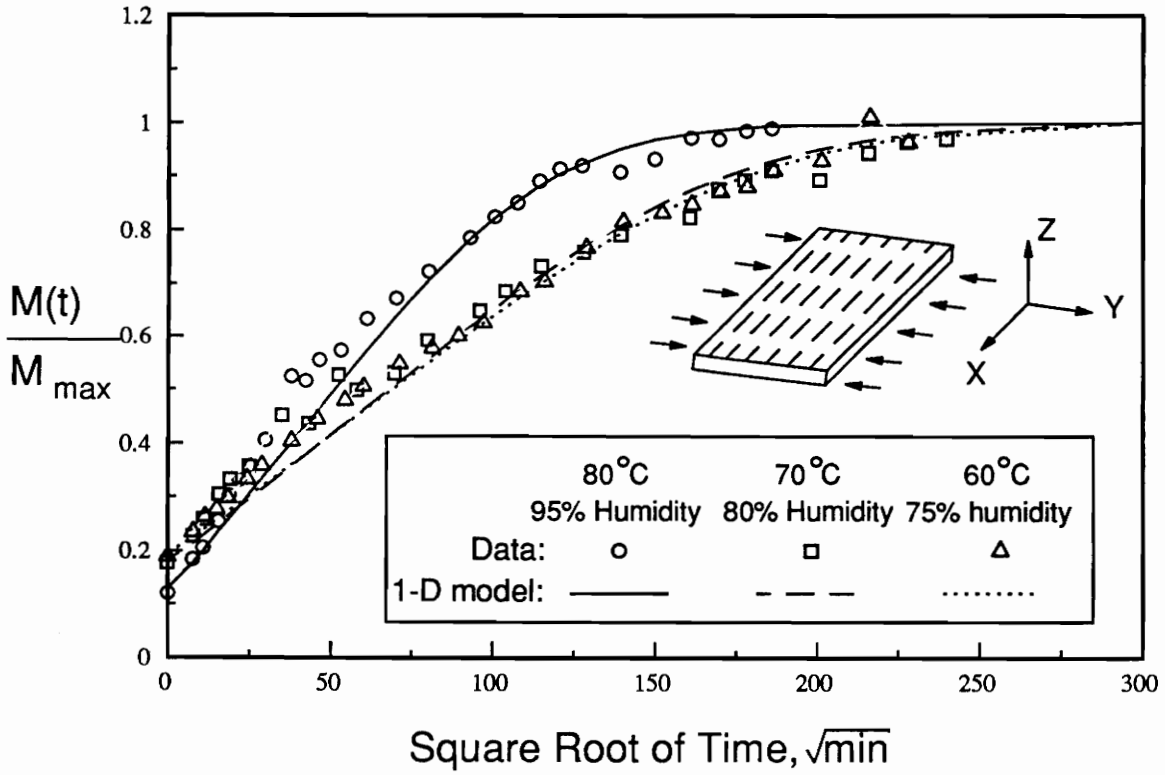

Figure 42. In-Plane (D_y)moisture absorption curves. The 1-D series solution to Fick's law fits experimental data points

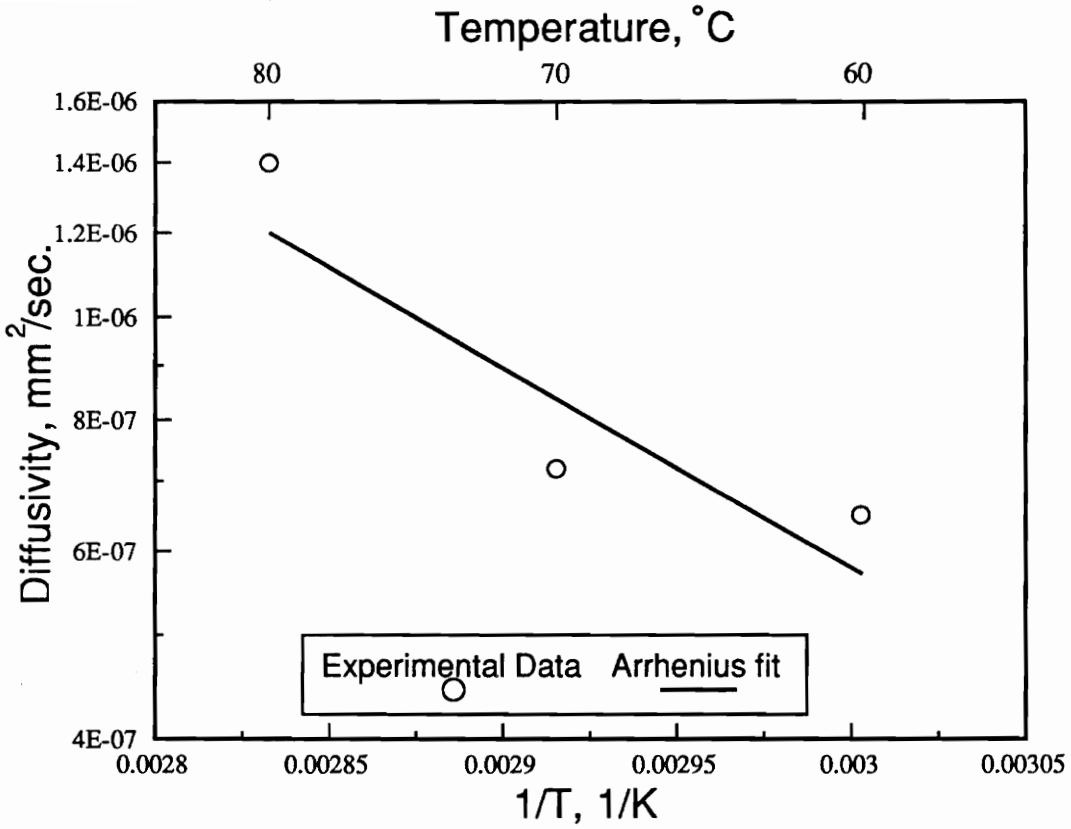

Figure 43. Plot of in-plane diffusivities versus temperature. The data is fit to the Arrhenius equation.

Diffusion along interfaces and moisture absorption around flaws are potential sources for any non-Arrhenius behavior in the data. The constant E_a/R and pre-exponential factor in equation (8) are found by plotting the logarithm of the diffusivity against the reciprocal of the absolute temperature. Then a linear least squares curve is fit to the data. The slope of the curve gives the activation energy which is 37.5 kJ/mol. The intercept of the curve gives the logarithm of the pre-exponential factor. A change in the slope of the line would indicate a change in the diffusion mechanism. Temperatures below 85 °C were chosen to avoid any changes in the diffusion mechanism associated with the glass transition temperature.

Finally, in Figure 44, the maximum moisture content is plotted as a function of relative humidity. For convenience the data were fit the power law formula, equation 7 in section 2.0.

$$M_{max}=0.038(RH)^{0.82}(\%)$$

The power law formula is a variation of Henry's law for ideal dilute solutions. When the humidity is raised to the first power the mixture obeys Henry's law.

6.7.2 Three-Dimensional Diffusion

Diffusivities calculated with the 3-D moisture absorption data and the procedure discussed in section 5.2 are shown in Table 11. The through-the-thickness diffusivities are comparable to literature values [30] for transverse diffusivities in AS4/3501 composite laminates. For temperatures between 45°C and 85°C transverse diffusivities for AS4/3501 composites will typically fall between 2.0e-8 mm^2/sec and 7.0e-7 mm^2/sec, respectively. The diffusivities do not show any consistent trend with the relative humidity. The through-the-thickness diffusivities (D_z) are nearly the same for each material. The stitching does not measurably increase the through-the-thickness diffusivity compared to the unstitched material. One consistent trend is the increase in the in-plane diffusivity as the thickness of

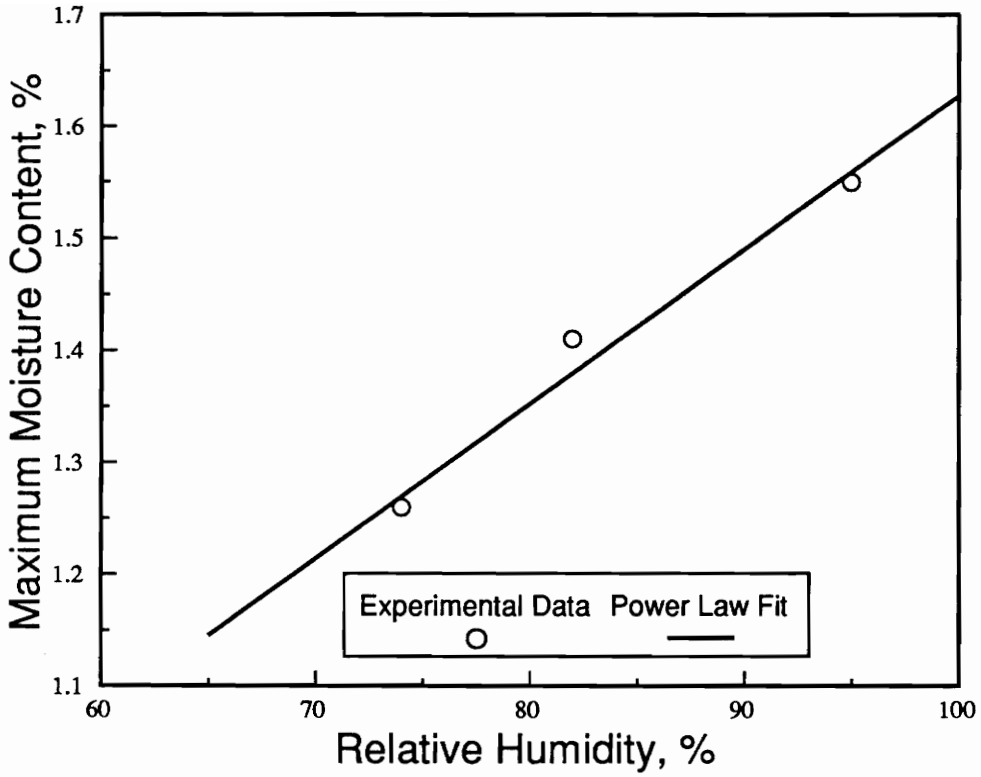

Figure 44. Maximum moisture content plotted as a function of relative humidity in the in-plane, 1-D experiments.

the specimen increases. Each material had the same number and lay-up of plies, but as shown previously in Table 4, the unstitched material was the thinnest and the glass stitched material was the thickest. This indicates a decrease in the fiber volume fraction which would result in the in-plane diffusivity increasing from the thinnest to the thickest material. The 45°C specimens were sealed around the edges. Therefore, only a through-the-thickness diffusivity was reported in Table 11.

Shown in Figures 45 through 53 are comparisons between the 1-D series solution (equation 5) and the 45°C data and the 3-D series solution (equation 12) and the 65°C and 85°C data. The 3-D series solution fits the data at short times in every case. At longer times, in the knee of curve, the series solution slightly over predicts the moisture content before reaching equilibrium. At 85°C and 95 percent humidity the series solution fits over the entire range.

After 2 months the sealant used on the 45°C specimens began to fail (i.e. the sealant began debonding from the specimens) resulting in low apparent moisture contents and high data scatter compared to the specimens with exposed edges. As a result only the initial slope was used to obtain the through-the-thickness diffusivity. The maximum moisture content for the tests conducted at 45°C and 75% relative humidity was taken to be the same as the maximum moisture content for the tests conducted at 65°C and 85°C and 75% relative humidity. Due to this approximation, the 45°C data does not approach a moisture uptake of one and the 1-D model fits the data only at very short times.

Arrhenius plots of the diffusivities obtained from the 3-D experiments are shown in Figures 54 and 55. The data were fit to the Arrhenius equation (equation 8) where the preexponential constants and the activation energies are shown in Table 12. The activation energies for the in-plane data are conspicuously high. Literature values for graphite epoxy composites [30] are typically in the 40 kJ/mol range. Different activation energies for the through-the-thickness and in-plane

Table 11. In-plane and through-the-thickness diffusivities for the unstitched and stitched materials determined using a 3-D analysis.

Diffusivity, (mm^2/sec)	RH, (%)	Unstitched	Kevlar Stitched	Glass Stitched
		Moisture Absorbed at 85° Celsius		
D_z	65	4.0E-7	4.3E-7	6.9E-7
	75	5.4E-7	4.9E-7	9.4E-7
	95	8.1E-7	1.0E-6	1.6E-7
D_x	65	2.7E-6	9.0E-6	1.6E-5
	75	3.2E-6	8.3E-6	3.0E-5
	95	9.7E-7	2.3E-6	2.7E-5
		Moisture Absorbed at 65° Celsius		
D_z	75	1.4E-7	2.4E-7	3.4E-7
D_x	75	6.2E-7	1.5E-6	5.9E-6
		Moisture Absorbed at 45° Celsius		
D_z	75	8.2E-8	1.3E-7	3.2E-7

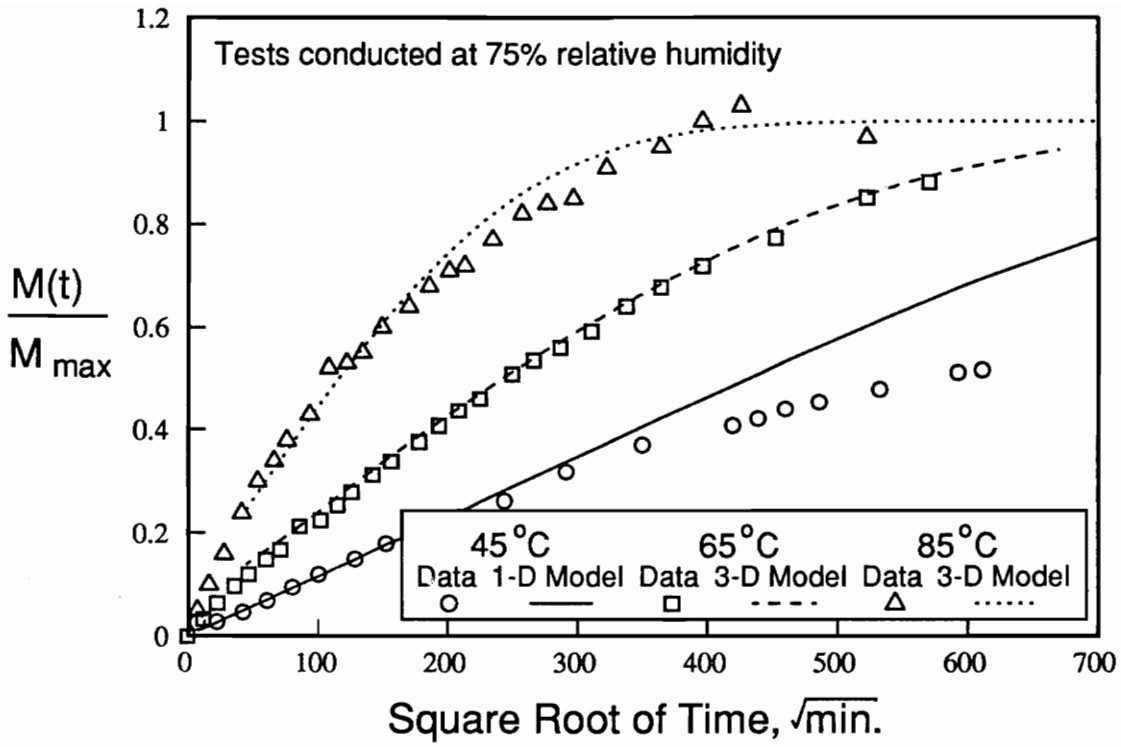

Figure 45. Moisture absorption curves for unstitched uniweave material at 45, 65, and 85°C and 75% RH. The 1-D or 3-D series solutions to Fick's Law are compared with the data.

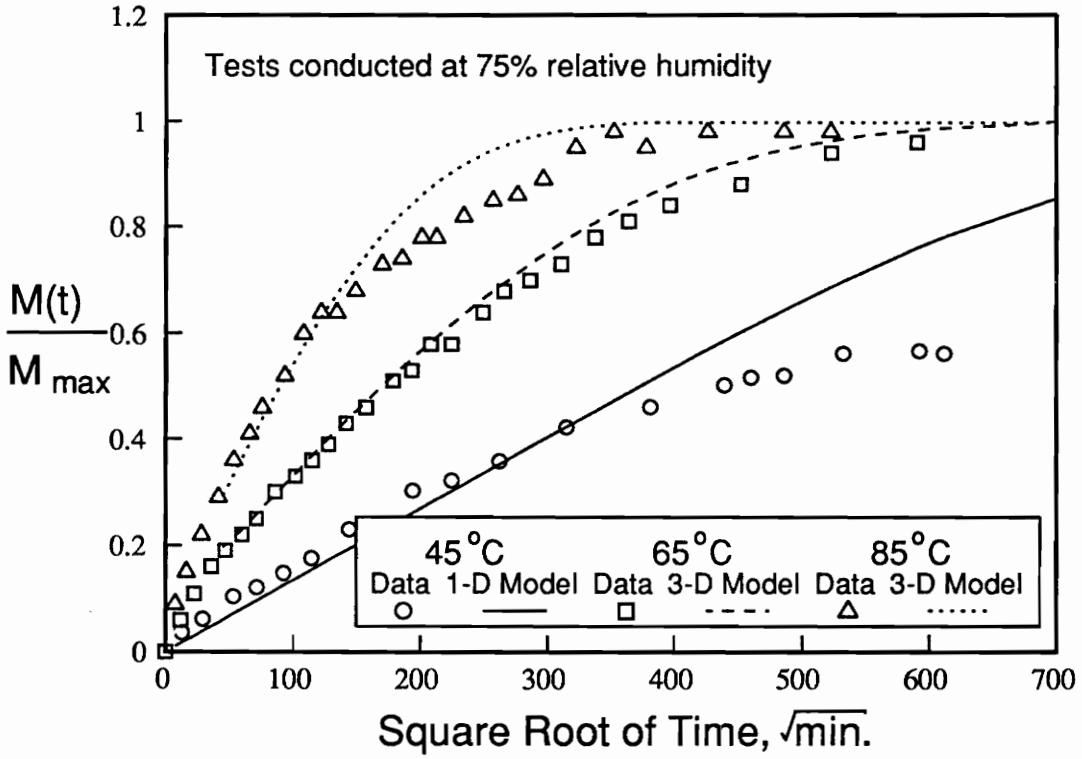

Figure 46. Moisture absorption curves for Kevlar stitched uniweave material at 45, 65 and 85°C and 75% RH. The 1-D or 3-D series solutions to Fick's Law are compared to the data.

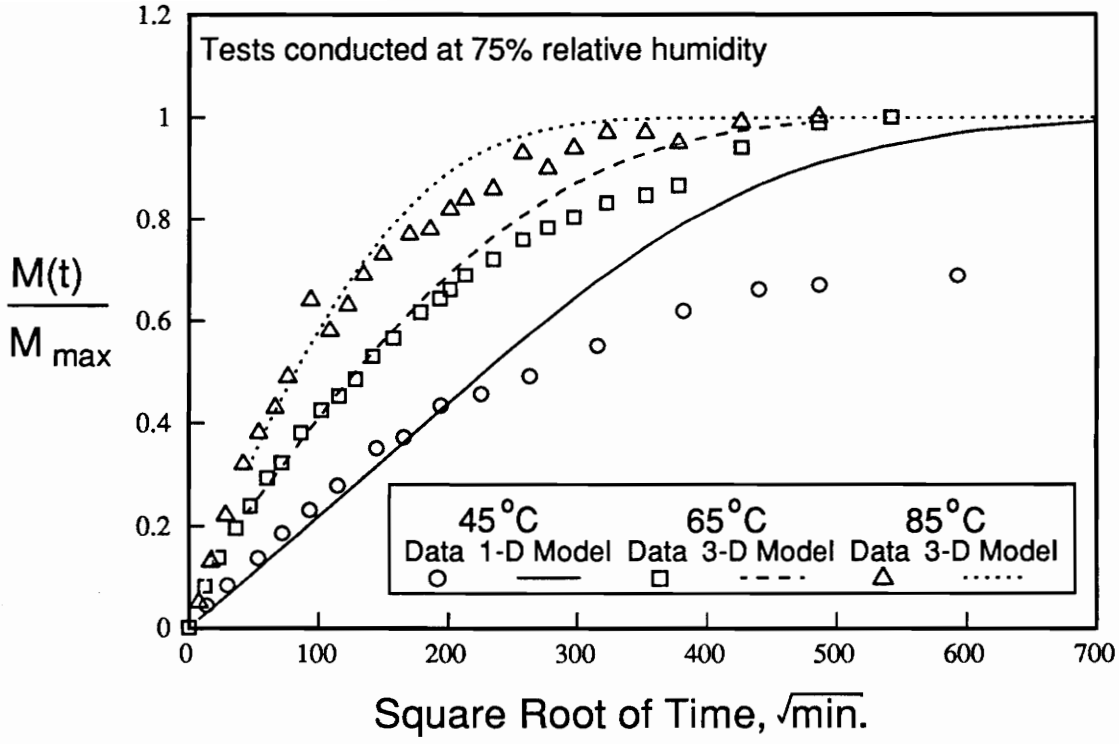

Figure 47. Moisture absorption curves for glass stitched uniweave material at 45, 65 and 85 °C and 75% RH. The 1-D or 3-D series solutions to Fick's Law are compared to the data.

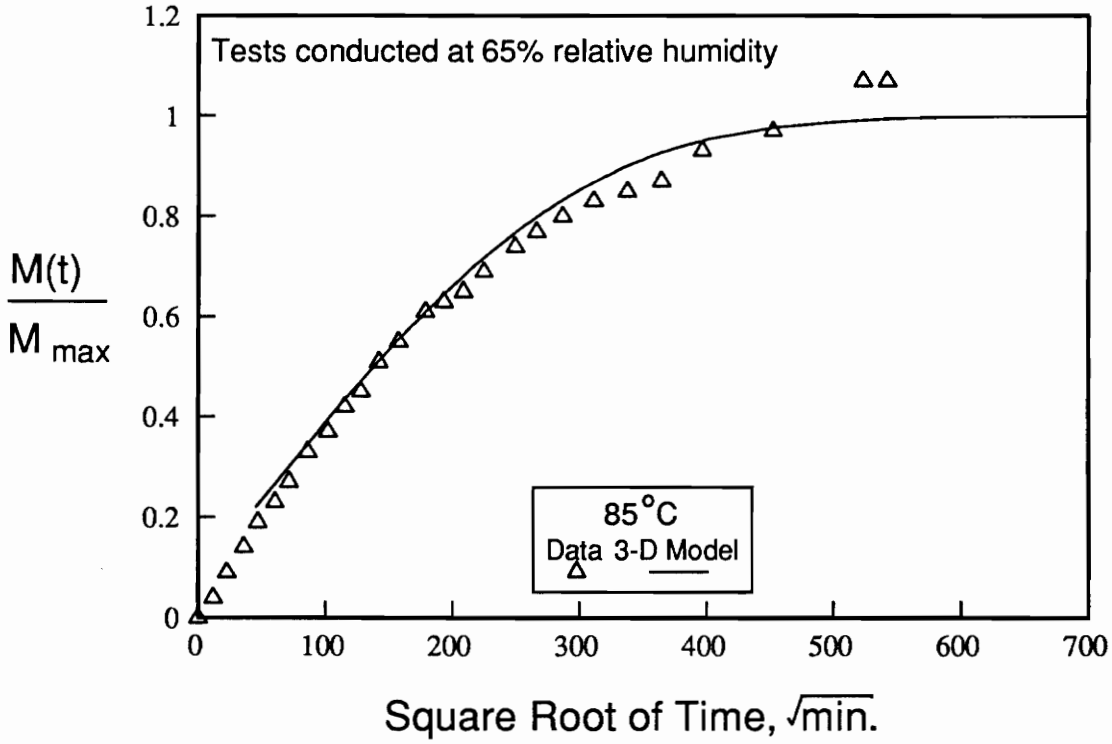

Figure 48. Moisture absorption curve for unstitched uniweave material at and 85°C and 65% RH. The 3-D series solution to Fick's Law is compared to the data.

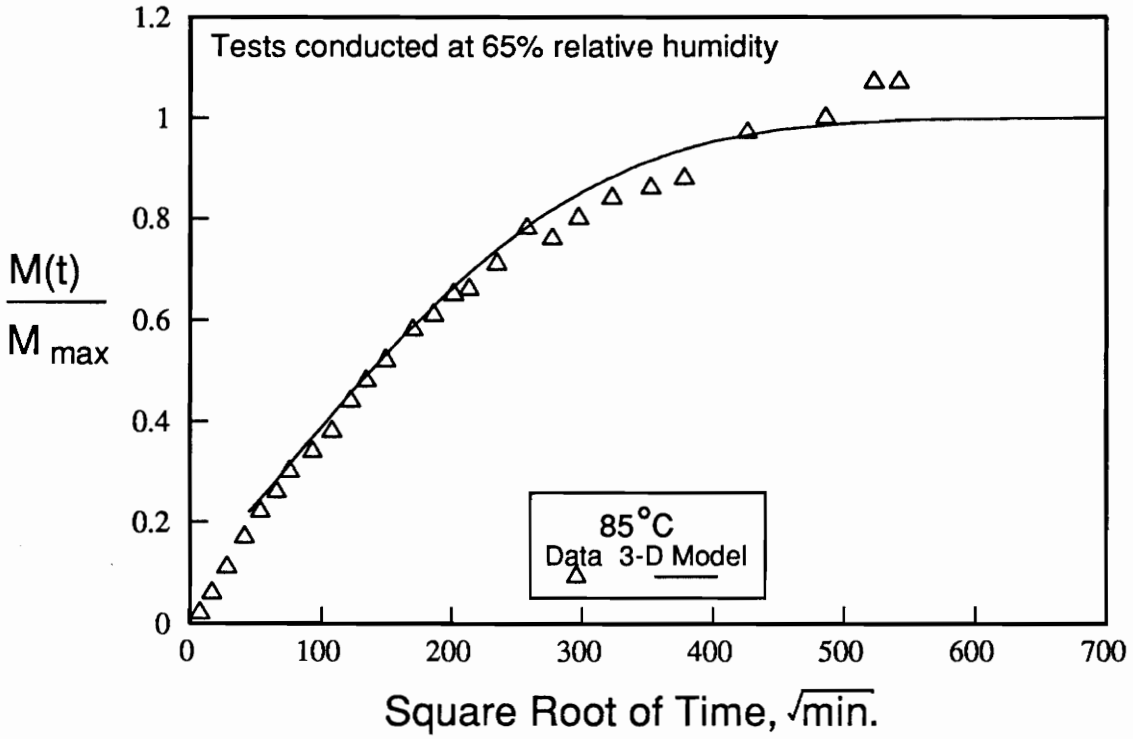

Figure 49. Moisture absorption curve for Kevlar stitched uniweave material at 85°C and 65% RH. The 3-D series solution to Fick's Law is compared to the data.

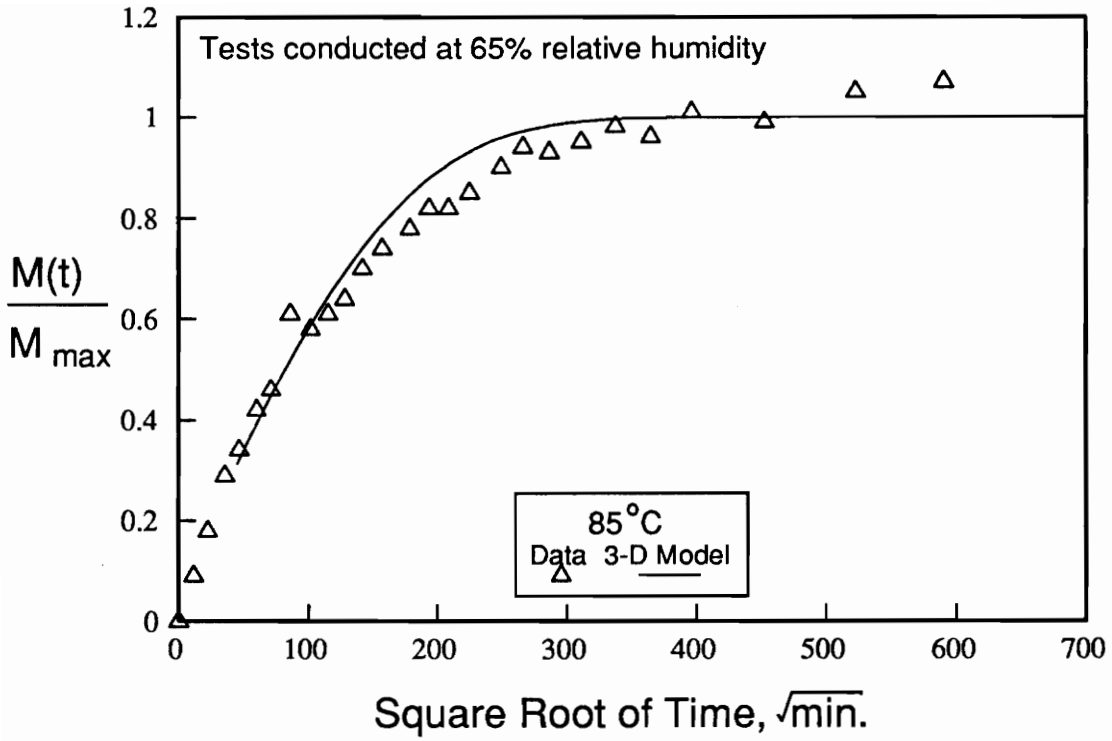

Figure 50. Moisture absorption curve for glass stitched uniweave material at 85°C and 65% RH. The 3-D series solution to Fick's Law is compared to the data.

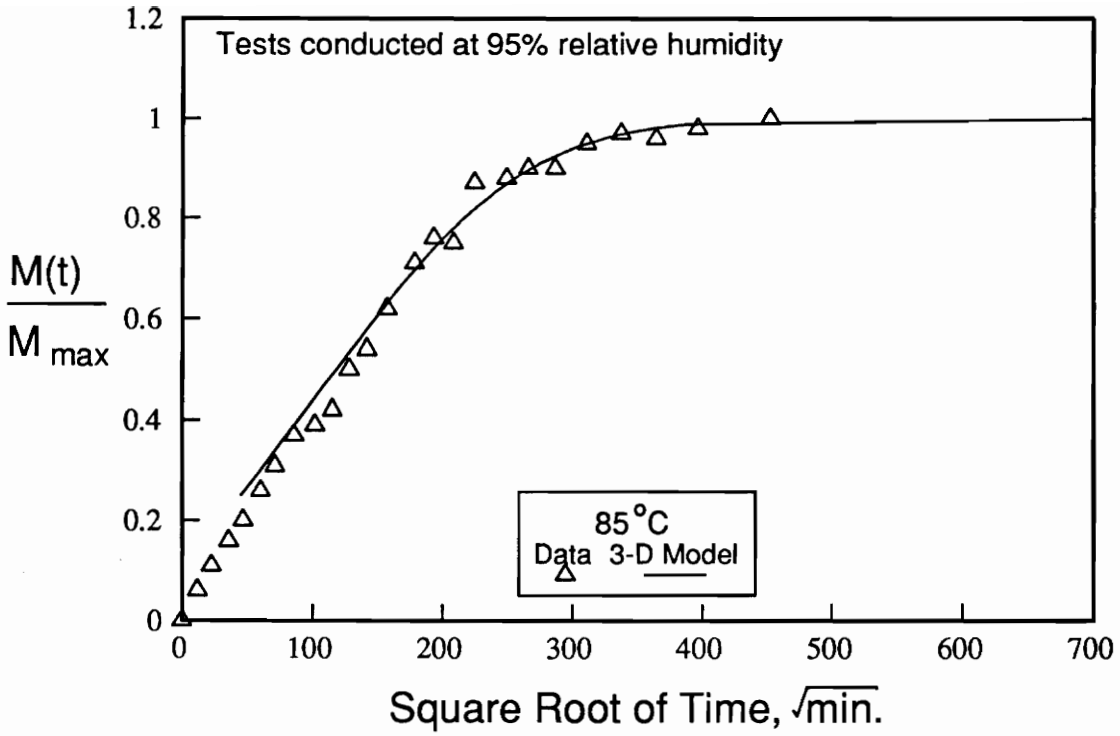

Figure 51. Moisture absorption curve for unstitched uniweave material at 85°C and 95% RH. The 3-D series solution to Fick's Law is compared to the data.

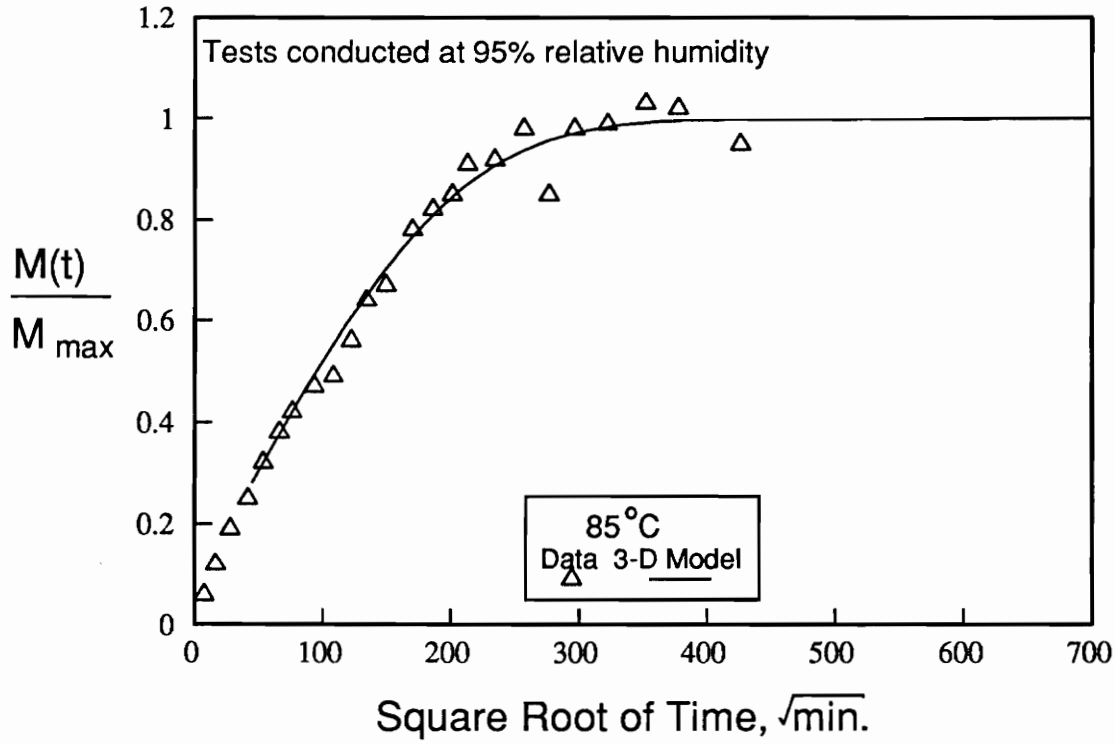

Figure 52. Moisture absorption curve for Kevlar stitched uniweave material at 85°C and 95% RH. The 3-D series solution to Fick's Law is compared to the data.

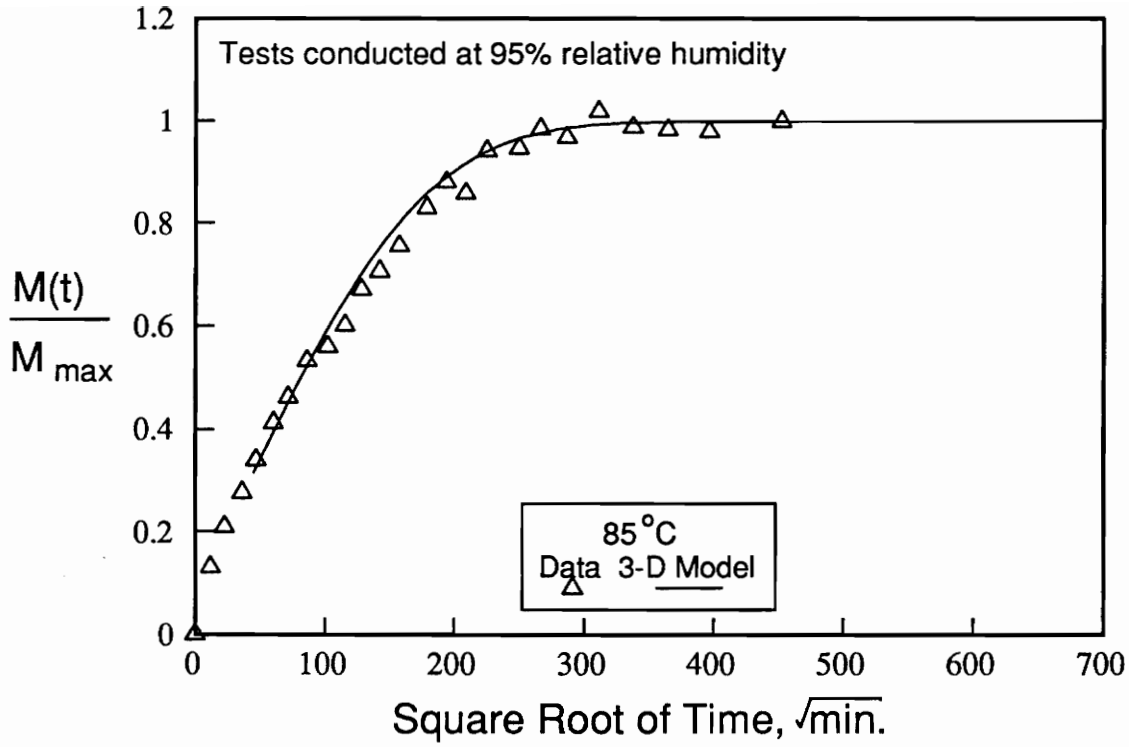

Figure 53. Moisture absorption curve for glass stitched uniweave material at 85°C and 95% RH. The 3-D series solution to Fick's Law is compared to the data.

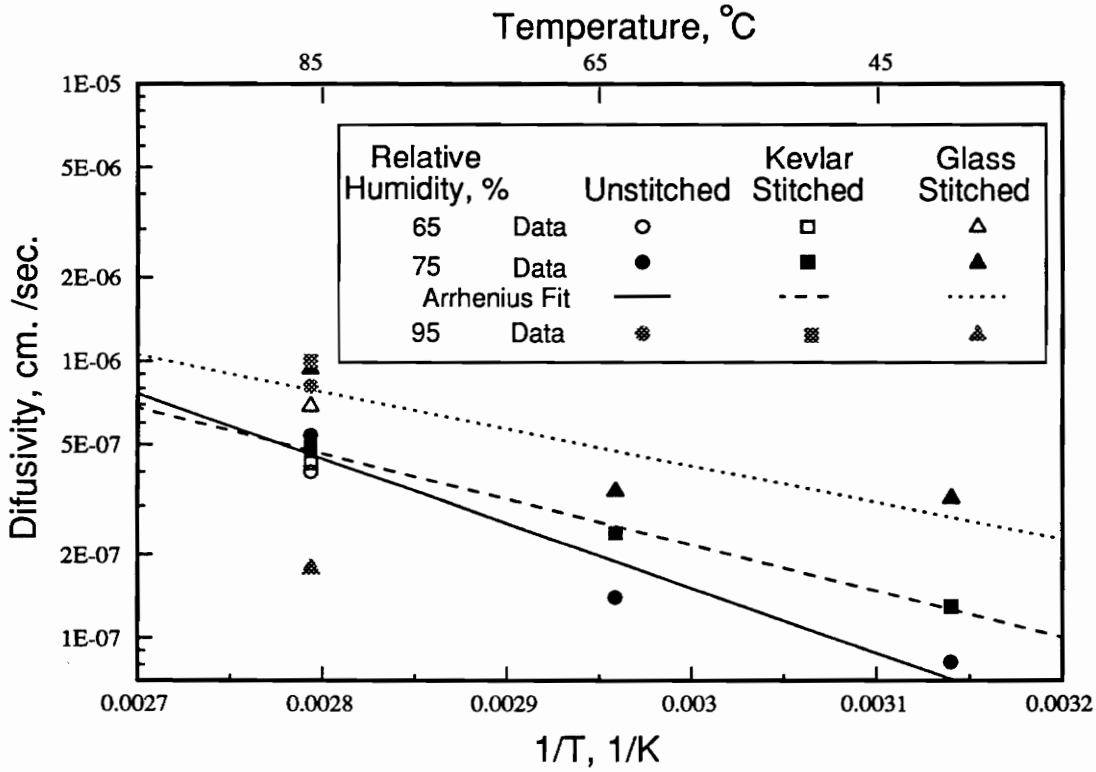

Figure 54. Arrhenius plot of the through-the-thickness diffusivities for the uniweave materials.

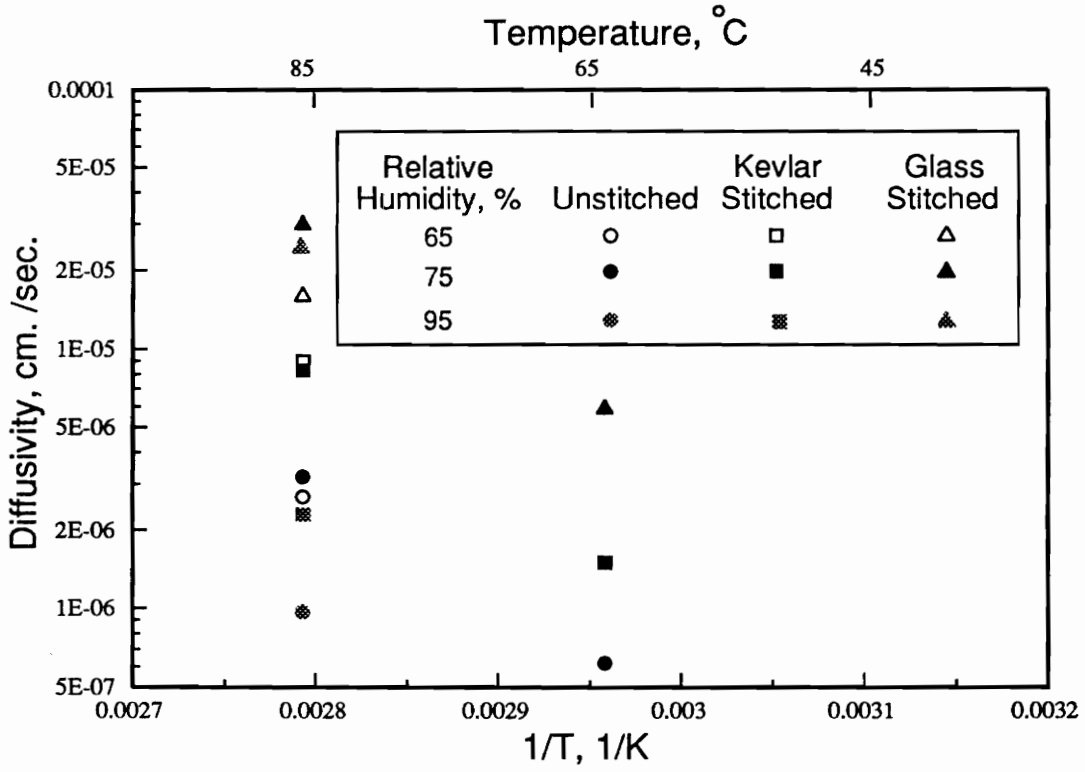

Figure 55. Arrhenius plot of the in-plane diffusivities for the uniweave materials.

Table 12. Constants for the Arrhenius equation obtained from the 3-D tests

Material	Diffusivity, mm^2/sec	E_a, kJ/mol	A, mm^2/sec
Unstitched	D_z	33.3	0.00237
	$D_x=D_y$	83.3	4.34E5
Kevlar Stitched	D_z	31.3	0.00157
	$D_x=D_y$	86.1	2.7E6
Glass Stitched	D_z	25.3	0.00035
	$D_x=D_y$	82.0	2.7E6

diffusivities would indicate different diffusion mechanisms for each direction. This is unlikely since the resin system is the same in each case. Furthermore, absorption mechanisms competing with diffusion through the polymer matrix would include moisture in cracks and flaws and diffusion along fiber matrix interfaces. These mechanisms may have different activation energies or they may not follow an Arrhenius type equation. Finally the in-plane diffusivities were measured at only two temperatures. Additional points may have resulted in a different activation energy.

Finally, in Figure 56, the maximum moisture content is plotted as a function of relative humidity. Although Kevlar fiber is known to absorb moisture, the Kevlar stitched material did not reach a higher maximum moisture content. For convenience the data are fit to a power law formula (equation 7).

$$M_{max}=0.023(RH)^{0.91}(\%)$$

The Relative humidity is not raised to the first power, indicating a deviation from Henry's law and ideal dilute solution behavior.

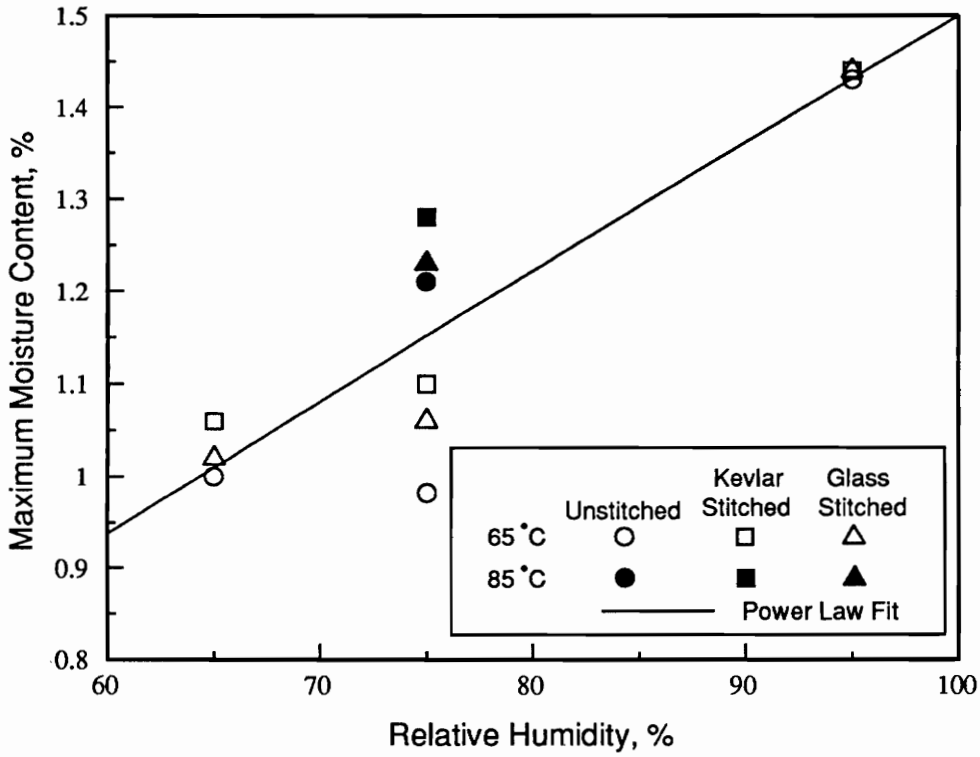

Figure 56. The maximum moisture content obtained in the 3-D experiments plotted as a function of relative humidity.

7.0 CONCLUSIONS AND FUTURE WORK

7.1 Uniweave Materials

Static compression and compression-compression fatigue tests were conducted on three AS4/3501-6 uniweave composites. Two of the composites were stitched through-the-thickness with either glass or Kevlar stitching and the third was unstitched. All three uniweave composites were exposed to three different temperature and humidity environments. The first environment cycled both temperature and humidity. The second environment cycled only the temperature at constant relative humidity. The last environment held constant temperature and humidity.

Stitching causes a decrease in the ultimate baseline static compression strength. Compared to the unstitched material, glass stitching reduces the compressive strength 16 percent and Kevlar stitching reduces the compressive strength 5 percent.

After 160 combined temperature and humidity cycles, the compressive strength of unstitched and Kevlar stitched material decreases about 5 percent. The glass stitched material did not lose compression strength after cycling. The strength loss was a function of moisture absorbed during combined temperature and humidity cycling.

Four days of temperature cycling at constant relative humidity causes a 6 percent decrease in compression strength of the unstitched and Kevlar stitched material. Additional cycling had no effect on compression strength.

Compressive strength decreases in all three uniweave materials after exposure to constant 60°C and 95 percent relative humidity. After 4 days, the unstitched and Kevlar stitched material had initial strength decreases of 9 and 6 percent, respectively. Following the initial strength reduction, the strength remains nearly constant through 40 days. After complete saturation, in water, compression strength of the unstitched and Kevlar stitched materials decreases about 18 percent. The glass stitched material loses 7 percent of its baseline compression strength after complete saturation.

Under compression-compression fatigue loading, Kevlar stitching does not adversely affect the baseline fatigue performance compared to the unstitched material. The glass stitched material, however, has lower baseline fatigue strength than either the Kevlar or the unstitched material.

Runout strength and fatigue sensitivity of the uniweave materials remains unchanged after temperature and humidity cycling when the test specimens are dried to their original weights before testing.

Exposure to constant temperature and humidity does not affect the fatigue properties of unstitched uniweave material until the material is saturated. After saturation the absorbed moisture reduces the runout strength of the unstitched material. The reduction in runout strength is nearly the same as the reduction in static strength caused by exposure to the hot/wet conditions. For the Kevlar stitched material exposed to the constant temperature and humidity environment, the fatigue sensitivity decreases while the runout strength remains unchanged. For the glass stitched material exposed to the constant temperature and humidity

environment, the runout strength decreases as the material reaches saturation. For each material, the runout strength was 50 to 60 percent of the ultimate compressive strength.

7.2 Braided Materials

An unstitched 2-D braided composite, a glass stitched 2-D braided composite and a 3-D braided composite were also exposed to combined temperature and humidity cycling. The braided materials had a E905L resin system which did not absorbed as much moisture as the 3501-6 system in the uniweave composites. Temperature and humidity cycling does not affect compression strengths of the unstitched 2-D and 3-D braided materials. Temperature and humidity cycling reduces the compression strength of the stitched 2-D braid by 8 percent compared to its baseline strength. Stitching reduces the baseline compressive strength of the 2-D braid 5 percent when compared to the unstitched material.

Compression-compression fatigue properties for the braided materials were also measured. Combined temperature and humidity cycling does not measurable affect the fatigue properties of the braided materials.

7.3 Fatigue Damage Progression and Failure Surfaces

Damage progression and failure surfaces do not change with environmental exposure or with maximum compressive fatigue loads below 65 percent of the static compression strength. Damage progression and failure surfaces varied considerably between stitched and unstitched materials. The unstitched specimens failed by delaminating. The stitched uniweave materials fail in shear. Once cracks appear throughout the thickness, the stitched specimens fail in a diagonal, shear mode type failure.

7.4 Microcracking

The baseline unstitched uniweave material did not show any microcracks resulting from the manufacturing process. Microcracking between some of the outer plies did develop after temperature and humidity cycling.

The baseline glass stitched uniweave material had significant microcracking around each individual stitch. These microcracks do not appear to grow with combined temperature and humidity cycling.

The baseline Kevlar stitched uniweave material also shows microcracking around the stitching; but not the degree of microcracking observed in the glass stitched materials. The microcracks in the Kevlar stitched material did not appear to increase in severity with combined temperature and humidity cycling.

7.5 Moisture Absorption in Uniweave Materials

The series solution to Fick's Law fits the in-plane moisture absorption data well at short times but in the knee of the curve the solution over predicts the moisture content before the specimen reaches the equilibrium moisture content. For the quasi-isotropic lay-up and the stitch pattern used in these materials, the two in-plane diffusivities are the same in each direction. The glass stitched material had higher in-plane diffusivities than the Kevlar or unstitched material.

The through-the-thickness diffusivities (D_z) are nearly the same for each of the uniweave materials. The stitching does not measurably increase the through-the-thickness diffusivity compared to the unstitched material. The 3-D series solution to Fick's Law fits the moisture absorption data at short times for the conditions studied. At longer times, in the knee of the curve, the series solution over predicts the moisture content before the specimen reaches equilibrium. At 85°C and 95 percent humidity the series solution fits over the entire range.

7.6 Future Work

Some areas of future work would include short-block-compression testing of specimens whose moisture content are between 0.8 and 1.5 percent. Static and fatigue testing at elevated temperatures should also be conducted since absorbed moisture has a greater effect at elevated temperature. Fatigue damage development in braided materials also should be pursued.

The 3-D diffusion analysis should be tested using a large flat plate and a smaller plate of the same thickness to determine if the analysis produces the same through-the-thickness and in-plane diffusivities in each case.

For the stitching and stitch pattern used in these tests, average values of diffusivities described the moisture absorption process. When preforms are stitched together in stiffeners or joints, however, a local diffusion model around the stitch may be required to adequately describe the diffusion process.

REFERENCES

1. Rhodes, M.D., Williams, J.G. and Starnes, J.H. Jr., "Effects of Low Velocity Impact Damage on the Compressive Strength of Graphite/Epoxy Hat-Stiffened Panels," **NASA-TN-D-8411**, 1977.

2. Starnes, J.H., Jr., Rhodes, M.D. and Williams, J.G., "The Effect of Impact Damage and Circular Holes on the Compressive Strength of Graphite-Epoxy Laminates," **NASA-TM-78796**, 1978.

3. Byers, B.A., "Behavior of Damaged Graphite/Epoxy Laminates Under Compression Loading," **NASA-CR-159293**, 1980.

4. Dow, M.B. and Smith, D.L., "Properties of Toughened Epoxy Resin and High-Strain Graphite Epoxy," **NASA-TP-2826**, 1988.

5. Rechak S. and Sun C.T., "Optimal Use of Adhesive Layers in Reducing Impact Damage in Composite Laminates" in I. H Marshall (ed.), **Composite Structures 4**, Elsevier Applied Science, London, 1987, p. 2.18.

6. Jang, B.Z., Chen, L.C., Wang, C.Z., Lin H.T. and Zee, R.H., "Impact Resistance and Energy Absorption Mechanisms in Hybrid Composites," **Composites Science and Technology**, Vol. 34, No. 4, April 1989, p. 305.

7. Su, B.K., "Delamination Resistance of Stitched Thermoplastic Matrix Composite Laminates," in G. M. Newaz (ed.), **Advances in Thermoplastic Matrix Composite Materials ASTM STP 1044,** ASTM, Philadelphia, 1989, p. 270.

8. Bucknall, C. B., **Toughened Plastics**, Applied Science Publishers Ltd., New York 1977.

9. Mignery, L.A., Tan, T.M., and Sun, C.T., "The Use of Stitching to Suppress Delamination in Laminated Composites," in W. S. Johnson (ed.), **Delamination and Debonding, ASTM STP 876**, ASTM, Philadelphia, 1985, p 371.

10. Dexter, H.B. and Funk, J.G., "Impact Resistance and Interlaminar Fracture Toughness of Through-the-Thickness Reinforced Composites," **27TH Structure, Structural Dynamics and Materials Conference**, AIAA, Washington, D.C., 1986, p 700.

11. Dow, M.B. and Smith D.L., "Damage Tolerant Composite Materials Produced by Stitching Carbon Fabrics," in R.F. Wegman, H. S. Kliger, H Edward (eds.), **21st International SAMPE Technical Conference**, SAMPE, Covina, Calif., 1989, p. 595.

12. Chung, W.C., Jang, B.Z., Chang, T.C., Hwang, L.R. and Wilcox R.C., "Fracture Behavior in Stitched Multidirectional Composites," **Materials Science and Engineering**, Vol. A112, June 1989, p. 157.

13. Pelstring, R.M. and Madan, R.C., "Stitching to Improve Damage Tolerance of Composites," in G. A. Zakrzewski (ed.), **34th International SAMPE Symposium**, SAMPE, Covina, California., 1989, p. 196.

14. Farley, G.L., Smith, B.T. and Maiden J., "Compression Response of Thick Layer Composite Laminates with Through the Thickness Reinforcement," **Journal of Reinforced Plastics and Composites**, Vol. 11, No. 7, July 1992, p. 787.

15. Farley, G.L. and Dickinson, L.C., "Removal of Surface Loop from Stitched Composites Can Improve Compression and Compression-after-Impact Strengths," **Journal of Reinforced Plastics and Composites**, Vol. 11, No. 6, June 1992, p. 633.

16. Portanova, M.A., Poe, C.C., Jr. and Whitcomb, J.D., "Open Hole and Post-Impact Compression Fatigue of Stitched and Unstitched Carbon/Epoxy Composites," **NASA-TM-102676**, June 1990.

17. Vandermey, N.E., Morris, D.H. and Masters, J.E., "Damage Development Under Compression-Compression Fatigue Loading in a Stitched Uniwoven Graphite/Epoxy Composite Material," Virginia Tech Center for Composite Materials and Structures, **CCMS-91-16** and **VPI-E-91-14**, July 1991.

18. Wagnecz L., "Mechanical Behavior and Damage Mechanisms of Woven Graphite-Polyamide Composite Materials," M.S. Thesis, Virginia Polytechnic Institute and State University, Blacksburg, Virginia, 1987.

19. Ko, F.K., "Three-Dimensional Fabrics for Composites," in Tsu-Wei Chou and Frank K. Ko (eds.), **Textile Structural Composites**, Elsevier, New York, 1989, p. 203.

20. Hirokawa, T., Yasuda J. Iwasaki Y. and Nogucki Y., "The Characteristics of 3-D Orthogonal Woven Fabric Reinforced Composites," in J. Stinson, R. Adsit (ed.), **36th International SAMPE Symposium**, SAMPE, Covina California, April 1991, p. 151.

21. Liao, D., Tan T.M. and Ko F.K., "Compressive Behavior of 3D Braided Composites, Part 1: Experimental Observations," in J. Stinson, R. Adsit (ed.), **36th International SAMPE Symposium**, SAMPE, Covina California, 1991, p. 129.

22. Ko, F.K. and Hartman D., "Impact Behavior of 2-D and 3-D Glass-Epoxy Composites," in J. L. Bauer (ed.), **31st International SAMPE Symposium**, SAMPE, Covina, Calif., April 1986, p. 1272.

23. Dickinson, L., Mohammed, M.H. and Klang, E., "Impact Resistance and Compression Properties of Three-Dimensional Woven Carbon/Epoxy Composites," in J. Fuller and G. Grunninger (eds.), **ECCM IV: Developments in the Science and Technology of Composite Materials**, Elsevier, New York, 1990, p. 659.

24. Chou, S., Chen, H. and Chen, H, "Effect of Structure on Mechanical Fracture Behavior of Three Dimensional Carbon Fiber Fabric Reinforced Epoxy Resin Composites," **Composite Science and Technology**, Vol. 45, No. 1, 1992, p. 23.

25. Springer, G.S., "Introduction," in G. S. Springer (ed.), **Environmental Effects on Composite Materials**, Technomic, Lancaster, Pennsylvania, 1981, p. 1.

26. Whiteside, J.B., Delasi, R.J. and Schult, R.L., "Measurement of Preferential Moisture Ingress in Composite Wing/Spar Joints," **Composite Science and Technology**, Vol. 24, No. 2, February 1985, p. 123.

27. Komorowski, J.P., "Hygrothermal Effects in Continuous Fibre Reinforced Composites, Part I: Thermal and Moisture Diffusion in Composite

Materials," **NAE-AN-4, NRC NO. 20974**, National Research Council Canada, 1983.

28. Komorowski, J.P., "Hygrothermal Effects in Continuous Fibre Reinforced Composites, Part II: Physical Properties," **NAE-AN-10, NRC NO. 22700**, National Research Council Canada, 1983.

29. Komorowski, J.P., "Hygrothermal Effects in Continuous Fibre Reinforced Composites, Part III: Mechanical Properties 1. Static Test," **NAE-AN-11, NRC NO. 21299**, National Research Council Canada, 1983.

30. Komorowski, J.P., "Hygrothermal Effects in Continuous Fibre Reinforced Composites, Part IV: Mechanical Properties 2. Fatigue and Time Dependant Properties," **NAE-AN-12, NRC NO. 21300**, National Research Council Canada, 1983.

31. Wolfe, E.G., "Polymer Matrix Composites: Moisture Effects and Dimensional Stability," **Encyclopedia of Composites, vol 4**, Wiley, New York, 1989, p. 279.

32. Crank, J.S. and Park, G.S., **Diffusion in Polymers**, Academic Press, New York, 1968.

33. Crank, J.S., **The Mathematics of Diffusion**, Oxford University Press, London, 1967.

34. Shen, C.H. and Springer, G.S., "Moisture Absorption and Desorption of Composite Materials," **Journal of Composite Materials**, Vol. 10, No. 2, April 1976, p. 2.

35. Cook, T.S., Wolrath, D.E. and Francis, P.H., "Moisture Absorption in Graphite-Epoxy Composite Materials," **22nd International SAMPE Symposium**, SAMPE, Azusa, Calif., 1977, p. 339.

36. Loos, A.C. and Springer, G.S., "Moisture Absorption of Graphite-Epoxy Compositions Immersed in Liquids and in Humid Air," in G. S. Springer (ed.), **Environmental Effects on Composite Materials**, Technomic, Lancaster, Pennsylvania 1978, p.34.

37. Deiasi, R. and Whiteside, J.B., "Effect of Moisture on Epoxy Resins and Composites," in J.B. Vinson (ed.), **Advanced Composite Materials: Environmental Effect, ASTM 658**, ASTM, Philadelphia, 1978, p. 2.

38. Shirell, C.D., "Diffusion of Water Vapor in Graphite/Epoxy Composites," in J. B. Vinson (ed.), **Advanced Composite Materials:Environmental Effect, ASTM 658**, ASTM, Philadelphia, 1978, p. 21.

39. Woo, M. and Piggott, M.R., "Water Absorption of Composites I. Epoxy Homopolymers and Copolymers," **Journal of Composite Technology and Research**, Vol, 9, No. 3, Fall 1987, p. 101.

40. Harper, B.D., Staab, G.H. and Chen, R.S., "Effects of Voids Upon the Hygral and Mechanical Properties of Composites," **Journal of Composite Materials**, Vol. 21, No. 3, March 1987, p. 280.

41. Weitsman, Y., "Coupled Damage and Moisture-Transport in Fiber Reinforced Polymeric Composites," **International Journal of Solids and Structures**, Vol. 23, No. 7, 1987, p. 1003.

42. Penn, L. and Larsen, F., "Physicochemical Properties of Kevlar Fibers," **Journal of Applied Polymer Science**, Vol. 23, No. 1, January 1979, p. 59.

43. Woo, M.S.W. and Piggott, M.R., "Water Absorption of Resins and Composites: II. Diffusion in Carbon and Glass Reinforced Epoxies," **Journal of Composite Technology and Research**, Vol. 9, No. 4, Winter 1987, p. 162.

44. Neuman S. and Marom G., "Prediction of Moisture Diffusion Parameters in Composite Materials Under Stress," **Journal of Composite Materials**, Vol. 21, No. 1, January 1987, p. 68.

45. Gillat O. and Broutman, L.J., "Effect of an External Stress on Moisture Diffusion and Degradation in a Graphite Reinforced Epoxy Laminates," in J.R. Vinson (ed.) **Advanced Composite Material-Environmental Effects, ASTM STP-658**, ASTM, Philadelphia, 1978, p. 61.

46. Blikstad, M., Sjöblom, P.O.W. and Johannesson, T.R., "Long-Term Moisture Absorption in Graphite/Epoxy Angle-Ply Laminate," **Journal of Composite Materials**, Vol. 18, No. 1, January 1984, p. 32.

47. Springer, G.S. and Tsai, S.W., "Thermal Conductivity of Unidirectional Material," in G.S. Springer (ed.), **Environmental Effects on Composite Materials**, Technomic, Lancaster, Pennsylvania 1978, p. 7.

48. Carslaw, H.S. and Jaeger, J.C., **Conduction of Heat in Solids**, Oxford, London, 1947.

49. Whitney, J.M., "Three Dimension Moisture Diffusion in Laminated Composites," **AIAA Journal**, Vol. 15, No. 9, September 1977, p. 1356.

50. Singh, K.S., Singh, P.N. and Rao, R.M., "Hygrothermal Effects on Chopped Fibre/Woven Fabric Reinforced Epoxy Composites. Part A: Moisture Adsorption Characterization," **Journal of Reinforced Plastics and Composites**, Vol. 10, No. 5, September 1991, p. 446.

51. Crossman, F.W., Mauri, R.E. and Warren W.J.,"Moisture-Altered Viscoelastic Response of Graphite/Epoxy Composites," in J. B. Vinson (ed.), **Advanced Composite Materials: Environmental Effect, ASTM 658**, ASTM, Philadelphia, 1978, p. 205.

52. Sykes, G.F., Funk, J.G., Slemp, W.S., "Assessment of Space Environment Induced Micro Damage in Toughened Composites," in J.T. Hoggatt, S.G. Hill, J.C. Johnson (eds.), **18th International SAMPE Technical Conference, Materials for Space-The Gathering Momentum**, Covina, California, SAMPE, 1986, p. 520.

53. Bergmann, H.W. and Hartung, W., "Thermal Cycling of Carbon Fiber-Reinforced Resin Systems," in **Advances in Fracture Research Proceedings of the 7th International Conference on Fracture**, Vol. 6, Pergamon, New York, 1989, p. 3585.

54. Morris, W.L., James, M.R. and Inman, R.V., "Accelerated Aging of the Thermal Expansion of Unidirectional Graphite/Epoxy Composites by Thermal Fatigue," **Journal of Engineering Materials and Technology**, Vol. 111, No. 4, October 1989, p. 331.

55. Adamson, J.M., "A Conceptual Model of the Thermal Spike Mechanism," in T.K. Obrien (ed.), **Long Term Behavior of Composites, ASTM STP 813**, ASTM, Philadelphia, 1983, p. 179.

56. McKague, E.L. Jr., Halkias, J.E and Reynolds, J.D., "Moisture in Composites: The Effect of Supersonic Service on Diffusion," **Journal of Composite Materials**, Vol. 9, No. 1, January 1975, p. 2.

57. Pritchard, G. and Stansfield, K., "The Thermal Spike Behavior of Carbon Fiber Reinforced Plastics," in F.L. Matthews (ed.), **ICCM 6/ECCM 2**,Vol. 4, Elsevier Applied Science, New York, 1987, p. 4.190.

58. Ankara, A., Weisgerber, D. and Vilsmeier J., "Influence of Thermal Spiking on Properties of Carbon Fibre Reinforced Plastic," **Materials Science and Technology**, Vol 2, No. 11, November 1986, p. 1081.

59. Bergmann, H. W., Gädke, M. and Goetting, H.C., "Performance Characteristics of Composite Materials," **Spacecraft Structures, Proceedings of a European Space Agency Conference**, esa-sp-238, 1985, p 353.

60. Ankara, A., Weisgerber, D. and Vilsmeir, J., "Influence of Moisture on the Mechanical Properties of Graphite Epoxy System," in G.C. Sih, S.F. Hsu (eds.), **Advanced Composite Materials and Structures**, Proceedings of an International Conference, 1986, p. 347.

61. Bishop, S.M., "Environmental Effects on the Shear Performance of Carbon Fiber Reinforced Plastics," in B.F. Dyson, D.R. Hayhurest (eds.), **Materials and Engineering Design**, Brookfield, London, Conference Proceedings: The Institute of Metal, 1988, p. 366.

62. Haque, A.,Mahmood, S., Walker, L. and Jeelani S., "Moisture and Temperature Induced Degradation in Tensile Properties of Kevlar-Graphite/Epoxy Hybrid Composites," **Journal of Reinforced Plastics and Composites**, Vol. 10, No. 2, March 1991, p. 132-145.

63. Shen, C. and Springer, G.S., "Effects of Moisture and Temperature on the Tensile Strength of Composite Materials," in G.S. Springer (ed.), **Environmental Effects on Composite Materials**, Technomic, Lancaster, Pennsylvania, 1981, p. 79.

64. Shen, C. and Springer, G.S., "Environmental Effects in the Elastic Moduli of Composite Materials," in G.S. Springer, **Environmental Effects on Composite Materials**, Technomic, Lancaster, Pennsylvania, 1981, p. 94.

65. Gibbins, M.N. and Hoffman, D.J., "Environmental Exposure Effects on Composite Materials for Commercial Aircraft," **NASA-CR-3502**, 1982.

66. Springer, G.S., "Numerical Procedures for the Solution of One Dimensional Fickian Diffusion Problems," in G.S. Springer (ed.), **Environmental Effects on Composite Materials**, Technomic, Lancaster, Pennsylvania, 1981, p. 166.

67. Cano, R.J., and Furrow, K.W., "Effects of Temperature and Humidity Cycling on the Strengths of Textile Reinforced Carbon/Epoxy Composite

Materials," Third NASA Advanced Composite Technology Conference, **NASA-CP-3178**, 1992, p.191.

68. Burr, S.T., "An Experimental Characterization of Micromechanical Fracture and & Failure Modes in a woven Fabric Composite," M.S. Thesis, Michigan Technological University, 1991.

69. Deaton, J.W. and Kullerd, S.M., "Mechanical Characterization of 2-D, 2-D Stitched, and 3-D Braided/RTM Materials," Third NASA Advanced Composites Technology Conference, **NASA CP-3178**, 1992, p. 209.

70. Aronhime, Marc T., Neumann, S. and Marom Gad, "The Anisotropic Diffusion of Water in Kevlar-Epoxy Composites," **Journal of Material Science**, Vol. 22, No. 7, July 1987, p. 2435.

VITA

The author was born January 1963 in Roanoke Virginia. After growing up in Waynesboro Virginia he attended VPI & SU where he grew up some more and earned a Bachelors Degree in Chemical Engineering. After graduation he began a five year career with Hercules Incorporated at the Radford Army Ammunition Plant. While with Hercules he researched and developed tank, cannon and rocket propellants for the U.S. government. A sudden surge of world peace foreshadowed an end to this career and the author took the opportunity to return to school and earn a Masters Degree in Engineering Mechanics. The author intends to return to an industrial career after graduation.